TOPOLOGY SHARED BETWEEN CLASSICAL AND QUANTUM MATERIALS

A Dissertation

Presented to the Faculty of the Graduate School

of Cornell University

in Partial Fulfillment of the Requirements for the Degree of

Doctor of Philosophy

by

Po-Wei Lo

August 2022

TOPOLOGY SHARED BETWEEN CLASSICAL AND QUANTUM MATERIALS

Po-Wei Lo, Ph.D.

Cornell University 2022

The concept of topology has been widely used to classify materials. Majority of works are focused on quantum systems. Until recently, many advancements have also been made in the field of topological mechanics. However, the connections between them are still limited to the linear level of mechanical systems which are naturally nonlinear. In this thesis, we expose this field with different approaches by studying topology of nonlinear classical systems and possible connections to quantum systems.

Firstly, we present a generic prescription of defining topological indices which accommodates nonlinear effects in mechanical systems without taking any approximation. Invoking the tools of differential geometry, a $\mathbb{Z}$-valued quantity in terms of a topological index μ in differential geometry known as the Poincaré-Hopf index, that features the topological invariant of nonlinear zero modes (ZMs), is predicted. We further identify one type of topologically protected solitons that are robust to disorders. Our prescription constitutes a new direction of searching for novel topologically protected nonlinear ZMs in the future.

Secondly, we connect this topological index μ to the Witten index W in supersymmetric quantum systems. To establish the connection, we study two topological number in isostatic mechanical systems and supersymmetric quantum systems respectively. On one hand, we define Q_{net} for an isostatic mechanical

system that counts the number of robust zero-energy configurations. On the other hand, we write a supersymmetric Hamiltonian that has a well-defined Witten index that tells us the number of robust zero-energy states. Finally, we show that $Q_{net} = W$ under very general conditions. Our result suggests a direct connection between nonlinear mechanical systems and interacting quantum systems, and therefore points out an alternative way to understand the topology of quantum systems.

Finally, we study topological frustration which is the existence of classical zero modes that are robust to many but not all distortions of the Hamiltonian. For a magnet whose classical limit exhibits topological frustration, an important question is what happens to this topology when the degrees of freedom are quantized and whether such frustration could lead to exotic quantum phases of matter like a spin liquid. In quantum spin ladders, we find low-energy eigenstates corresponding to known symmetry protected topological (SPT) ground states, and a special role of $SU(2)$ symmetry that demands the existence of extra dimensions of classical zero modes—the phenomena we call symmetry-enriched topological frustration (SETF). These results suggest that in the absence of magnetic order, classical topological frustration manifests at finite spin as asymptotically low energy modes with support for exotic quantum phenomena.

BIOGRAPHICAL SKETCH

Po-Wei was born on November 11, 1989 in Taiwan. He studied electrical engineering and computer science graduated from National Chia Tung University with a B.E. in June 2012. After that, he switched to physics and entered the graduate school in National Taiwan University. He got a M.S. 2 years later. He began studies at Cornell University in August 2016. He completed the Ph.D. thesis in 2022, under the supervision of Michael J. Lawler.

This document is dedicated to all Cornell graduate students.

ACKNOWLEDGEMENTS

I much appreciate all the help leads to the completion of my Ph.D. thesis. During this Ph.D. program, I have gone through a lot of training which has strengthened my abilities and skills in research, collaborations, and communication. I am really grateful to Cornell University for giving me this opportunity to improve myself.

First of all, I must first thank my supervisor, Dr. Michael J. Lawler. During the discussion with him, I found that I have many shortcomings. Through his careful guidance, I have learned a lot of research methods and concepts. In addition, I particularly thank Dr. Christian D Santangelo who taught me many basic computational skills and fundamental mathematics. Moreover, I also thank Dr. Chao-Ming Jiang who taught me a lot of rigorous ways of proving handwaving ideas. Overall, I would like to thank everyone at Cornell. All the kind people have given me considerable assistance, so that I am no longer a lost lamb. Finally, I must especially thank my family, who fully supported me to study for a Ph.D. degree and gave me strong spiritual support.

TABLE OF CONTENTS

LIST OF TABLES

LIST OF FIGURES

CHAPTER 1

INTRODUCTION

One way to study the connections of topology between classical mechanics and quantum mechanics is starting with mechanical systems. Mechanical systems offer a remarkable connection between physics and engineering. Through their simplicity, they have inspired both ideas at the foundation of theoretical physics and a sense of control over our physical world. In the recent field of topological condensed matter, following hints that topology can play a role in nonlinear fine-tuned mechanical systems[30], Kane and Lubensky[26] uncovered a connection between topological insulators[21, 46, 28, 23] and linearized balls-and-springs models. With importance in the field of metamaterials[37, 44, 71, 50, 38, 62, 64, 56, 63, 42, 45, 55, 72, 51, 74] and magnetics[48, 47], they realized if constraints define the system, zero modes (ZMs) can be topologically protected by TKNN-like topological invariant[57].

It was quickly realized that Kane and Lubensky's ZMs in the case of a chain model they construct can survive back into the nonlinear regime and become bulk solitons[14]. But a formally identical origami system was identified that does not exhibit these solitons[13]. More nonlinear ZMs were found in mechanical systems in numerical simulations[41, 73]. In a one-dimensional chain, a domain wall separating two distinct polarizations can be identified by constructing a sequence of consecutive maps on the space of ZMs of a single unit cell[75]. However, that does not quite guarantee that this domain wall can move continuously along the chain like a soliton. Thus, the existence of a soliton relies on the exact parameters of a model[52]. To the best of our knowledge, however, it remains unclear if solitons observed in generic mechanical systems are always

topologically protected or not, and if so, what is the topology to classify them?

To answer these questions, we develop an exact theory to study the topological protection of the kinematics of periodic mechanisms satisfying holonomic constraints such as those that arise in *e.g.* linkages and origami. Using the concept of differential geometry, our theory predicts the existence of a $\mathbb{Z}$-type topological index μ which can be used to classify nonlinear ZMs such as solitons.

The topological index $\mu(p)$ defined for a zero-energy configuration point p in an isostatic mechanical system has a similar mathematical expression that is used to calculate the supersymmetric partition function in the topological quantum field theory[36, 5]. For a certain "symmetric" case, the sum over all $\mu(p)$ is exactly equal to the Witten index of the BRST type supersymmetric model[2, 60, 3]. The definition of this "symmetric" case will be provided below. In this model, the Hamiltonian can be interpreted as complex fermions that conserve fermion numbers, such as electrons in a normal metal, coupled to anharmonic phonons. However, in a mechanical system, constraints, in general, do not have this symmetry. So this connection seems restricted to limited cases.

Fortunately, a more general supersymmetric Hamiltonian can be written in a way that does not require the constraint functions to obey this symmetry[31]. In this case, $U(1)$ symmetry of the fermion systems is broken and thus the Hamiltonian can then be interpreted as Majorana fermions (which can realize a p-wave superconductor[29]) coupled to anharmonic phonons. Although the fermion number is no longer conserved, the fermion parity is still well-defined. Thus, we can calculate the Witten index even in a "non-symmetric" case. Then a question arises: for a generic set of constraint functions, what is the relation between the Witten index and the topological index $\mu(p)$?

Another candidate to study the connections of topology between classical mechanics and quantum mechanics is frustrated spin systems. Geometric frustration in physics brings many exotic phenomena. Spin lattices such as triangular, kagome, and pyrochlore latticesmay possess novel quantum phenomena[4, 9, 10, 8, 54] and novel classical phenomena arising from a large degeneracy of classical ground states such as spin origami[53, 43, 49]. These classical phenomena seem at first sight disconnected from the quantum phenomena but perhaps not. If we could solve some of these frustrated spin systems in the large-but-finite spin regime, what kinds of quantum phenomena would be revealed?

In many cases, it is known that the degeneracy of classical ground states is lifted by quantum fluctuations and the ground state becomes magnetically ordered in two or three-dimensional space. This order-by-disorder phenomenon has been established by performing perturbative expansions or spin-wave approximation approaches in the large spin S limit. We know for example that in Heisenberg antiferromagnets on a triangular, square, or kagome lattice, order-by-disorder occurs[15, 69, 32]. However, a magnetically ordered phase may not always be the fate of a frustrated spin system. Taking into account higher-order corrections in $1/S$, it has been shown that a magnetic order ground state is not easily established and may even be absent in some frustrated spin systems, including some square lattice models[11, 70] and the pyrochlore Heisenberg antiferromagnet[22, 24]. In the cases where an ordered phase is not the fate of frustration, can frustration support exotic quantum phenomena? If so, what kinds of frustration can support these phenomena?

We consider the case of geometric frustration and whether it can support ex-

otic quantum phenomena at large-but-finite S. In particular, we are focused on the case where the Hamiltonian of a geometrically frustrated spin system can be written as a classical frustration-free form. In this case, the classical ground state can be understood as zero modes of a constrained problem. The zero modes of classical spins then obey Moessner-Chalker-Maxwell counting[20] and form mechanical analogs of topological mechanics[27] like spin origami[49]. We call this phenomenon "topological frustration" and wonder whether it supports topological quantum states, quantum spin liquids, or other exotic quantum phenomena.

Some of the results presented in this thesis have previously been published in Refs. [36] or submitted to arXiv (https://arxiv.org/abs/2207.10045 and https://arxiv.org/abs/2207.10045)[34, 35].

CHAPTER 2

TOPOLOGY IN NONLINEAR MECHANICAL SYSTEMS

In this chapter, we introduce the definition of the topological index μ in nonlinear mechanical systems. To illuminate its applications, we further use this topological index to generate another topological index we call I that reveals whether or not a topologically protected ZM can propagate through the system. Applying this to the Kane-Lubensky (KL) chain, we realize the topology to classify the (two) distinct phases of the KL chain, namely the "flipper" and the "spinner", and further show that the existence of the spinner soliton is topologically protected and robust to disorders (unlike the flipper). In distinction, the origami chain does not support any soliton despite the superficial similarity of its linear ZMs to those of the KL chain.

2.1 The mechanics of constrained systems

We start by characterizing the type of mechanical system we are interested in. We assume that the state of the system can be described by generalized degrees of freedom, $\theta = (\theta_1, \theta_2, \cdots, \theta_n)$, and that the system is characterized by a set of (spring) extensions $\mathbf{e}(\theta) = (e_1(\theta), \cdots, e_m(\theta))$. While the elastic energy of such a system can be written as $E(\theta) = \sum_i k_i e_i(\theta)^2$ for a set of moduli $k_i > 0$, here we will only be interested in the ground state configurations specified by $\bar{\theta}$ such that $\mathbf{e}(\bar{\theta}) = \mathbf{0}$. If we work with a mechanical linkage or a spring network as in Ref.[26], we can think of θ representing the positions of the vertices of our network and $e_i(\theta)$, the extension of the springs (from their equilibrium lengths). In this language, the Jacobian $\partial e_i(\theta)/\partial\theta_j$ is termed the rigidity matrix.

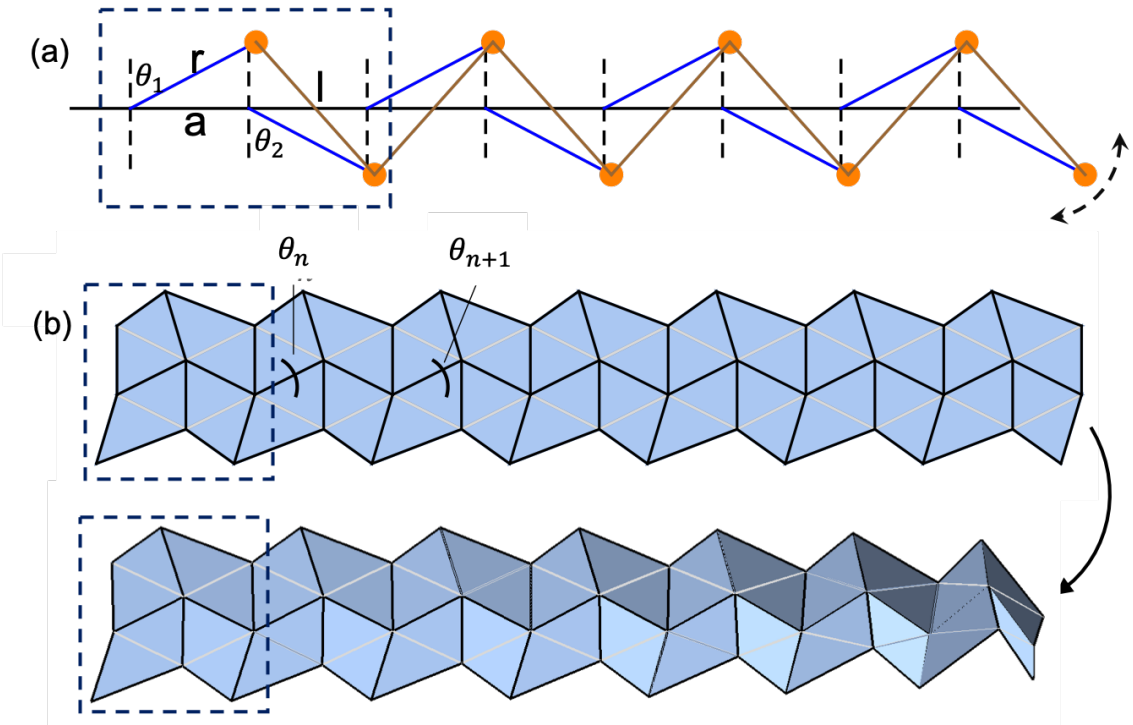

Figure 2.1: (a)The KL chain has an edge mode on either the left or right edge. (b) The origami chain has an edge mode on either the left or right edge.

Before presenting our prescription of defining topological indices, it is useful to review two examples that pose some apparent paradoxes in defining the topological invariant of the linear ZMs. First, for the KL chain, it is often easier to express the generalized coordinates in terms of the rotation angle of a series of rotors so that θ_i is the angle between the ith rotor and the vertical axis as shown in Fig. E.1 (a). The extension of the ith spring which connects the ith rotor with the $(i+1)^{th}$ rotor then takes the form $e_i(\theta) = f(\theta_i, \theta_{i+1})$, where

$$\begin{aligned} f(\theta_i, \theta_{i+1}) &= [(a + r\sin\theta_{i+1} - r\sin\theta_i)^2 \\ &\quad +(r\cos\theta_{i+1} + r\cos\theta_i)^2]^{1/2} - L, \end{aligned} \tag{2.1}$$

a, r, and L are the distance between two consecutive pivot points, the radius of

the rotors, and the equilibrium length of the springs, respectively. For an open chain of n springs (and $n+1$ rotors), if we choose $\theta_{n+1} = \theta_1$, then we have exactly as many constraints as the degrees of freedom, making the system isostatic.

In the second example of the origami chain[13], we instead use θ_i to denote the supplement of the dihedral angle of one of the folds of each vertex, also called the fold angle [Fig. E.1 (b)] (see Appendix). In this case,

$$f(\theta_i, \theta_{i+1}) = A \sin^2(\theta_i/2) - B \sin^2(\theta_{i+1}/2) + \epsilon, \tag{2.2}$$

where $0 < A < 1$, $0 < B < 1$, and ϵ are defined in Appendix A. While it is straightforward to generalize the above equations to any periodic structure, for simplicity, we specialize to the examples mentioned above focusing on Eq. (2.1)-(2.2) for the remainder of this paper.

In both the KL chain and the origami chain, if we assume a uniform solution of $\mathbf{e}(\bar{\theta}) = \mathbf{0}$, following Ref. [26], the polarization is defined as the integer

$$Q = \frac{1}{2\pi i} \int_{\pi}^{\pi} \mathrm{d}q \, \frac{\partial}{\partial q} \ln \left[\partial_1 f(\bar{\theta}, \bar{\theta}) + \partial_2 f(\bar{\theta}, \bar{\theta}) e^{iq} \right]. \tag{2.3}$$

where ∂_a implies the derivative with respect to the ath variable in the argument of f. When $|\partial_2 f(\bar{\theta}, \bar{\theta})| > |\partial_1 f(\bar{\theta}, \bar{\theta})|$, $Q = 0$ and when $|\partial_2 f(\bar{\theta}, \bar{\theta})| < |\partial_1 f(\bar{\theta}, \bar{\theta})|$, $Q = 1$. These two values of Q define two distinct topological phases. For finite systems, the bulk is rigid for both $Q = 0$ and 1, however, the feature that distinguishes these two phases is the location of the linear ZM.

The behavior above is exhibited by the linear ZMs in both the KL chain and the origami chain, as it should. But in the KL chain (and not the origami chain), certain non-linear deformations can propagate across the system resulting in the edge mode appearing on the other side. In that sense, the polarization defined by Eq. (2.3), though an integer, is not necessarily topologically robust.

2.2 A topological index for isostatic systems

To understand why the two models discussed above behave so differently in presence of non-linearity, we introduce a prescription of defining topological indices in terms of the Poincaré-Hopf index[7] The definition of the index involves a generic non-linear map $\mathbf{e}(\theta)$ (Eq.2.1 and Eq.2.2 are two examples we are focused on in this work) which can be thought of as the vector field on the space of generalized coordinates as shown in Fig. 2.2 (a). In the isostatic case ($m = n$), for a solution $\bar{\theta}$ satisfying $\mathbf{e}(\bar{\theta}) = \mathbf{0}$, we can define an index $\mu(\bar{\theta})$ by computing the winding number of the map $\mathbf{e}(\theta)$ on the $(n-1)$-dimensional sphere enclosing $\bar{\theta}$, $S_{\bar{\theta}}$ by integrating the differential form

$$\mu(\bar{\theta}) = \frac{1}{(n-1)!A_{n-1}} \oint_{S_{\bar{\theta}}} \frac{e_{i_1} de_{i_2} \wedge ... \wedge de_{i_n} \epsilon^{i_1, i_2, ..., i_n}}{(e_1^2 + e_2^2 + ... + e_n^2)^{n/2}}, \tag{2.4}$$

where A_{n-1} is the surface area of a unit $(n-1)$-dimensional sphere. When, for example, $n = 2$, it yields the so-called first Chern number which frequently appears in classifying the topology in electronic band structures. $\mu(\bar{\theta})$ is well-defined for any isolated solution $\bar{\theta}$ even when the Jacobian is not full rank. It is also known as the degree of a map[40] which implies $\mu(\bar{\theta})$ predicts the minimum number of non-linear ZMs that would pass through the configuration $\bar{\theta}$ after releasing one constraint.

When the Jacobian is full rank, $\mu(\bar{\theta}) = \text{sgn}[\det(\partial e_i(\bar{\theta})/\partial\theta_j)]$[19]. Under this condition, the configuration $\bar{\theta}$ is structurally stable meaning that $\mu(\bar{\theta})$ is invariant under small, continuous deformations of the constraint functions $\mathbf{e}(\theta)$. The idea of topological protection in a linear theory can now be cast as the following: without any symmetry, the phonon spectrum is characterized by a $\mathbb{Z}_2$ invariant protected by a bulk gap that closes when the Jacobian is not full rank.

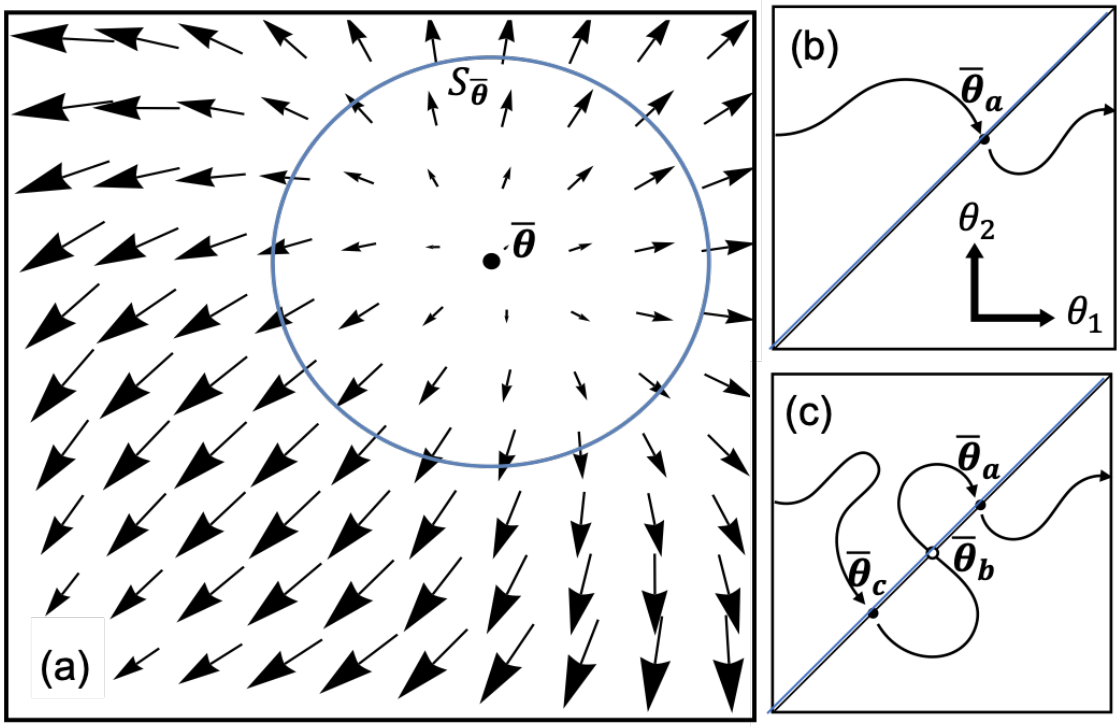

Figure 2.2: (a) The vector field $\mathbf{e}(\bar{\theta})$ is indicated by arrows. The winding number $\mu(\bar{\theta})$ is a topological index which measures how many times the vector field rotates along $S_{\bar{\theta}}$. (b) The total intersection number I is a homotopy invariant of a ZM and counts the minimal number of periodic configurations along that ZM. (c) A ZM with a deformed trajectory has the same total intersection number as (b).

A deeper physical meaning of $\mu(\bar{\theta})$ relies on the form of constraints. For example, in the KL and origami chain with periodic boundary conditions, for a uniform solution $\bar{\theta}$, $\mu_{PBC}(\bar{\theta})$ can be simplified to $\mu_{PBC}(\bar{\theta}) = \text{sgn}\{[\partial_1 f(\bar{\theta},\bar{\theta})]^n - [-\partial_2 f(\bar{\theta},\bar{\theta})]^n\}$ which only depends on the magnitude of $\partial_1 f(\bar{\theta},\bar{\theta})$ and $\partial_2 f(\bar{\theta},\bar{\theta})$. Consequently, $\mu_{PBC}(\bar{\theta}) = 1$ when $|\partial_1 f(\bar{\theta},\bar{\theta})| > |\partial_2 f(\bar{\theta},\bar{\theta})|$ and $\mu_{PBC}(\bar{\theta}) = -1$ when $|\partial_1 f(\bar{\theta},\bar{\theta})| < |\partial_2 f(\bar{\theta},\bar{\theta})|$. Therefore, $\mu_{PBC}(\bar{\theta}) = 2Q - 1$, where Q is the topological polarization discovered by Kane and Lubensky [26].

2.3 examples and applications

The topological index $\mu(p)$ is well-defined for any isolated solution points even when the rigidity matrix is not full rank. This provides us a new way to study what happens at the gapless point. By the definition, the magnitude of the topological index tells us the minimum number of points in the coordinate space which are mapped into the same nonzero $\mathbf{f}$ around the solution point p. Therefore, the physical meaning of the topological index $\mu(p)$ is the (minimum) number of zero modes passing through the point p after dropping one constraint.

A one-dimensional nonlinear ZM (drop one constraint in an isostatic system) can then be studied by tracking those topological indices as we continuously deform one of the constraints in an isostatic system. Because the net topological index Q_{net}, defined as the sum over all the topological indices at the solution points, is conserved, the only way to annihilate charges Q_{net} is combining one positive charge with one negative charge. Therefore, the topology of the nonlinear ZMs can be predicted by drawing the possible ways of connecting two topological indices with the opposite signs.

2.3.1 Two-rotor model

Let's take a two-rotor model for example. As shown in Fig.E.2(a), each site has a rotor with radius r, and the distance between two pivot points of adjacent rotors is a. Two adjacent rotors are constrained by a spring with rest length L_1. The rotating angle θ_i is defined clockwisely with respect to $+y$-axis for the first rotor, and counterclockwisely with respect to $-y$-axis for the second rotor. Imag-

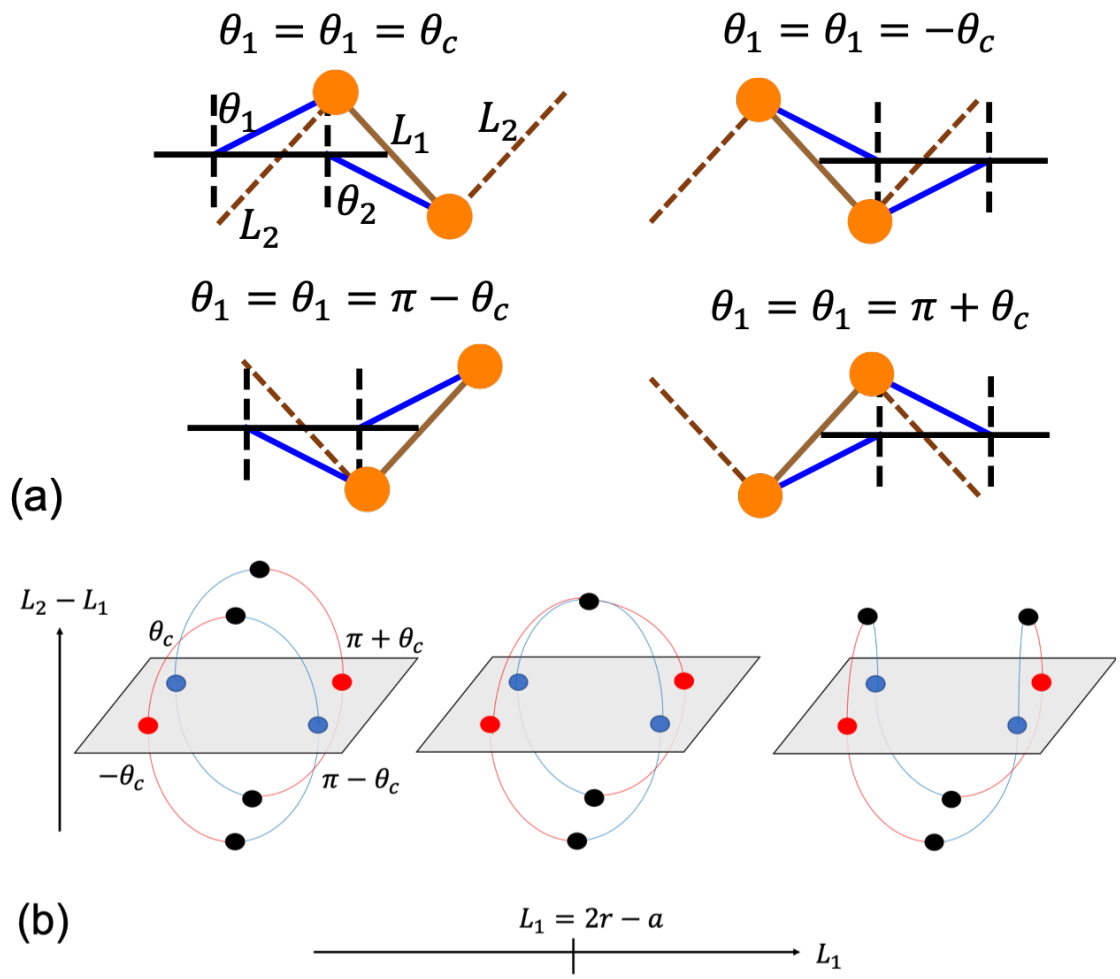

Figure 2.3: (a)Four different solutions for the two-rotor model with an extra spring connecting the second spring back to the first spring like a periodic boundary condition. (b)Nonlinear zero modes in the the two-rotor model. The blue (red) circles are the solution points for the periodic boundary condition ($w = 0$) with topological index +1 (−1). The blue (red) lines are the solution points with topological index +1 (−1) as we continuously change L_2. The black circles are the points where one positive and one negative topological index combine. Two topologically different nonlinear zero modes are separated by the phase transition point $L_1 = 2r - a$ where two black circles merge.

ine that we connect the second rotor back to the first rotor by one extra spring with length L_2 like a periodic boundary condition. Then the two-rotor model becomes an isostatic system with four different zero-energy points, namely, $\theta_i = \theta_c$, $-\theta_c$, $\pi - \theta_c$, $\pi + \theta_c$ where $\theta_c = sin^{-1}(\frac{\sqrt{a^2+4r^2-l^2}}{2r})$.

We can then predict the topology of nonlinear zero modes of the two-rotor model (after dropping the extra spring which connects the second spring back to the first spring) by connecting those topological indices with opposite signs. As shown in Fig.E.2(b), there are two topologically different ways to connect those four topological indices. For Phase I, two pairs of +1 and -1 form two separated loops. The solution $\theta_s = \theta_c$ is connected to the solution $\theta_s = \pi + \theta_c$, while the solution $\theta_s = -\theta_c$ is connected to the solution $\theta_s = \pi - \theta_c$. On the other hand, Phase II has four solutions connected and form a single loop. These two topologically different phases have been found in Ref.[14] by explicitly solving the model.

The ways of connecting topological indices are governed by the points where one positive and one negative topological index combine. Those points themselves are structurally unstable because any small change of w would either separate the two topological indices or annihilate them. The ways of connecting charges change when two structurally unstable points merge. As shown in Fig.E.2(a) and (b), the topological phase transition occurs when two structurally unstable points merge at $l = 2r - a$.

2.3.2 Other examples

Consider a coordinate space R^n with the element $(x_1, x_2, ..., x_n)$ where x_i is the degree of freedom in the system. A constraint space has the element $(f_1, f_2, ..., f_n)$ where f_i is a function of $x_1, x_2, ..., x_n$ and $f_i = 0$ is the constraint. In R^n space, the net topological index is invariant as long as no charge leaves finite region or comes from infinity and all solution points are isolated. If we think $\mathbf{f}$ is an n-dimensional vector field in the R^n space, the net topological index is indeed the index of the vector field in the Poincare-Hopf theorem. The rules of connecting topological indices are similar to the example of the KL chain, but now topological indices can end up or come from infinity.

Let's consider an example, $f_1 = x^2 - 1$ and $f_2 = x - y$[see Fig.3.2(a)]. There are two solution points, $(1, 1)$ and $(-1, -1)$. The corresponding topological indices are $+1$ and -1 respectively. There are three possible configurations. One can draw a loop passing through both solution points, one line passing through both solution points, or two lines passing through two solution points separately. The ZMs can be found by directly dropping f_1 or f_2. As shown in Fig.3.2(a), when we drop f_1 we get $x = y$ which is a ZM passing through both solution points. On the other hand, when we drop f_2 we get $x = 1$ and $x = -1$ which are two ZMs passing through two solution points separately.

Consider another example, $f_1 = x^2 - y^2$ and $f_2 = 2xy$[see Fig.3.2(b)]. There is only a $+2$ topological index at $(0, 0)$. The only configuration is two lines intersecting at point $(0, 0)$. As shown in Fig.3.2(b), when we drop f_1, we get $x = 0$ and $y = 0$ which are two ZMs passing through the point $(0, 0)$. On the other hand, when we drop f_2, we get $x = y$ and $x = -y$, which are two ZMs passing through the point $(0, 0)$ as well.

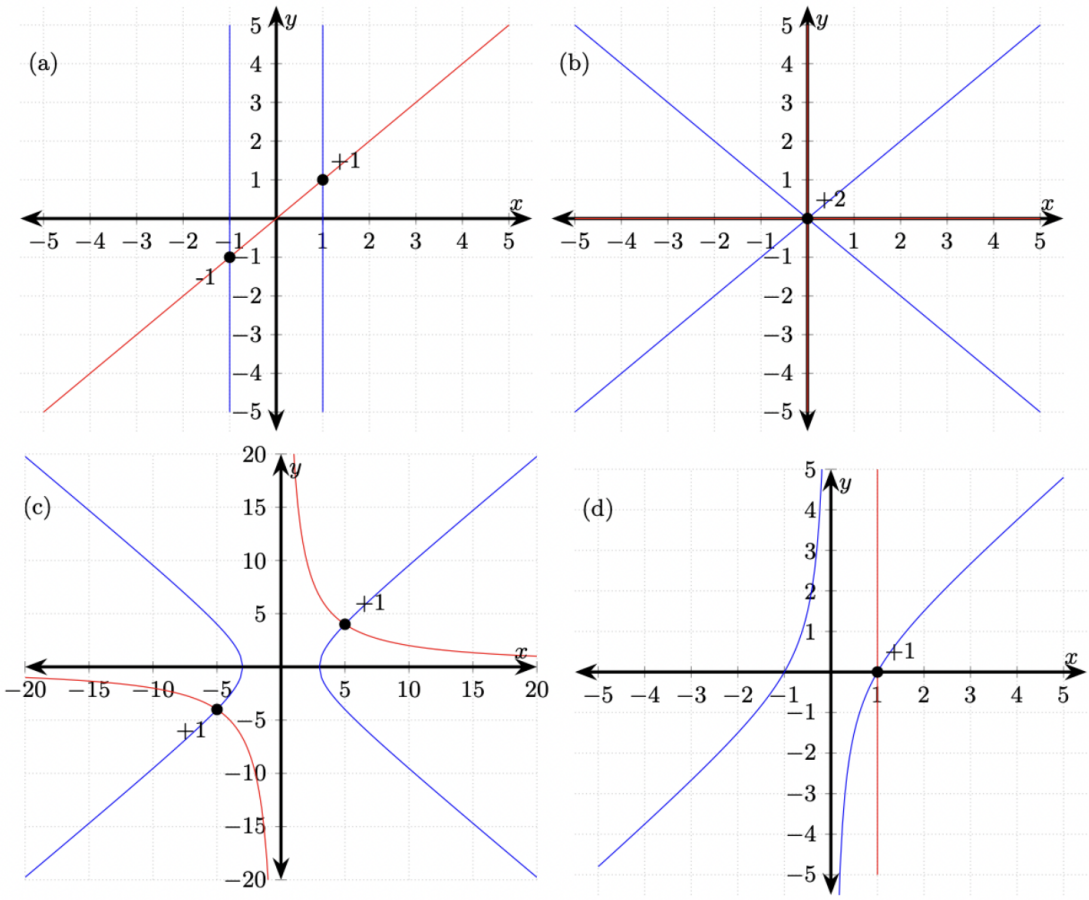

Figure 2.4: (a)Example of $f_1 = x^2 - 1$ and $f_2 = x - y$. Two topological indices $+1$ and -1 are at point $(1, 1)$ and $(-1, -1)$ respectively. The red line is the zero mode after dropping f_1, and the blue lines are the zero modes after dropping f_2. (b)Example of $f_1 = x^2 - y^2$ and $f_2 = 2xy$. One topological index $+2$ is at point $(0, 0)$. The red lines are the zero modes after dropping f_1, and the blue lines are the zero modes after dropping f_2. (c)Example of $f_1 = x^2 - y^2 - 9$ and $f_2 = xy - 20$. Two $+1$ topological indices are at point $(5, 4)$ and $(-5, -4)$ respectively. The red lines are the zero modes after dropping f_1, and the blue lines are the zero modes after dropping f_2. (d)Example of $f_1 = x(x - y) - 1$ and $f_2 = x - 1$. One topological indices $+1$ at point $(1, 0)$. The red line is the zero mode after dropping f_1, and the blue lines are the zero modes after dropping f_2. One of the blue lines is a hidden zero mode which does not directly pass through the critical point.

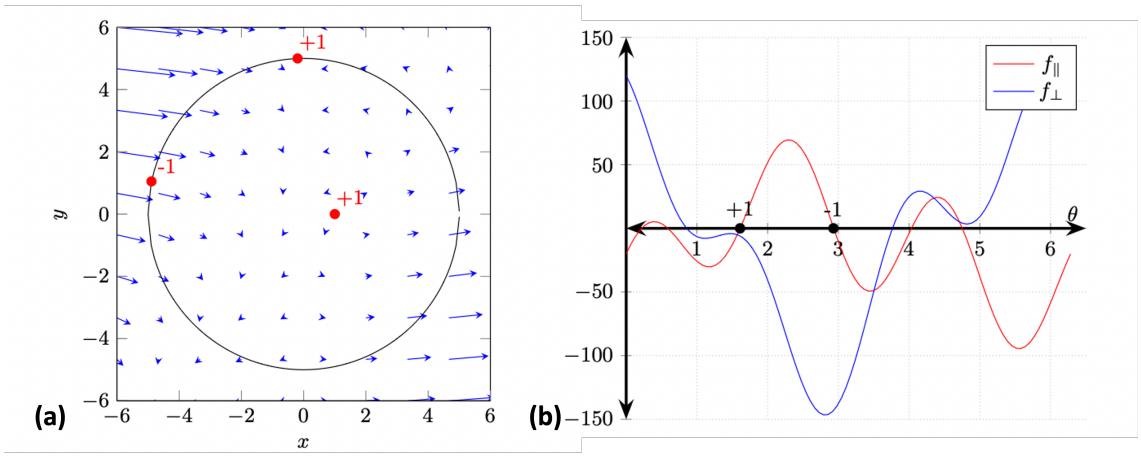

Figure 2.5: (a)The vector field $\mathbf{f} = (x(x-y)-1, x-1)$ in $x-y$ plane is plotted in blue color. The black circle with radius 5 is the boundary. The red points are critical points or boundary critical points. There are one critical point $(1,0)$ inside the circle with a $+1$ topological index and two boundary topological indices with $+1$ and -1 charges respectively. (b)The red curve $f_{\parallel}$ is the projection of $\mathbf{f}$ on the tangent direction and the blue curve $f_{\perp}$ is the projection of $\mathbf{f}$ on the normal direction. There are six boundary critical points at boundary and only two of them with $\mathbf{f}$ pointing inward (negative $f_{\perp}$) marked with black points. The boundary topological index are $+1$ and -1 respectively.

The third example is $f_1 = x^2 - y^2 - 9$ and $f_2 = xy - 20$[see Fig.3.2(c)]. There are two $+1$ topological index at two solution points $(5,4)$ and $(-5,-4)$ separately. Because two $+1$ charges can not be connected, the only possible configuration is two lines passing through two solution points separately. As shown in Fig.3.2(c), when we drop either f_1 or f_2 we both get two hyperbolas passing though two solution points separately.

Finally, we look at an example in which a charge leaves finite region or comes from infinity. Assume that we have two constraints $f_1 = x(x-y)-1$ and $f_2 = x-1$ which have a single solution $(1,0)$. As shown in Fig.3.2(d), when we drop f_1, we get a ZM $x = 1$ passing through the solution point $(1,0)$. On the other hand,

when we drop f_2, since the determinant of the Jacobian matrix is x, as continuously changing f_2, the sign of the topological index would change. This implies that a single topological index could leave finite region or come from infinity. As shown in Fig.3.2(d), after dropping f_2, two ZMs show up. One passes through the solution point $(1, 0)$, but the other one does not pass through the solution point. The latter one is a hidden ZM which arises from the boundary charge at infinity.

The boundary topological index Q_b at infinity can be defined by the similar concept and combines with the net topological index Q_{net} being the Euler characteristic χ which only depends on the manifold. Assume that $\mathbf{f}$ is a vector field on the coordinate space. We draw a large $(n-1)$-dimensional sphere (boundary) covering all finite region, and project $\mathbf{f}$ onto the $(n-1)$-dimensional sphere. Then we define the boundary critical points on the boundary as the points where the projection of $\mathbf{f}$ vanishes. Locally for each boundary critical point, we can define a topological index and only the boundary critical points with $\mathbf{f}$ pointing inward contribute as the boundary topological indices. As a result, we can write

$$\chi(V_n) = Q_{net}(\mathbf{f}) + Q_b(\mathbf{f}) = 1 \tag{2.5}$$

For the example of $f_1 = x(x-y) - 1$ and $f_2 = x - 1$, the vector field in R^2 is plotted in Fig.2.5(a). There is only one solution point $(1, 1)$ at finite region which has $+1$ topological index. Imagine that a circle at origin with radius 5 is drew as the boundary. In Fig.2.5(b), the projection of $\mathbf{f}$ on the tangent direction $f_{\parallel}$ and on the normal direction $f_{\perp}$ are plotted. There are six boundary critical points at boundary (when $f_{\parallel} = 0$) and two of them with $\mathbf{f}$ pointing inward (negative $f_{\perp}$). The boundary topological index are $+1$ and -1 respectively. Thus, $Q_b(\mathbf{f}) = 1 + (-1) = 0$ and $\chi(V_2) = 1 + 0 = 1$ which is the Euler characteristic of a disk.

2.4 A topological index for non-isostatic systems

So far, the topological index μ discussed above only applies to an isolated zero-energy configuration $\bar{\theta}$ in an isostatic system. To capture the topology of a non-linear ZM in a non-isostatic system, we now extend to derive another similar topological index ν. To do so, we look at this topological index from another perspective by first defining a tangent d-form

$$T^{i_1 \cdots i_d} = \epsilon^{i_1 \cdots i_d j_1 \cdots j_{n-d}} \partial_{j_1} e_1 \cdots \partial_{j_{n-d}} e_{n-d}, \tag{2.6}$$

where d denotes the dimension of the non-linear ZM. Since $T^{i_1 \cdots i_d}(\theta_{\mathbf{i_1}} \cdots \theta_{\mathbf{i_d}}) = 0$ for any vector $\theta_{\mathbf{i_j}}$ normal to the space of ZMs, we can think of $T^{i_1 \cdots i_d}$ as defining the tangent space of non-linear ZMs. For an open KL chain, the number of constraints is one less than the number of the degrees of freedom, and so $d = 1$. Then T is a vector field that is everywhere tangent to a non-linear ZM. In this case, the non-linear ZM can be found as the solution to the first-order differential equation $\partial_s \theta(s) = T\,[\theta(s)]$. So long as $T(\theta)$ is a smooth non-vanishing function of θ, the integral curves of $T(\theta)$ will be smooth as well. For any surface not parallel to the tangent $T(\theta)$, we can define an intersection number at the point $\bar{\theta}$ where the ZM intersects with the surface as $\nu(\bar{\theta}) = \text{sgn}\left[T(\bar{\theta}) \cdot \hat{N}(\bar{\theta})\right]$ where $\hat{N}(\bar{\theta})$ is the unit normal to the surface at $\bar{\theta}$. Alternatively, we can define a vector $\mathbf{g}(\theta) = (e_1, e_2, ..., e_{n-1}, h)$ where h is the function describing the surface. Then $\nu(\bar{\theta})$ can be computed as

$$\nu(\bar{\theta}) = \frac{1}{(n-1)! A_{n-1}} \oint_{S_{\bar{u}}} \frac{g_{j_1} dg_{j_2} \wedge \cdots \wedge dg_{j_n} \epsilon^{j_1 j_2 \ldots j_n}}{(g_1^2 + g_2^2 + ... + g_n^2)^{n/2}}, \tag{2.7}$$

similar to the way μ was defined earlier in Eq. 3.2. This results in $\nu(\bar{\theta}) = \text{sgn}\,[\det \nabla g(\bar{\theta})]$ when the Jacobian of g, denoted $\nabla g(\bar{\theta})$, is full rank. The function h can also be thought as an auxiliary constraint used to obtain information of a

non-linear ZM. For example, in the KL and origami chain, when $h = e_n = f(\theta_n, \theta_1)$ as defined previously, $\nu(\bar{\theta})$ would be $\mu_{PBC}(\bar{\theta})$.

2.5 Topological distinctions between the KL chain and origami chain

Based on the earlier discussion of μ, there always exists, at least, one non-linear ZM passing through a uniform solution in both the open KL and open origami chain because $\mu_{PBC} = \pm 1$ for each uniform solution in both cases. However, to understand whether this non-linear ZM can propagate from one site to another, we need to specialize to a local topological index $\nu_{loc}(\bar{\theta})$ in a single cell (which contains two sites with one constraint) with a two-dimensional space specified by (θ_1, θ_2) and consider h specified by $\theta_2 - \theta_1 = 0$. In this example, every time the non-linear ZM for a single cell (SCZM) crosses this plane at $\bar{\theta}$, we can associate an index $\nu_{loc}(\bar{\theta})$ with the intersection point as defined above [see Fig. 2.2 (b)]. With this in mind, for continuous deformations of the trajectory of the SCZM [see Fig. 2.2 (c)], new uniform configurations can be created or annihilated in pairs of opposite indices, but the total intersection number $I = \sum_i \nu_{loc}(\bar{\theta}_i)$ of the SCZM remains invariant.

The idea of topological protection, defined as it is in terms of an inherently linear concept of the phonon spectrum as highlighted before, can be carried over in a robust way to non-linear mechanical systems as follows: the space of ZMs for one set of constraints can be continuously deformed into the space of ZMs of another set of constraints as long as no ZM intersects with others or itself during deformations. Then it will become clearer why the KL chain and

the origami chain behave so differently despite their superficial similarity after computing the intersection number of a single cell.

First, Fig. 2.6 (a)-(b) show the solutions to Eq. (2.1) for a single cell of the KL chain (consisting of a pair of rotors). Uniform solutions, namely, $\theta_1 = \theta_2$ (there are four) correspond to the points where the non-linear SCZMs cross the plane $\theta_1 - \theta_2 = 0$. We note that, in the non-linear model, the trajectory of a non-linear SCZM passes through either two or all four of these (uniform) solutions depending on the values of L, r, and a. The total intersection number I of a non-linear SCZM satisfies the following condition: when $a < L < 2r - a$, there are two distinct SCZMs with $I = +2$ [blue in Fig. 2.6 (a)] and $I = -2$ [red in Fig. 2.6 (a)]. Thus, each SCZM passes two distinct uniform solutions at least twice and these two uniform solutions are necessarily connected via the trajectory of the SCZM. This case is known as the "spinner" phase of the KL chain, characterized by spinner solitons whose existence is topologically protected. When $2r - a < L < 2r + a$, on the other hand, we have only one SCZM with a total intersection number $I = 0$ [this SCZM passes through all four solutions as in Fig. 2.6 (b)]. This is dubbed the "flipper" phase. In this phase, the trajectory of the SCZM can be continuously deformed by tuning, *e.g.* L, such that all four solutions get annihilated in pairs of opposite intersection numbers exactly at $L = 2r + a$, and no solution exists beyond that.

Next, we consider the origami chain. A single cell in this model is described by Eq. 2.2. The uniform solutions are given by the zeros of $f(\theta, \theta) = (A - B)\sin^2(\theta/2) + \epsilon$, which only exist when $(B - A)/\epsilon > 1$. As shown in Fig. 2.6 (c)-(d), there are two distinct regimes: (*i*) $0 < \epsilon < A - B$, and (*ii*) $A - B < \epsilon < 0$, both of which have two uniform solutions with opposite sign of ν_{loc} and the two

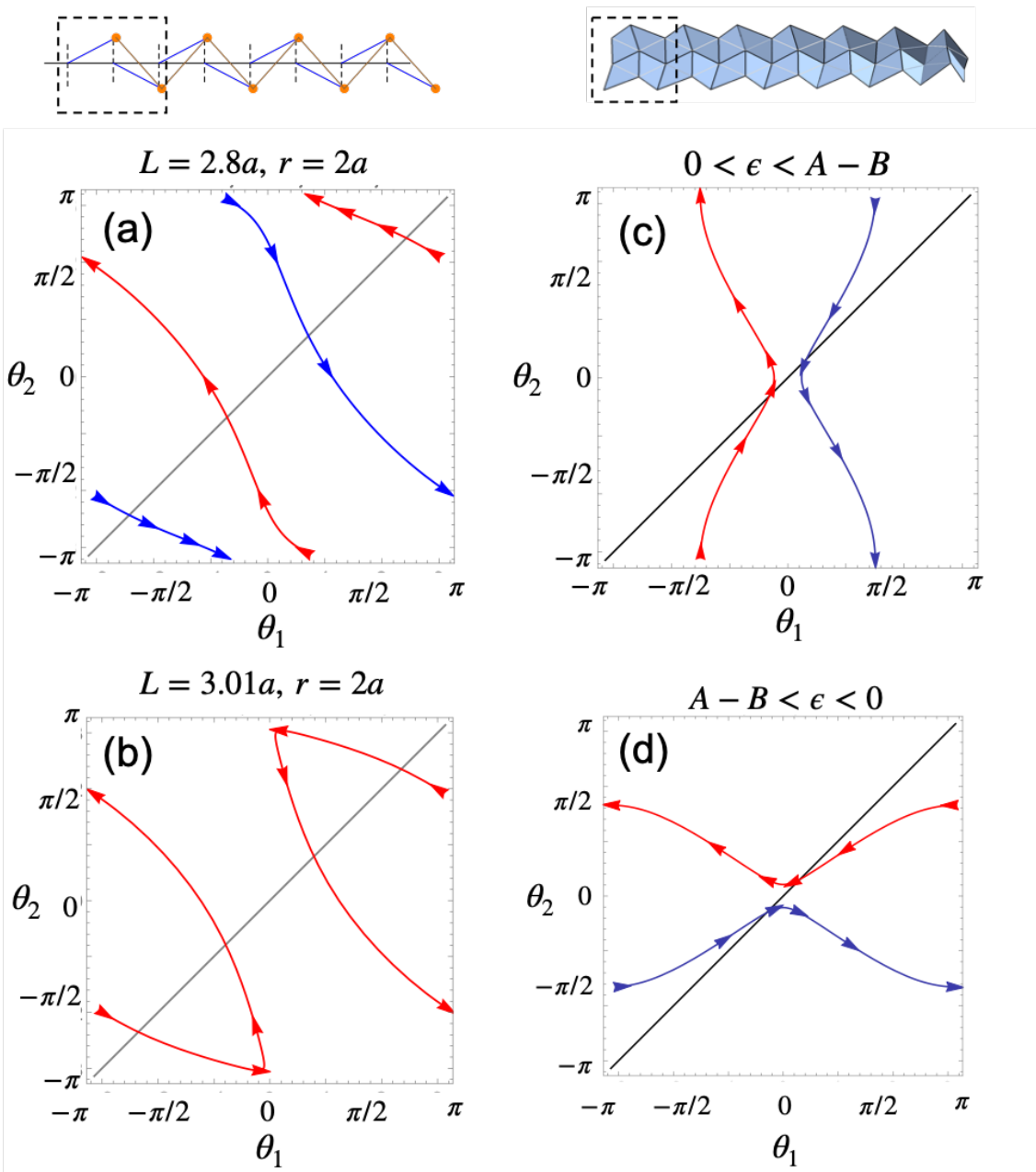

Figure 2.6: (a)-(b) are the spaces of ZMs of a single cell for the KL chain. (c)-(d) are the spaces of ZMs of a single cell for the origami chain. The color is only a label (blue for $I > 0$ and red for $I \leq 0$) and does not have a quantitative meaning.

SCZMs correspond to the total intersection number of $I = +1$ [blue in Fig 2.6 (c) or (d)] or $I = -1$ [red in Fig 2.6 (c) or (d)]. As seen in Fig 2.6 (c)-(d), each SCZM crosses the line defined by $\theta_1 = \theta_2$ at least once. If the system is distorted, it is possible to cross this line multiple times, but the total intersection number remains unchanged. We conclude that the existence of uniform solutions is, indeed, topologically protected. To eliminate them, it is necessary to distort the system through a topological phase transition by joining the trajectories of the two SCZMs. Ultimately, this requires tuning the system through one of the two situations: $\epsilon = 0$ or $A - B + \epsilon = 0$.

2.6 Topologically protected solitons

It is clear that when a SCZM has a total intersection number $|I| \geq 2$, it must have at least two uniform solutions joined by a smooth trajectory. However, this does not immediately extend to a larger chain of n ($n > 2$) unless the following (sufficient) condition P is met: for a given SCZM, either the map from θ_i to θ_{i+1} $\forall i$ or the reverse map is injective.

Lets take the spinner for an example and denote a ZM for the n-site chain, which contains n rotors and $n-1$ springs, by C_n. In this notation, the black curve on the bottom plane in Fig. 2.7(a) is C_2 and the red curve is C_3. Since, in this case, we have $|I| = 2$, the projection of C_3 onto a constant θ_3 plane always yields C_2 (it, in fact, extends to $|I| \geq 2$). This statement can be understood in the following way: we are looking for a solution for $f(\theta_2, \theta_3) = 0$ provided $f(\theta_1, \theta_2) = 0$. A sufficient condition for this is that the solution of $f(\theta_2, \theta_3) = 0$ on the $\theta_2 - \theta_3$ plane wraps around θ_2 at least once (this holds when $|I| \geq 2$) guaranteeing a θ_3 for a

given θ_2 that also satisfies $f(\theta_1, \theta_2) = 0$. If the above condition is met, there must exist at least one θ_3 for a given (θ_1, θ_2) that satisfies both the constraints. Thus, for each point on the black curve C_2, we can always find at least one point on the red curve C_3 projected onto it.

We can now prove that the two uniform solutions are connected by C_3 which we have shown to hold for C_2 previously. This we prove by contradiction. If we assume that there are two disconnected parts of C_3 while C_2 is connected, there must exist two points that have the same θ_1 and θ_2 but distinct θ_3. However, this contradicts the fact that the map from θ_3 to θ_2 is injective, and thus, C_3 must be connected. The argument can easily be generalized to C_n for $n > 3$. Thus, we conclude that there must exist at least two uniform solutions joined by a ZM in a n-site chain. This ZM is a soliton (for the non-linear model) that is topologically protected and robust to disorders as long as each SCZM corresponds to a total intersection number $|I| \geq 2$ and satisfies the condition P mentioned above. We emphasize, a soliton of this kind exists even in a disordered ($a < L_i < 2r - a$, L_i chosen randomly) KL chain which has the total intersection number $I = \pm 2$ in each cell as shown in Fig.2.7 (b).

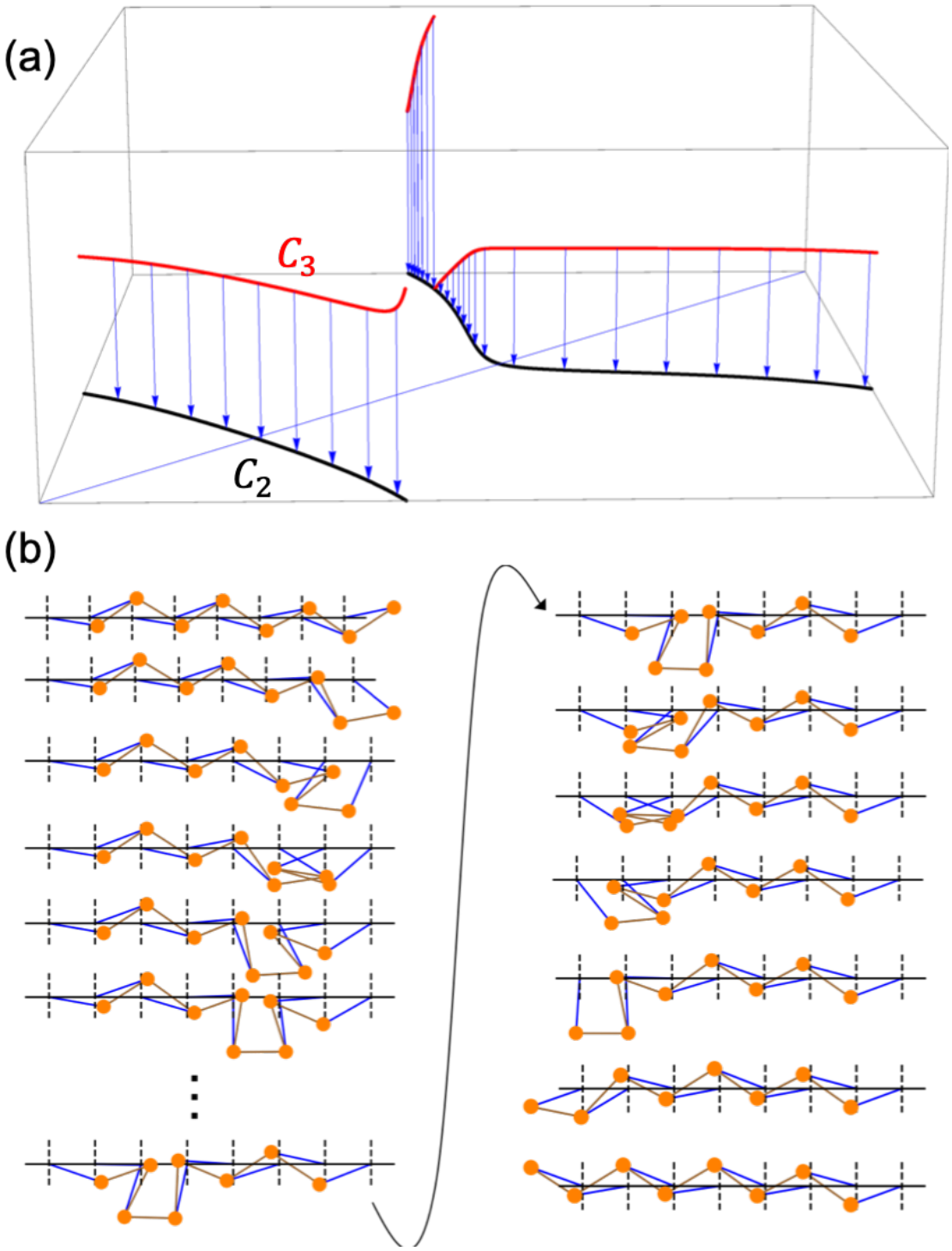

Figure 2.7: (a) The ZM for the $n = 2, 3$ KL chain (the spinner case). The black curve C_2 on the bottom plane is a single loop on two-dimensional torus, and the red curve C_3 is a single loop on three-dimensional torus. (b) A soliton on the disordered KL chain.

CHAPTER 3

TOPOLOGY SHARED BETWEEN CLASSICAL METAMATERIALS AND INTERACTING SUPERCONDUCTORS

3.1 Introduction

In this Chapter, we study the topology shared between classical constraint problems and interacting metals or superconductors. Firstly, we define Q_{net} for an isostatic mechanical system as the sum over all $\mu(p)$ and find that its magnitude is the minimum number of zero-energy configurations. Secondly, we write a supersymmetric Hamiltonian that has a well-defined Witten index W for a generic set of nonlinear constraint functions. We show that this Hamiltonian can describe a superconductor interacting with phonons, including any anharomonicity they may have. $|W|$ for this Hamiltonian also turns out to be the minimum number of zero-energy states. Finally, we make a topological connection between these two systems by showing that $Q_{net} = W$ for a set of nonlinear and non-symmetric constraints under very general conditions (specified below) as shown in Fig.3.1.

3.2 zero-energy configurations in an isostatic mechanical system

Firstly, we consider an isostatic mechanical system described by a Hamiltonian

$$H_{iso} = \sum_i \left(\frac{p_i^2}{2} + \frac{f_i^2}{2} \right) \tag{3.1}$$

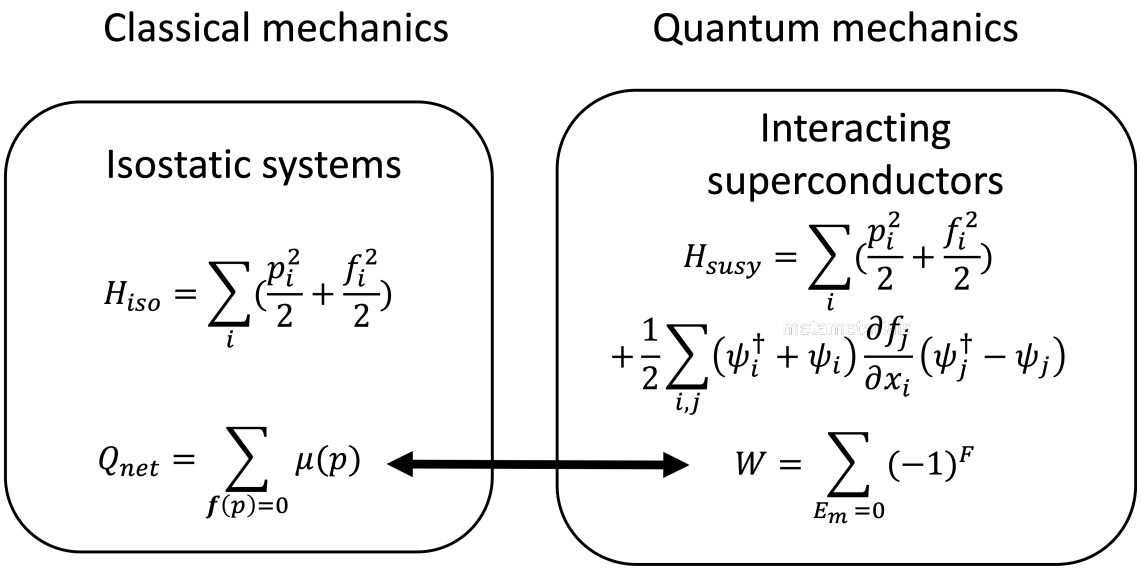

Figure 3.1: Topology shared between classical metamaterials and interacting superconductors via the topological index Q_{net} and the Witten index W.

which has zero-energy configurations satisfying a set of constraints $f_1 = 0, f_2 = 0, ..., f_n = 0$ where f_i is a function of $x_1, x_2, ..., x_n$ such as those that arise in *e.g.* springs, linkages, and origami. When f_i is a linear function, H_{iso} describes n simple harmonic oscillators. Following the definition in Ref.[36], a topological index $\mu(p)$ at a zero-energy configuration p can be calculated by an integration of a differential form

$$\mu(p) = \frac{1}{s_{n-1}(n-1)!} \oint_{S_p} \frac{f_{i_1} df_{i_2} \wedge ... \wedge df_{i_n} \epsilon^{i_1, i_2, ..., i_n}}{(f_1^2 + f_2^2 + ... + f_n^2)^{\frac{n}{2}}} \tag{3.2}$$

where S_p is an $(n-1)$-dimensional sphere in the configuration space which encloses the point p, s_{n-1} is the surface area of a unit $(n-1)$-dimensional sphere. When the Jacobian $\partial f_i / \partial x_j$ at p is full rank, $\mu(p) = \text{sgn}[\det(\partial f_i / \partial x_j)]$.

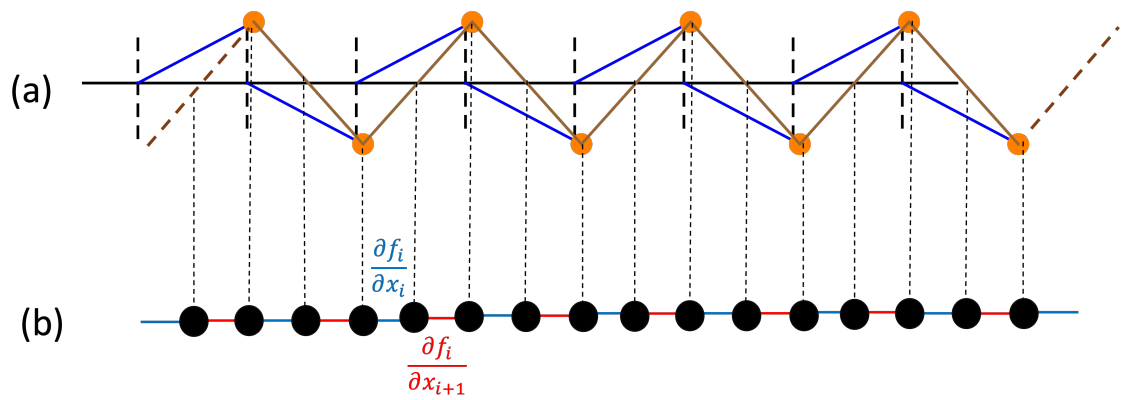

Figure 3.2: (a)The Kane-Lubensky chain with periodic boundary conditions. (b)The Kitaev chain. For each constraint (spring) or degree of freedom (ball) of the KL chain, we put a Majorana fermion that hops to its nearest neighbors with the parameters $\frac{\partial f_i}{\partial x_i}$ and $\frac{\partial f_i}{\partial x_{i+1}}$.

Here we further define another topological index Q_{net} as the sum over $\mu(p)$ of all zero-energy configurations.

$$Q_{net} = \sum_{\mathbf{f}(p)=\mathbf{0}} \mu(p) = \sum_{\mathbf{f}(p)=\mathbf{0}} \mathrm{sgn}\left[\det\left(\frac{\partial f_i}{\partial x_j}\right)\Big|_p\right] \tag{3.3}$$

which counts the difference between the number of zero-energy configurations with $\mu = +1$ and $\mu = -1$. Because μ can only be created or annihilated in pairs, $|Q_{net}|$ is the minimum number of zero-energy configurations that always exist under finite local deformations.

Let's consider an example, the Kane-Lubensky(KL) chain[26] with periodic boundary conditions as shown in Fig.3.2(a). This example is an anharmonic-oscillator system that naturally exists in nonlinear mechanical systems. There are many zero-energy configurations, but the sum over $\mu(p)$ is zero. Therefore, $Q_{net} = 0$ suggests that all zero-energy configurations can be annihilated by deforming constraints. For example, if we choose one of the spring lengths larger than twice the length of rotors plus the distance between the two nearest pivot

points, then there will be no zero-energy configuration in the KL chain.

3.3 zero-energy states in a supersymmetric quantum system

Secondly, we consider a supersymmetric quantum system similar to Ref.[31] described by a supersymmetric Hamiltonian

$$H_{susy} = \{Q, Q\} \tag{3.4}$$

where $Q = \frac{1}{2}\sum_i[\psi_i(p_i + if_i) + \psi_i^\dagger(p_i - if_i)]$ and ψ_i is a fermion operator. In the Euclidean quantum theory, we can replace p_i by $i\frac{\partial}{\partial x_i}$. Then H_{susy} can be rewritten as

$$H_{susy} = \sum_i \left(\frac{p_i^2}{2} + \frac{f_i^2}{2}\right) + \frac{1}{2}\sum_{i,j}(\psi_i^\dagger + \psi_i)\frac{\partial f_j}{\partial x_i}(\psi_j^\dagger - \psi_j) \tag{3.5}$$

which can also be written in terms of Majorana fermion operators $\gamma_{a,i} = \psi_i^\dagger + \psi_i$ and $\gamma_{b,i} = -i(\psi_i^\dagger - \psi_i)$ as

$$H_{susy} = \sum_i \left(\frac{p_i^2}{2} + \frac{f_i^2}{2}\right) + \frac{i}{2}\sum_{i,j}\gamma_{a,i}\frac{\partial f_j}{\partial x_i}\gamma_{b,j} \tag{3.6}$$

Here we can see that H_{susy} and H_{iso} only differ by additional terms described by the interacting between fermions and bosons. When f_i is a linear function, H_{susy} is simply two independent systems, n simple harmonic oscillators and a non-interacting Majorana fermion system. In general, a constraint function f_i is nonlinear. We can get some insights by expanding f_i around a zero-energy configuration point to second highest order terms ($f_i = \sum_j a_{i,j}x_j + \sum_{j,k} b_{i,j,k}x_jx_k$). By doing so, we will get

$$\begin{aligned}\tilde{H}_{susy} = &\sum_i \left(\frac{p_i^2}{2} + \frac{(\sum_j a_{i,j}x_j + \sum_{j,k} b_{j,i,k}x_jx_k)^2}{2}\right) \\ &+\frac{i}{2}\sum_{i,j}\gamma_{a,i}a_{j,i}\gamma_{b,j} + \frac{i}{2}\sum_{i,j,k}\gamma_{a,i}b_{j,i,k}x_k\gamma_{b,j}\end{aligned} \tag{3.7}$$

The first and second terms describe anharmonic phonons and a non-interacting Majorana fermion system, respectively, and the last term is the coupling between Majorana fermions and anharmonic phonons.

In the supersymmetric quantum system, nonzero-energy states are always paired with opposite fermion parities. Thus, we can calculate the Witten index

$$W = \sum_{E_m=0} (-1)^F \tag{3.8}$$

where E_m is an eigenenergy of H_{susy} and $(-1)^F$ is the fermion parity operator. Because the Witten index tells us the difference between the number of even and odd fermion parity zero-energy states, its magnitude $|W|$ is the minimum number of zero-energy states that always exist under finite local deformations.

In a symmetric case where $\partial f_i/\partial x_j$ is a symmetric matrix (with respect to the matrix indices i, j). We can find a function V such that $f_i = \frac{\partial V}{\partial x_i}$. H_{susy} is reduced to

$$H_{susy}^{sym} = \sum_i \left(\frac{p_i^2}{2} + \frac{f_i^2}{2} \right) + \frac{1}{2} \sum_{i,j} \frac{\partial f_j}{\partial x_i} (\psi_i \psi_j^\dagger - \psi_i^\dagger \psi_j) \tag{3.9}$$

whose path integral can be viewed as a Witten-type supersymmetric topological quantum field theory[5]. Similar to Eq.3.6, but now it describes fermions (electrons in a metal) coupling to anharmonic phonons. In this case, it has been shown that $W = \sum_{\frac{\partial V}{\partial x_i}=0} \mathrm{sgn}[\det(\frac{\partial^2 V}{\partial x_i \partial x_j}\Big|_p)]$ which is exactly the same as Q_{net}.

Given those similar physical interpretations of Q_{net} and W plus the result of symmetric cases, it seems that Q_{net} might still be related to W in a certain way even for non-symmetric cases.

3.4 Derivation of symmetric cases

We use an approach similar to the Faddeev-Popov gauge-fixing procedure[18]. First, we generalize Q_{net} to a family of sets of constraints $\mathbf{f}(\mathbf{x}) + \mathbf{w} = \mathbf{0}$ where $\mathbf{w}$ is some constant vector. The net topological index $Q_{net}(\mathbf{w})$ depending on $\mathbf{w}$ is written as

$$\begin{aligned} Q_{net}(\mathbf{w}) &= \sum_{\mathbf{f}(p_{\mathbf{w}})+\mathbf{w}=\mathbf{0}} \mu(p_{\mathbf{w}}) = \sum_{\mathbf{f}(p_{\mathbf{w}})+\mathbf{w}=\mathbf{0}} \left[\det\left(\frac{\partial f_i}{\partial x_j}\right)\right] \\ &= \sum_{\mathbf{f}(p_{\mathbf{w}})+\mathbf{w}=\mathbf{0}} \left|\det\left(\frac{\partial f_i}{\partial x_j}\right)\right|^{-1} \det\left(\frac{\partial f_i}{\partial x_j}\right) \\ &= \int d\mathbf{x} \prod_{i=1}^{n} \delta(f_i + w_i) \det\left(\frac{\partial f_i}{\partial x_j}\right) \end{aligned} \tag{3.10}$$

In the first line, we assume that all solution points are non-degenerate. In the last line, we replace the sum of Jacobian by an integration over delta functions. $Q_{net}(\mathbf{w})$ can also be calculated by drawing a lager sphere that encloses all solution points and calculating the integration of a differential form in Eq.3.2. Thus, $Q_{net}(\mathbf{w})$ only depends on the asymptotic behavior of $\mathbf{f}(\mathbf{x}) + \mathbf{w}$ on the boundaries of $\mathbf{x}$ ($||\mathbf{x}|| \to \infty$).

In the next step, we compute the average of the net topological indices over this family of sets of constraints by using the the weight $\prod_{i=1}^{n} e^{-\frac{w_i^2}{2}}$. Then the average of the net topological indices is

$$Q_{ave} = \int \prod_{i=1}^{n} \frac{dw_i}{\sqrt{2\pi}} e^{-\frac{w_i^2}{2}} \left[\int d\mathbf{x} \prod_{i=1}^{n} \delta(f_i + w_i) \det\left(\frac{\partial f_i}{\partial x_j}\right)\right] \tag{3.11}$$

Under the condition that $||\mathbf{f}(\mathbf{x})|| \to \infty$ on the boundaries of $\mathbf{x}$, the asymptotic behavior of $\mathbf{f}(\mathbf{x})$ is unchanged under any finite local deformations (e.g., the deformation $\tilde{\mathbf{f}} = \mathbf{f}+\mathbf{w}$). Therefore, when $||\mathbf{f}(\mathbf{x})|| \to \infty$ as $||\mathbf{x}|| \to \infty$, $Q_{net}(\mathbf{w})$ is independent of $\mathbf{w}$ and Q_{ave} is equal to the original Q_{net} in Eq.3.3

Then after integrating over w_i and writing $\det(\frac{\partial f_i}{\partial x_j})$ as an integral over complex Grassmann numbers, Q_{ave} can be rewritten as

$$Q_{ave} = \int \frac{\mathbf{dx d\Psi d\bar{\Psi}}}{(i\sqrt{2\pi})^n} \exp\left[-\sum_{i=1}^{n} \frac{1}{2} f_i^2 \right. \\ \left. -i \sum_{i=1}^{n} \sum_{j=1}^{n} (\bar{\Psi}_i \frac{\partial f_i}{\partial x_j} \Psi_j)\right] \tag{3.12}$$

where $\bar{\Psi}_i$ and Ψ_i are complex Grassmann numbers. We can see that Q_{ave} plays a similar role as the partition function.

To promote the classical theory to a quantum theory, we consider another similar constrained problem by replacing $\mathbf{f}(\mathbf{x})$ by $\frac{d\mathbf{x}}{d\tau} + \mathbf{f}(\mathbf{x})$ where τ is the imaginary time. Following the same approach, the new topological index can be written as

$$W = \int \mathbf{DxD\Psi D\bar{\Psi}} \exp\left(-\oint d\tau \left[\sum_{i=1}^{n} \frac{1}{2}\left(\frac{dx_i}{d\tau} + f_i\right)^2 \right.\right. \\ \left.\left. +i \sum_{i=1}^{n} \sum_{j=1}^{n} \bar{\Psi}_i \left(\delta_{i,j} \frac{d}{d\tau} + \frac{\partial f_i}{\partial x_j}\right) \Psi_j \right]\right), \tag{3.13}$$

All constants are absorbed in $\mathbf{DxD\Psi D\bar{\Psi}}$. Here we emphasize that W is not a regular partition function because it requires periodic boundary conditions along the imaginary time circle for both bosons and fermions.

When $\partial f_i / \partial x_j$ is symmetric, namely when $f_i = \frac{\partial V}{\partial x_i}$, the path integral Eq. 3.13 describes a supersymmetric quantum mechanics model with BRST symmetry [5]. In the following, we review some key aspects of this supersymmetric quantum mechanics model with BRST symmetry. The discussion below follows Ref. tft. We assume $f_i = \frac{\partial V}{\partial x_i}$ from now on.

It can be shown that only the configurations with $\frac{d\mathbf{x}}{d\tau} + \mathbf{f}(\mathbf{x}) = \mathbf{0}$ contributes to the path integral. Naively, there can be two types of solutions, dynamical

solutions ($\frac{d\mathbf{x}}{d\tau} \neq 0$) and stationary solutions ($\frac{d\mathbf{x}}{d\tau} = 0$). First, we notice that $\frac{d\mathbf{x}}{d\tau}+\mathbf{f}(\mathbf{x}) = \mathbf{0}$ implies that

$$\begin{aligned} 0 &= \oint d\tau \sum_{i=1}^{n} \left(\frac{dx_i}{d\tau} + f_i\right)^2 \\ &= \oint d\tau \sum_{i=1}^{n} \left(\frac{dx_i}{d\tau}\right)^2 + \oint d\tau \sum_{i=1}^{n} f_i^2 + 2\oint d\tau \sum_{i=1}^{n} \frac{dx_i}{d\tau} f_i \end{aligned} \tag{3.14}$$

Notice that $f_i = \frac{\partial V}{\partial x_i}$. the last term becomes $2\oint d\tau \frac{dV}{d\tau}$ which is zero due to the periodic boundary condition. Hence, $\frac{dx_i}{d\tau} = 0$ and $f_i = 0$, namely there are only stationary solutions. For a stationary solution, the system stays at rest in a solution point p. The fermion contribution to the topological index W for each stationary solution can be calculated by transforming the field to Fourier series. The sign only comes from the zero frequency term because nonzero frequency terms all comes in complex conjugate pairs and the product of a complex conjugate pair is always positive. Note the fermion has periodic boundary condition along the time direction, which permits zero-frequency modes. Therefore, the total contribution from a stationary solution is the same as the topological index $\mu(p)$ defined in Eq. 3.2. As a result, W is equal to Q_{ave} when $f_i = \frac{\partial V}{\partial x_i}$.

The BRST formulation can be recovered by adding auxiliary field $\mathbf{B}$. We rewrite W as

$$\begin{aligned} W = \int \mathbf{DxD\Psi D\bar{\Psi}DB} \exp\Bigg(-\oint \Bigg[& d\tau \sum_{i=1}^{n} \frac{1}{2} B_i^2 \\ & -i \sum_{i=1}^{n} B_i \left(\frac{dx_i}{d\tau} + f_i\right) + i \sum_{i=1}^{n} \sum_{j=1}^{n} \bar{\Psi}_i \left(\delta_{i,j} \frac{d}{d\tau} + \frac{\partial f_i}{\partial x_j}\right) \Psi_j \Bigg]\Bigg) \end{aligned} \tag{3.15}$$

The supersymmetry relation is defined via a nilpotent generator $Q = \sum_{i=1}^{n} \Psi_i B_i$. The transformation rules are

$$\{Q, x_i\} = \Psi_i \quad \{Q, B_i\} = 0 \quad \{Q, \Psi_i\} = 0 \quad \{Q, \bar{\Psi}_i\} = B_i \tag{3.16}$$

The Hamiltonian of the BRST-symmetric model can then be written as

$$\begin{aligned} H_{BRST} &= \frac{1}{2}\sum_{i=1}^{n} p_i^2 + \frac{1}{2}\sum_{i=1}^{n} f_i^2 \\ &+ \frac{1}{2}\sum_{i=1}^{n}\sum_{j=1}^{n} \frac{\partial f_j}{\partial x_i}(\Psi_i\Psi_j^\dagger - \Psi_i^\dagger\Psi_j) \end{aligned} \tag{3.17}$$

In the Hamiltonian formalism, the topological index W can be calculated by taking the trace or summing over eigenstates. For each fermion, there will an extra π phase as a manifestation of the periodic boundary condition along the time circle in the path integral. As a result, the topological index W is

$$W = \sum_m (-1)^{n_F} e^{-\beta E_m} = \sum_{E_m=0} (-1)^{n_F} \tag{3.18}$$

which is indeed the Witten index.

3.4.1 linear functions

To find their connections, we first look at linear-constraint cases to get some insights. Assume that the constraints are $\mathbf{Rx} = \mathbf{0}$. Then the corresponding H_{susy} is

$$H_{susy}^L = \sum_i \frac{p_i^2}{2} + \sum_{i,j,k} \frac{x_i \mathbf{R}_{i,j}^T \mathbf{R}_{j,k} x_k}{2} + \frac{i}{2}\sum_{i,j} \gamma_{a,i}\mathbf{R}_{i,j}\gamma_{b,j} \tag{3.19}$$

By performing the singular value decomposition to obtain $\mathbf{R} = \mathbf{U\Sigma V^T}$, and rotating $x_i' = \mathbf{V}_{i,j}x_j$, $\gamma_{a,i}' = \mathbf{U}_{i,j}^T\gamma_{a,j}$ and $\gamma_{b,i}' = \mathbf{V}_{i,j}\gamma_{b,j}$, we get

$$H_{susy}^L = \sum_i \left[\frac{(p_i')^2}{2} + \frac{(\lambda_i x_i')^2}{2} + \frac{i\lambda_i}{2}\gamma_{a,i}'\gamma_{b,j}'\right] \tag{3.20}$$

where $\lambda_i = \mathbf{\Sigma}_{i,i}$ is the singular value of $\mathbf{R}$. H_{susy}^L contains two non-interacting systems. The first one described by the first two terms in Eq.3.20 is n-simple-harmonic-oscillators with ground state energy equal to $\sum_i \frac{\lambda_i}{2}$. The last term is a

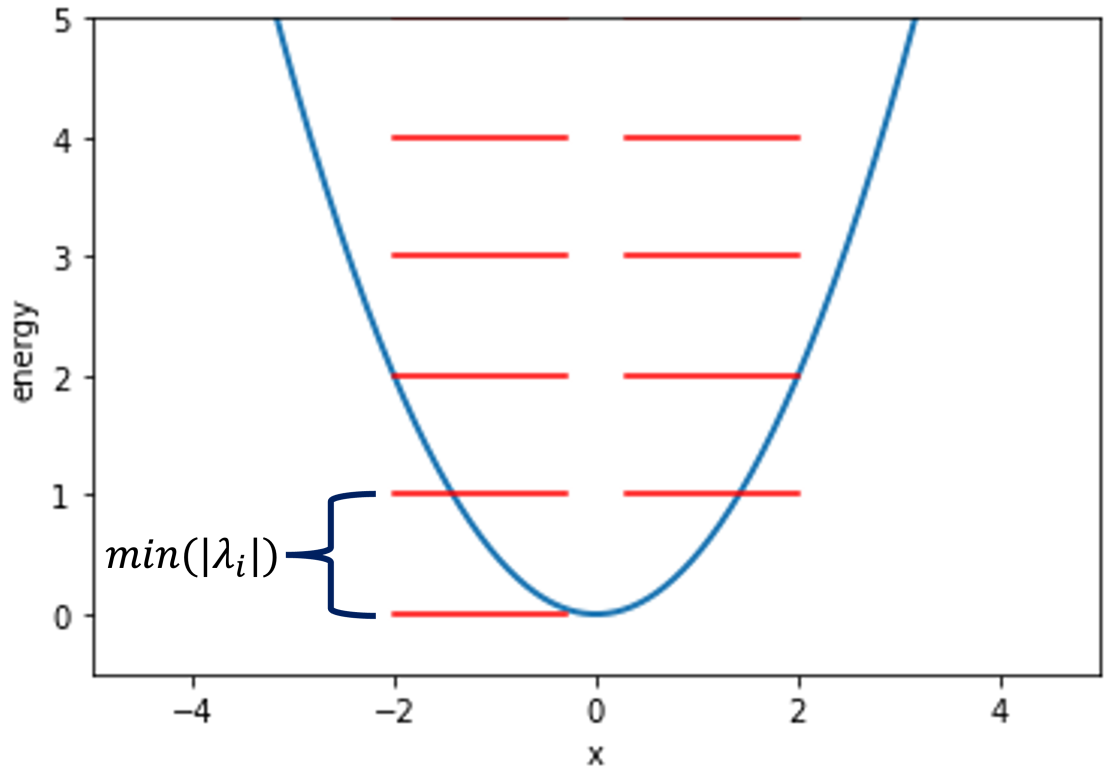

Figure 3.3: Spectrum of H^L_{susy} with a single linear constraint function $f(x) = x$.

Majorana fermion system that has energy $\sum_i \pm\frac{\lambda_i}{2}$ in different Majorana fermion sectors. The ground state energy of the Majorana fermion system is $-\sum_i \frac{\lambda_i}{2}$ and its fermion parity equates to the Pfaffian of the Hamiltonian in the Majorana basis which is simply [det($\mathbf{R}$)][29]. Combining the two systems, the lowest energy state of H^L_{susy} has exact zero energy with a gap min($\{\lambda_i\}$) as shown in Fig.3.3. Because H^L_{susy} only has one single zero-energy state, W = [det($\mathbf{R}$)] which is equal to Q_{net}.

For example, in the periodic KL chain, if we linearize the constraints at a uniform solution point[26, 36], $\frac{\partial f_i}{\partial x_i}$ and $\frac{\partial f_i}{\partial x_{i+1}}$ would be constants. In the fermionic part, we will get the Kitaev chain as shown in Fig.3.2(b) which is a p-wave

superconductor[29].

3.4.2 nonlinear functions

Now let's go back to generic nonlinear-constraint cases. Here we specify three general conditions for the constraint functions $\mathbf{f}$ that we are interested in. (1)$\frac{\partial f_i}{\partial x_j}$ is continuous everywhere. This makes sure that potential energy is continuous in the whole space.(2)$||\mathbf{f}|| \to \infty$ as $||\mathbf{x}|| \to \infty$. This guarantees that wavefunctions are confined in finite regions. (3)The Jacobian $\frac{\partial f_i}{\partial x_j}$ is full rank at all solution points $\mathbf{f} = \mathbf{0}$.

To find W, we rescale the constraint functions f_i by a positive constant g and rewrite the Hamiltonian as

$$H_{susy}(g) = \sum_i \left(\frac{p_i^2}{2} + \frac{g^2 f_i^2}{2} \right) + \frac{ig}{2} \sum_{i,j} \gamma_{a,i} \frac{\partial f_j}{\partial x_i} \gamma_{b,j} \tag{3.21}$$

and first look at large g cases.

When g is very large, the potential energy is dominated by $\frac{g^2 f_i^2}{2}$ term. Thus, we can focus on those points where $\mathbf{f} = \mathbf{0}$ to study low-energy states. Assume that we have N points satisfying $\mathbf{f} = \mathbf{0}$ labeled as $z_{\alpha=1,2,\ldots,N}$. At each z_α, we take the linear order of f_i to obtain a Hamiltonian which locally looks like a potential well described by Eq.3.20. The structure of the low energy states is, therefore, similar to a linear-constraint case in which a system has a zero-energy state gapped by $\min(\{g\lambda_{\alpha,i}\})$ where $\lambda_{\alpha,i}$ is a singular value of the matrix $\frac{\partial f_i}{\partial x_j}$ at point z_α.

Two types of perturbations can lift or lower energy. Firstly, we consider the overlap between two wave functions localized at different z_α. The overlap is estimated as $\sim e^{-\epsilon g}$ where ϵ is some positive constant that depends on the

distance between two wells. Thus, the energy will only be increased or lowered by an amount of order of $e^{-\epsilon g}$.

The second perturbation is the higher order corrections terms around each well. We expand f_i at each z_α as $f_i = \sum_j a_{i,j,\alpha} x_j + \sum_{j,k} b_{i,j,k,\alpha} x_j x_k + ...$ Then we rescale x_i with a prefactor $g^{-1/2}$, namely, $x_i \to g^{-1/2} x_i$ and $p_i \to g^{1/2} p_i$. We get $g f_i \to g^{1/2} \sum_j a_{i,j,\alpha} x_j + \sum_{j,k} b_{i,j,k,\alpha} x_j x_k + ...$, and $g \frac{\partial f_j}{\partial x_i} \to g a_{j,i,\alpha} + g^{1/2} \sum_j b_{j,i,k,\alpha} x_k + ...$ As a result, we can rewrite the Hamiltonian around z_α as

$$\begin{aligned}\tilde{H}_{susy}(g) = g\Bigg[\sum_i \left(\frac{p_i^2}{2} + \frac{(\sum_j a_{i,j,\alpha} x_j)^2}{2}\right) \\ + \frac{i}{2}\sum_{i,j} \gamma_{a,i} a_{j,i,\alpha} \gamma_{b,j}\Bigg] \\ + g^{1/2}\Bigg[\sum_{i,j,k,l} \frac{a_{i,j,\alpha} b_{i,k,l,\alpha} x_j x_k x_l}{2} \\ + \frac{i}{2}\sum_{i,j,k} \gamma_{a,i} b_{j,i,k,\alpha} x_k \gamma_{b,j}\Bigg] + O(1)\end{aligned} \tag{3.22}$$

Therefore, the energy lifted or lowered due to the higher order corrections terms is of the order of $g^{1/2}$. As a result, if we choose large enough g, we can always guarantee that an energy window from $-\frac{1}{2}\min(\{g\lambda_{\alpha,i}\})$ to $\frac{1}{2}\min(\{g\lambda_{\alpha,i}\})$ only contains the N states that have almost or exact zero-energy as shown in Fig.3.4. These N states have exactly zero energy if we only consider the first two lines in $\tilde{H}_{susy}(g)$.

Then we can calculate the Witten index by only focusing on these N states because all other nonzero energy states are paired, and thus contributes zero to the Witten index. From the result of linear-constraint cases, the fermion parity of the lowest energy state at z_α is $[\det(\frac{\partial f_i}{\partial x_j})]$. As a result, $W = \sum_\alpha [\det(\frac{\partial f_i}{\partial x_j}|_{z_\alpha})]$ which is exactly equal to Q_{net}.

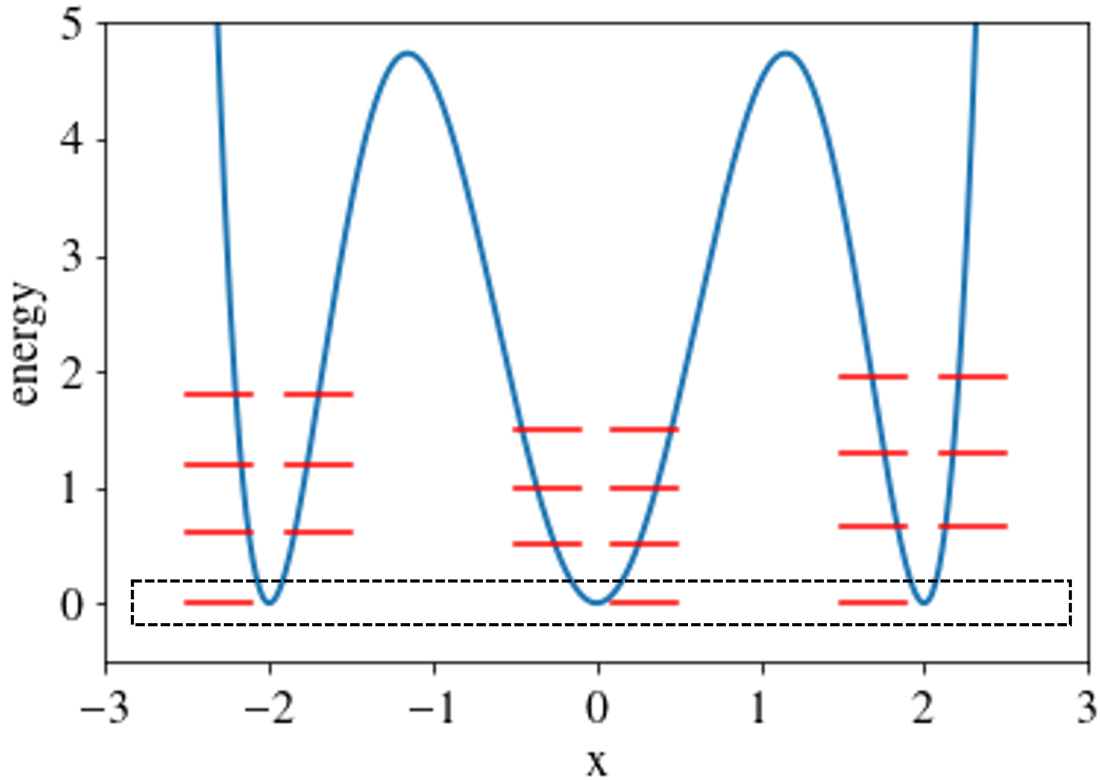

Figure 3.4: Low-energy spectrum of $H_{susy}(g)$ with nonlinear constraint functions in the large g limit.

In the next step, we are going to show that the Witten index W is independent of g, namely, $\frac{dW}{dg} = 0$. First, we write

$$\begin{aligned} W = &\sum_{m_1} \langle B_{m_1} | e^{-\beta H_{susy}(g)} | B_{m_1} \rangle \\ &- \sum_{m_2} \langle F_{m_2} | e^{-\beta H_{susy}(g)} | F_{m_2} \rangle \end{aligned} \tag{3.23}$$

where $|B_{m_1}\rangle$ is an even fermion parity state and $|F_{m_2}\rangle$ is an odd fermion parity state. Then we can calculate

$$\begin{aligned} \frac{dW}{dg} = &-\beta \sum_{m_1} \langle B_{m_1} | \frac{dH_{susy}(g)}{dg} e^{-\beta H_{susy}(g)} | B_{m_1} \rangle \\ &+\beta \sum_{m_2} \langle F_{m_2} | \frac{dH_{susy}(g)}{dg} e^{-\beta H_{susy}(g)} | F_{m_2} \rangle \end{aligned} \tag{3.24}$$

The change of the Witten index due to the change of states is zero because the Witten index is independent of basis. Mathematically, we can write

$$\begin{aligned}\frac{d\langle m|}{dg}e^{-\beta H_{susy}(g)}|m\rangle + \langle m|e^{-\beta H_{susy}(g)}\frac{d|m\rangle}{dg} \\ = e^{-\beta E_m}\frac{d\langle m|m\rangle}{dg} = 0\end{aligned} \tag{3.25}$$

Then use the fact that $\frac{dH_{susy}(g)}{dg} = 2\{\frac{dQ}{dg}, Q\}$ where $Q = \sum_i[(\psi_i(p_i + igf_i) + \psi_i^\dagger(p_i - igf_i)]$, we get

$$\begin{aligned}\frac{dW}{dg} = -2\beta\sum_{m_1}\langle B_{m_1}|\left\{\frac{dQ}{dg}, Q\right\}e^{-\beta H_{susy}(g)}|B_{m_1}\rangle \\ +2\beta\sum_{m_2}\langle F_{m_2}|\left\{\frac{dQ}{dg}, Q\right\}e^{-\beta H_{susy}(g)}|F_{m_2}\rangle\end{aligned} \tag{3.26}$$

This expression only receives contribution from states $|B_{m_1}\rangle$ and $|F_{m_2}\rangle$ with finite energies, which always come in pairs. A pair of states $|B_m\rangle$ and $|F_m\rangle$ are related by $\sqrt{\frac{E_m}{2}}|F_m\rangle = Q|B_m\rangle$ and $\sqrt{\frac{E_m}{2}}|B_m\rangle = Q|F_m\rangle$ where $E_m \neq 0$ is the eigenenergy of this pair of states. A unpaired state must be annihilated by Q and, hence, has zero energy. Thus, we have

$$\begin{aligned}\frac{dW}{dg} = &-\sqrt{2E_m}\beta\sum_m\langle F_m|\frac{dQ(g)}{dg}e^{-\beta H_{susy}(g)}|B_m\rangle \\ &-\sqrt{2E_m}\beta\sum_m\langle B_m|\frac{dQ(g)}{dg}e^{-\beta H_{susy}(g)}|F_m\rangle \\ &+\sqrt{2E_m}\beta\sum_m\langle B_m|\frac{dQ(g)}{dg}e^{-\beta H_{susy}(g)}|F_m\rangle \\ &+\sqrt{2E_m}\beta\sum_m\langle F_m|\frac{dQ(g)}{dg}e^{-\beta H_{susy}(g)}|B_m\rangle\end{aligned} \tag{3.27}$$

which is zero as long as $\frac{dQ(g)}{dg}$ is a regular function. In our case, $\frac{dQ(g)}{dg} = i\sum_i(\psi_i - \psi_i^\dagger)f_i$, and thus $\frac{dW}{dg} = 0$. Now, we have shown that for any constraint functions $\mathbf{f}$ that satisfy the three conditions, $Q_{net} = W$.

Conceptually, we start with a purely classical system described by Eq. 3.1 which has some zero-energy classical configurations characterized by the topological index Q_{net}. Now, imaging "turning on" quantum mechanics by treating

Eq. 3.1 as a quantum mechanical Hamiltonian. Generically, due to the Heisenberg uncertain principle, we do not expect any zero-energy eigenstates for Eq. 3.1 anymore. However, we can "recover" the zero-energy states by further including extra Majorana fermions interacting with the existing bosons and considering the Hamiltonian Eq. 3.6. As a result, there will be a few zero-energy states that protected by supersymmetry. The number of these zero-energy states is characterized by the Witten index W. Physically, we can make an analogy between the two topological numbers Q_{net} and W in the following way:

$$\begin{aligned} &\text{minimum \# of zero-energy configurations} \\ &= \text{minimum \# of zero-energy states} \end{aligned} \tag{3.28}$$

In the example of the KL chain, there is no supersymmetry-protected zero-energy state in the quantum system described Eq. 3.6 analogy to the KL chain because $W = Q_{net} = 0$.

3.5 conclusion

We show metamaterials can be used to study the topology of interacting quantum materials with the aid of supersymmetry. Specifically, we map a classical constrained problem to Bogoliubov quasiparticles of a superfluid/superconductor coupled to a boson such as a phonon. Hence, classical metamaterials can be used to study some aspects of the most challenging problems in quantum condensed matter physics.

Necessarily, the connection between classical metamaterials and quantum materials requires fine tuning. The Debye temperatures in real materials range from $O(10)$ to $O(10^3)$ K could match the order of the hopping strength of elec-

trons in some materials. If the phonon band structure is similar to the electron band structure, and we fine-tune the anharmonicity of the phonon to match the coupling between Majorana fermions and phonon, it is possible to realize such a supersymmeric quantum system that shares the same topology of a classical mechanical systems. Perhaps a search through a database of all materials may find some that approximately meet these conditions. But even if not, the connection may still prove useful for the fine tuned problems may provide insight into the general behavior of interacting metals and superconductors.

Potentially, there are many possible ways of defining topological indices following the prescription in Ref.[36]. Perhaps studying connections between these topological indices and existing topological numbers in quantum theory, as we have done in this manuscript, may yield further connections between metamaterials and quantum materials. If so, classical metamaterials may provide explanations of otherwise inexplicable behavior of some quantum materials.

CHAPTER 4

THE FATE OF TOPOLOGICAL FRUSTRATION IN A QUANTUM SPIN LADDER

4.1 Introduction

In this chapter, we study the connections between topological frustration and quantum magnets in one-dimensional space where an ordered phase is naturally prevented. We do so by studying quantum spin ladders[65] in a special regime where the classical spins exhibit geometric frustration on each plaquette similar to classical spins on each tetrahedron of pyrochlore Heisenberg antiferromagnets. A key distinction from the pyrochlore case beyond dimension is the additional existence of infinitely many conservation laws owing to the existence of symmetry we call "staggered swap" symmetry. Using these conservation laws, we show that the fate of classical topological frustration in the quantum regime is to emerge as asymptotically-in-S low energy low-entanglement eigenstates. These eigenstates violate the eigenstate thermalization hypothesis, have area law entanglement, and correspond to known symmetry-protected topological (SPT) ground states enabled by the staggered swap symmetry. We further identify a special role of $SU(2)$ symmetry, that it demands the existence of extra dimensions of classical zero modes the phenomena we call symmetry-enriched topological frustration (SETF). We conclude with a discussion of a) how small violations of the special symmetries used to obtain results in this paper would likely lead to quantum scars, b) the model generalizes to higher dimensions proposing a bilayer triangular lattice model which shares many similar properties with our quantum spin ladders, and c) a discussion of why we think these

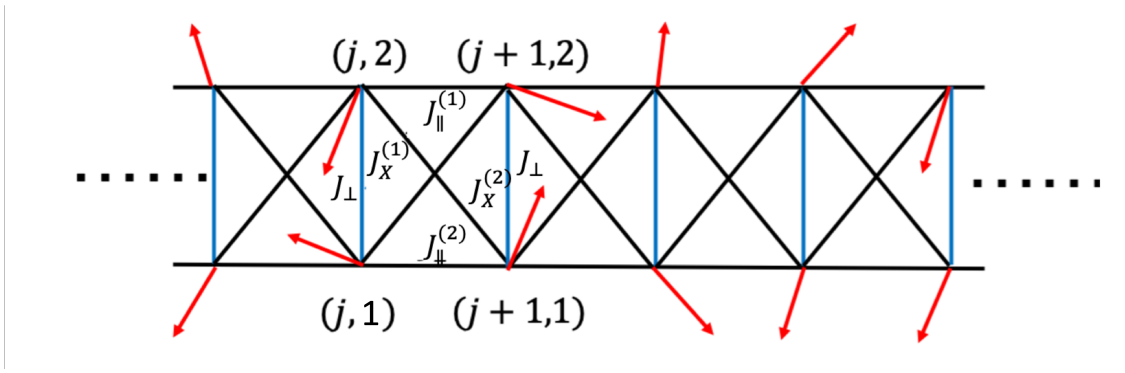

Figure 4.1: The frustrated spin ladder model

results suggest tensor network methods are a powerful approach to the study of large-S antiferromagnets.

4.2 Geometrically frustrated spin ladders

We start with a frustrated spin ladder model (Fig.4.1) which possesses classical frustration, local conserved quantities, or both in some regimes. The Hamiltonian is written as

$$\begin{aligned} H_{ladder} = & \frac{J_{\perp}}{S(S+1)} \sum_i \vec{S}_{i,1} \cdot \vec{S}_{i,2} \\ & + \frac{J_{\parallel,1}}{S(S+1)} \sum_i \vec{S}_{i,1} \cdot \vec{S}_{i+1,1} \\ & + \frac{J_{\parallel,2}}{S(S+1)} \sum_i \vec{S}_{i,2} \cdot \vec{S}_{i+1,2} \\ & + \frac{J_{X,1}}{S(S+1)} \sum_i \vec{S}_{i,1} \cdot \vec{S}_{i+1,2} \\ & + \frac{J_{X,2}}{S(S+1)} \sum_i \vec{S}_{i,2} \cdot \vec{S}_{i+1,1} \end{aligned} \tag{4.1}$$

where $\vec{S}_{i,m}$ is the spin operator at the site (i, m), and $J_{\perp}$, $J_{\parallel,1}$, $J_{\parallel,2}$, $J_{X,1}$, and $J_{X,2}$ are the antiferromagnetic coupling strengths depicted in Fig.4.1. We divide the

antiferromagnetic coupling strength by $(S+1)S$ so that as spin increasing we only increase the number of degrees of freedom but keep unit length for the spin.

This spin ladder model looks complex but has been studied for the spin-half case in many different regimes[6, 67, 65]. In general, it relies on numerical simulations to find the ground state[65] except for some regimes which can be studied analytically[6, 67]. For example, in the limit $J_\perp \gg J_{\|,1}, J_{\|,2}, J_{X,1}, J_{X,2}$, the ground state is a gapped rung singlet[6]. Another well-controlled regime is the case where $J_1 = J_{\|,1} = J_{\|,2} = J_{X,1} = J_{X,2}$[67]. In this regime, the Hamiltonian has two competing phases. One of the phases is the rung singlet in which the coupling $J_\perp$ between two spins at the same rung dominates, and thus the system forms a singlet spin state at each rung. The other phase is the spin-one Haldane phase in which two spins at the same rung are aligned to the same direction forming an equivalently spin-one quasiparticle that couples to its two neighbors and behaves just as the Heisenberg spin-one chain. Despite the simple structure of the phase diagram, this well-controlled regime can be highly frustrated in the classical limit and thus a good candidate to study any connections between classical geometric frustration and quantum magnetism.

4.3 Phase diagram

To establish the connections, we generalize the spin ladder model to arbitrary spin S. First, in the classical $S \to \infty$ limit, the spin operator $\vec{S}_{i,m}$ is reduced to a three-dimensional vector. One can use Lagrange multipliers to fix the length of each spin, and then the ground states are obtained by minimizing the energy

with respect to each spin component. Interestingly, there exists a special regime where the Hamiltonian can be written in a frustration-free form

$$H_{fru} = \frac{J}{S(S+1)} \sum_i (a_1 \vec{S}_{i,1} + a_2 \vec{S}_{i,2} + a_3 \vec{S}_{i+1,1} + a_4 \vec{S}_{i+1,2})^2 \tag{4.2}$$

which requires two conditions $J_{\|,1} J_{\|,2} = J_{X,1} J_{X,2}$ and $J_\perp \geq 2\sqrt{J_{\|,1} J_{\|,2}}$. The Hamiltonian H_{fru} has large ground state degeneracy, and thus the system is highly frustrated. In this type of highly frustrated regime, the classical ground state can be understood as zero modes of a constraint problem. In the spin ladder model, the configurations of zero modes can be obtained by sequentially add two spins on the ith rung that satisfy the constraint

$$a_1 \vec{S}_{i,1} + a_2 \vec{S}_{i,2} + a_3 \vec{S}_{i+1,1} + a_4 \vec{S}_{i+1,2} = 0. \tag{4.3}$$

In the quantum finite S regime, similarly to the spin-half case, only some regimes can be studied analytically. Especially, we are interested in the frustrated but well-controlled regime where $J_1 = J_{\|,1} = J_{\|,2} = J_{X,1} = J_{X,2}$. In this regime, the ladder has global staggered swap symmetry: the Hamiltonian is invariant by swapping the two spins on all the even rungs or all the odd rungs. In this regime the Hamiltonian also has the local conservation law with the conserved quantum number $T_i(T_i + 1)$ where T_i is the total spin quantum number on a rung with spin operator defined as $\vec{T}_i = \vec{S}_{i,1} + \vec{S}_{i,2}$. Thus, we can rewrite the Hamiltonian as

$$H_{con} = \frac{J_\perp/2}{S(S+1)} \sum_i \vec{T}_i^2 + \frac{J_1}{S(S+1)} \sum_i \vec{T}_i \cdot \vec{T}_{i+1} + const. \tag{4.4}$$

For a given spin S, there are $2S + 1$ competing phases, one for each value of spin representation T_i including the rung singlet ($T_i = 0$) and the well-known

SPT Haldane phases from $T_i = 1$ to $T_i = 2S$. However, only the rung singlet and the spin-$2S$ Haldane state can be the ground state depending on the ratio of the antiferromagnetic coupling strengths $J_\perp/J_1$. When $J_\perp$ dominates, two spins on the same rung form a spin-singlet. When the coupling J_1 between two neighbor rungs dominates, each rung forms a maximum spin-$2S$ quasiparticle which antiferromagnetically couples to its two neighbors, and the spin ladder model is equivalent to the spin-$2S$ Heisenberg chain.

To elaborate on the phase diagram, let's look at the $S = 3/2$ case. The density-matrix renormalization group calculation[66] is performed to obtain the energy of the rung singlet plus the spin-one, spin-two, and spin-three Haldane phases for different values of $J_\perp/J_1$ as shown in Fig.4.2a. The spin-three Haldane state is the ground state when $J_\perp/J_1$ is smaller than a critical value $J_\perp/J_1 \approx 1.68$. When $J_\perp/J_1$ is larger than this critical value, the ground state is the rung singlet. We can further find the critical point that separates two distinct phases for other spin values. The critical point would finally move toward $J_\perp/J_1 = 2$ as S goes to infinity. As a result, we draw a schematic phase diagram as shown in Fig.4.2b where a quantum phase transition line separates the rung singlet and the spin-$2S$ Haldane phase.

The region of the phase diagram where H_{ladder} can be placed in the form of H_{fru} lies on the upper part of Fig.4.2(b) where $J_\perp/J_1 \geq 2$ and labeled "classical frustration". But we also restricted parameters so that we can write H_{ladder} as H_{con}, as discussed above. Thus there is an overlap between H_{con} and H_{fru} where the spin ladder is classically frustrated and has local conserved quantities (See Fig.4.3a). In the overlap case, the Hamiltonian can always be written in

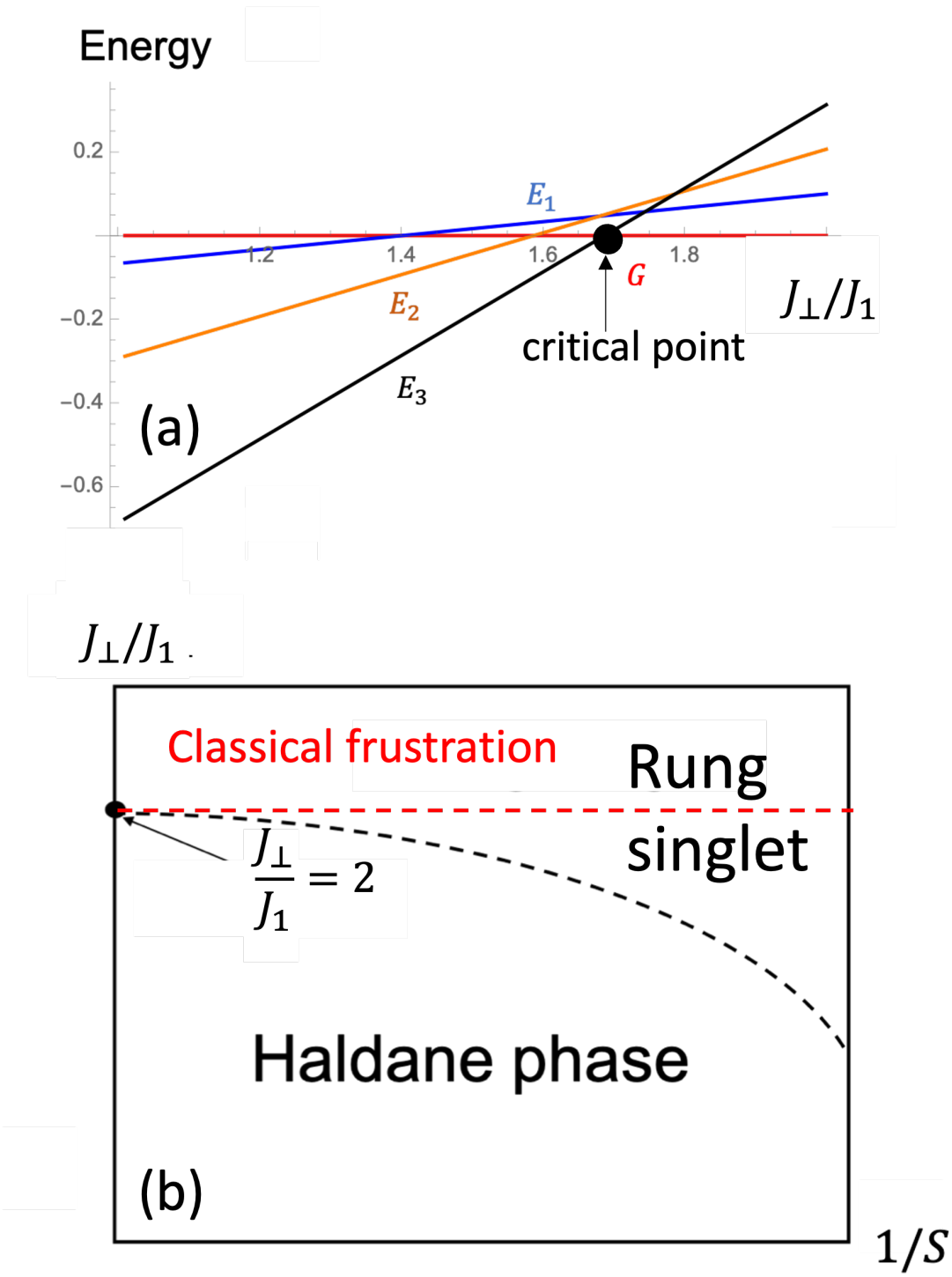

Figure 4.2: (a)The density-matrix renormalization group calculation for the eigenenergy of the spin-3/2 frustated spin ladder model (50 rungs) for different values of $J_\perp/J_1$. Here we fix $J_1 = 1$. G: the rung singlet; E_i: the spin-i Haldane state.(b)A schematic phase diagram of the frustrated spin ladder model

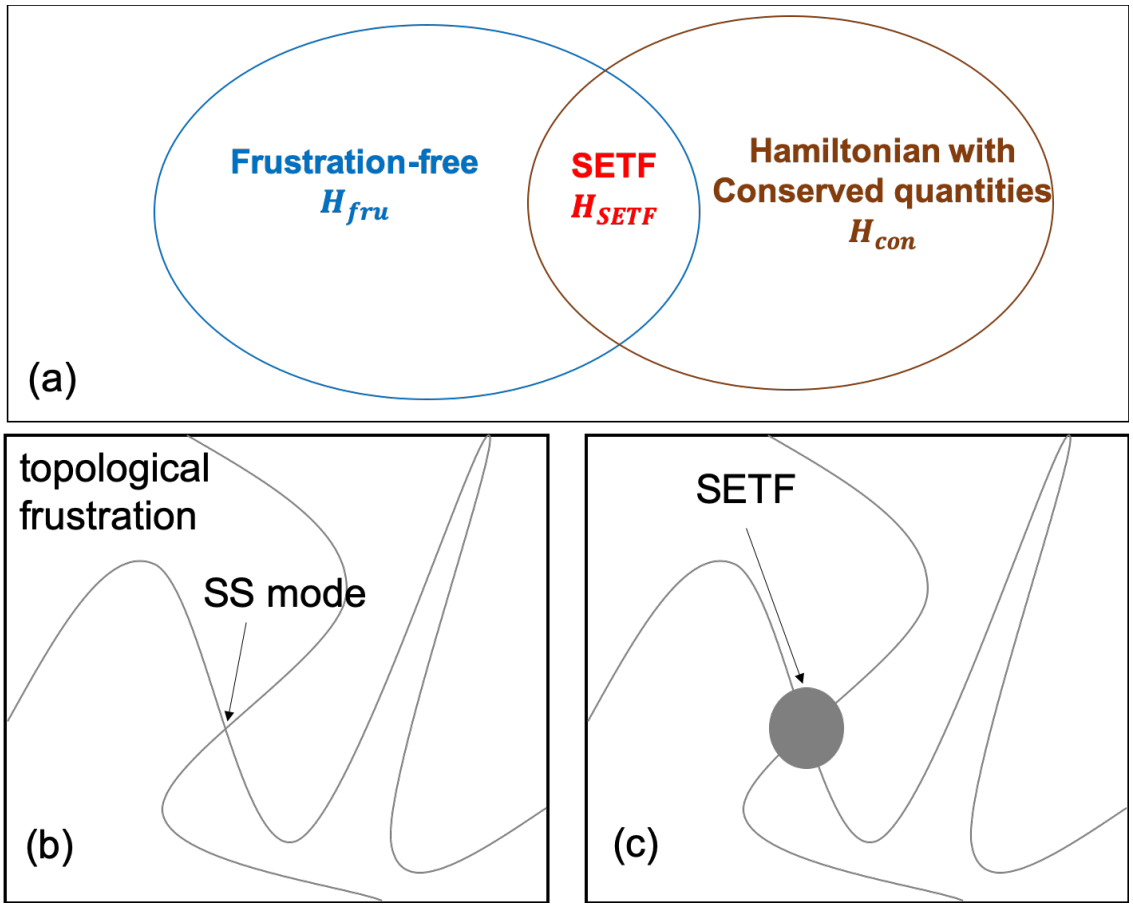

Figure 4.3: (a)Relations among symmetry-enriched topological frustration(SETF), frustration-free Hamiltonian, and the Hamiltonian with conserved quantities. (b)The topological space of zero modes with a self-stress(SS) mode (c)The topological space of zero modes with a regime where the zero modes have extra dimensions.

a frustration-free form

$$H_{SETF} = \frac{J_1}{2S(S+1)} \sum_i (b_1 \vec{T}_i + \vec{b}_2 T_{i+1})^2 \tag{4.5}$$

which we will turn out to be the regime where the SETF occurs.

4.4 The fate of topological frustration

Now we have enough ingredients to study the connections between topological frustration and quantum magnetism. Especially, we will begin on the classical side to understand topological frustration and then to see what the fate of this topological frustration would be after turning on quantum mechanics.

To do so, we start with the purely classical problem of finding the ground state of H_{fru} in which the zero modes are the configurations which satisfy a set of constraints $a_1\overrightarrow{S}_{i,1} + a_2\overrightarrow{S}_{i,2} + a_3\overrightarrow{S}_{i+1,1} + a_4\overrightarrow{S}_{i+1,2} = 0$. Based on Maxwell's counting[20], since each rung of the ladder has four degrees of freedom and three constraints (in average) the zero mode has one remaining degree of freedom for each rung. For example, when $a_1/a_2 = ca_3/a_4$ where c is some constant, we can define a vector $\overrightarrow{V}_i = a_1\overrightarrow{S}_{i,1} + a_2\overrightarrow{S}_{i,2}$ and rewrite the constraint as $\overrightarrow{V}_i + c\overrightarrow{V}_{i+1} = 0$. In this case the system has a local zero mode at each rung in which two spins combined can rotate as $U(1)$ symmetry about the axis described by $\overrightarrow{V}_i$.

Maxwell's count is, however, incomplete, as discussed by Kane and Lubensky to linear level for balls-and-springs models[27]. For example, considering that we have n degrees of freedom and $n-1$ constraints. In a generic case, the topological space of zero modes would look like a one-dimensional manifold except for some points where two curves (or more than two curves) intersect (See Fig.4.3b). Those intersecting points are the places where self-stress modes appear and give an extra number of zero modes in a linear theory.

In a full nonlinear problem, the topological space of zero modes can change dramatically due to certain symmetry that makes some constraints become redundant. This gives extra dimensions to zero modes, the phenomenon we call

SETF (See Fig.4.3c). In the Hamiltonian H_{fru}, for example, when $a_1 = a_2$ and $a_3 = a_4$, which corresponds to $J_{\|,1} = J_{\|,2} = J_{X,1} = J_{X,2}$, the configurations with two spins at the same rung pointing into opposite directions ($\vec{S}_{i,1} = -\vec{S}_{i,2}$) is a local zero mode in which two spins combined can rotate as $SU(2)$ symmetry which has two continuous degrees of freedom that is one more than Maxwell's counting. In this SETF regime, we can always rewrite H_{fru} in a form of H_{SETF} by defining $\vec{T}_i = \vec{S}_{i,1} + \vec{S}_{i,2}$. Thus, the regime where SETF occurs is exactly the overlap between H_{con} and H_{fru}.

To understand how this SETF is preserved from infinite S to finite S, let's take a highly frustrated point $J_\perp/J_1 = 2$ for an example. The corresponding Hamiltonian is written as

$$H_2 = \frac{J_1}{2S(S+1)} \sum_i (\vec{T}_{i,1} + T_{i+1,1})^2. \tag{4.6}$$

As we move from infinite S to finite S, the strict zero modes of the classical limit all get lifted by quantum fluctuations and we are left with a unique rung singlet ground state G (Fig.4.4). But the SETF at finite but large S is preserved as the existence of many very low energy excitations. We know this exactly by mapping them to the SPT spin-n Haldane states E_n whose topological properties are protected by the staggered swap symmetry (See Appendix A).

It turns out there is a simple argument that predicts the lifting of the classical zero modes by quantum fluctuations. The recently developed theory of nonlinear topological mechanics[36] identifies a topological invariant that protects the existence of classical zero modes by surface integrals over phase space. If these constraints only involve position variables, the surfaces are well defined both at the quantum and classical levels. So it could be the topology is preserved by quantum fluctuations and captured by a quantum version of nonlinear topolog-

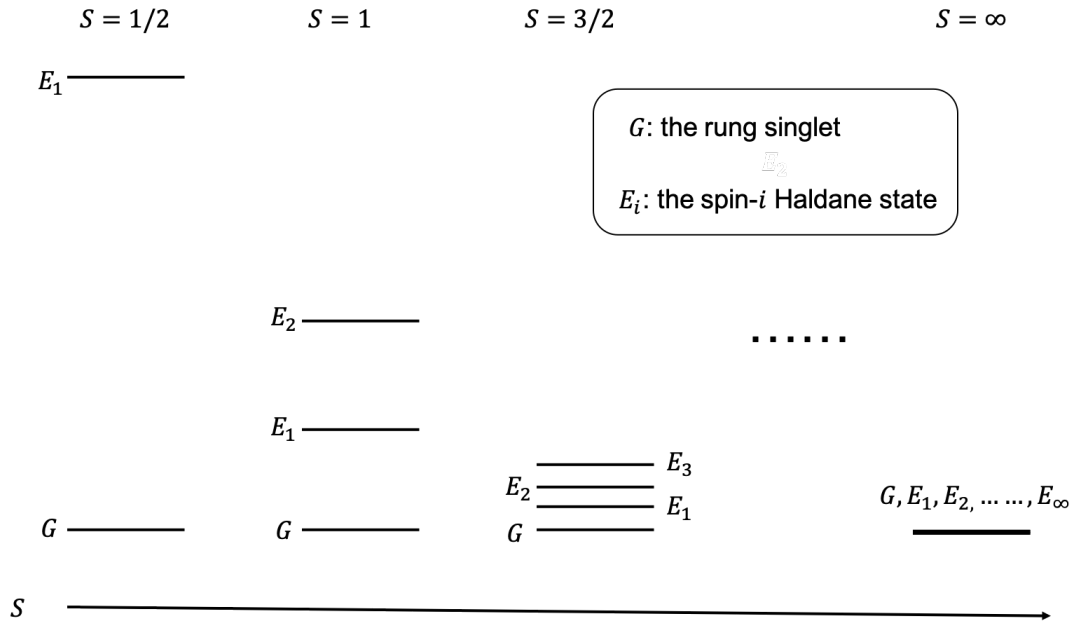

Figure 4.4: Low energy eigenstates at different spins for the spin ladder model.

ical mechanics. However, in the present case, these surfaces are defined by the constraints in Eq. 4.3 that arise from angular momentum variables that involve position and momentum variables. So, upon quantizing the system, the surfaces cease to exist by the Heisenberg uncertainty principle and the topological invariant becomes undefined. As a result, it is not surprising the topology is lost in the finite S model.

Though the zero modes are lifted at finite S, the staggered swap symmetry allows some of them to become SPT states. This symmetry allows us to rewrite the frustration-free Hamiltonian in terms of a new spin operator defined by a pair of spins ($\vec{T}_\alpha = \vec{S}_b + \vec{S}_c$), the resulting Hamiltonian would have a local conserved quantity T_α^2. In classical theory, this symmetry demands one more degree of freedom than Maxwell's counting would predict. The conservation of T_α^2 groups the Hilbert space into different sectors each labeled by its eigenval-

ues $T_\alpha(T_\alpha + 1)$. Each sector is characterized by its own Hamiltonian with its own "ground states" and set of excitations. Therefore, the classical SETF phase in the spin ladder has asymptotically low-energy topological eigenstates whose presence is the quantum manifestation of a combination of topological frustration and the staggered swap symmetry.

4.5 conclusion and outlook

Topological frustration is a classical phenomenon that is able to study in most frustrated spin systems, but does not draw much attention due to the ignorance of the connections between classical frustration and quantum magnets. In particular, combined with the role of symmetry, the fate of SETF and how SETF is preserved from infinite spin to a finite spin points out a new direction to study unsolved frustrated spin systems such as kagome and pyrochlore antiferromagnets. Several future directions this research motivates includes the potential observation of quantum scars, two-dimensional topological frustration systems with a similar set of conservation laws, and the potential use of tensor network methods to study large-S frustrated magnets.

4.5.1 Existence of quantum scars

In the nearly SETF regime where the conservation laws are violated due to some small perturbation, we speculate the quantum scars could be observed. An isolated quantum system was believed to be thermalized in a way such that the system can be described by equilibrium statistical mechanics that we call the

eigenstate thermalization hypothesis (ETH). However, some quantum systems were found disobeying the ETH[16]. In particular, when there exist many conserved quantities in a quantum system the ETH is strongly violated which is essentially the case where SETF occurs. If we move slightly away from the SETF regime by adding some small perturbation, the system becomes weakly ETF breaking, and quantum scars might be observed[58].

To illustrate the idea, let's look at quantum spin ladders as a concrete example. For quantum spin ladders with the staggered swap symmetry, the ground states (the Haldane states) in different sectors are gapped to their excited states of the same sector. With a small perturbation, interactions can be introduced between two states with the same energy but in different sectors. For example, the ground states in two sectors $(|T_1|, |T_2|, |T_3|, |T_4|, ...) = (0, 1, 0, 1, ...)$ and $(|T_1|, |T_2|, |T_3|, |T_4|, ...) = (1, 0, 1, 0, ...)$ have the same energy but are non-interacting when staggered swap symmetry holds. With small perturbation that breaks the staggered swap symmetry, those two states can become interacting. In this case, if we prepare the ground state in the sector $(|T_1|, |T_2|, |T_3|, |T_4|, ...) = (0, 1, 0, 1, ...)$ as an initial state, we speculate that similar to a quantum scarred eigenstates in a Rydberg atom chain[59, 58], an oscillation between the two states $(0, 1, 0, 1, ...)$ and $(1, 0, 1, 0, ...)$ might be observed. Similarly, other initial states could also lead to different patterns of quantum scars in the nearly SETF regime.

4.5.2 Generalization to higher dimensions

Based on the special role of $SU(2)$ symmetry in SETF, we design a bilayer triangular lattice model as shown in Fig.4.5. The Hamiltonian is

$$\begin{aligned} H_{bilayer} = \frac{J_A}{S(S+1)} \sum_{i,j,m} (\vec{S}_{i,j,m} \cdot \vec{S}_{i+1,j,m} \\ + \vec{S}_{i,j,m} \cdot \vec{S}_{i,j+1,m} + \vec{S}_{i+1,j,m} \cdot \vec{S}_{i,j+1,m}) \\ + \frac{J_B}{S(S+1)} \sum_{i,j} (\vec{S}_{i,j,1} \cdot \vec{S}_{i+1,j,2} + \vec{S}_{i,j,1} \cdot \vec{S}_{i,j+1,2} \\ + \vec{S}_{i+1,j,1} \cdot \vec{S}_{i,j+1,2} + \vec{S}_{i,j,2} \cdot \vec{S}_{i+1,j,1} \\ + \vec{S}_{i,j,2} \cdot \vec{S}_{i,j+1,1} + \vec{S}_{i+1,j,2} \cdot \vec{S}_{i,j+1,1}) \\ + \frac{J_C}{S(S+1)} \sum_{i,j} \vec{S}_{i,j,1} \cdot \vec{S}_{i,j,2} \end{aligned} \tag{4.7}$$

where $\vec{S}_{i,j,m}$ is the spin operator at the site (i, j, m), and J_A, J_B, and J_C are the antiferromagnetic coupling strengths depicted in Fig.4.5.

Topological frustration occurs when $J_C = 2J_B$. Under this condition, the Hamiltonian can be written in a frustration-free form

$$\begin{aligned} H_{bilayer(fru)} = \frac{J_B}{2S(S+1)} \sum_{i,j} (\vec{S}_{i,j,1} + \frac{J_A}{J_B} \vec{S}_{i,j,2} \\ \vec{S}_{i+1,j,1} + \frac{J_A}{J_B} \vec{S}_{i+1,j,2} \\ + \vec{S}_{i,j+1,1} + \frac{J_A}{J_B} \vec{S}_{i,j+1,2})^2 \end{aligned} \tag{4.8}$$

which can then be understood as a constraint problem in the classical limit. Similar to the spin ladder model, each vertex of triangles has two spins and thus four degrees of freedom. In average, there are three constraint for each vertex, so the zero mode has one remaining degree of freedom on each vertex shared by two spins.

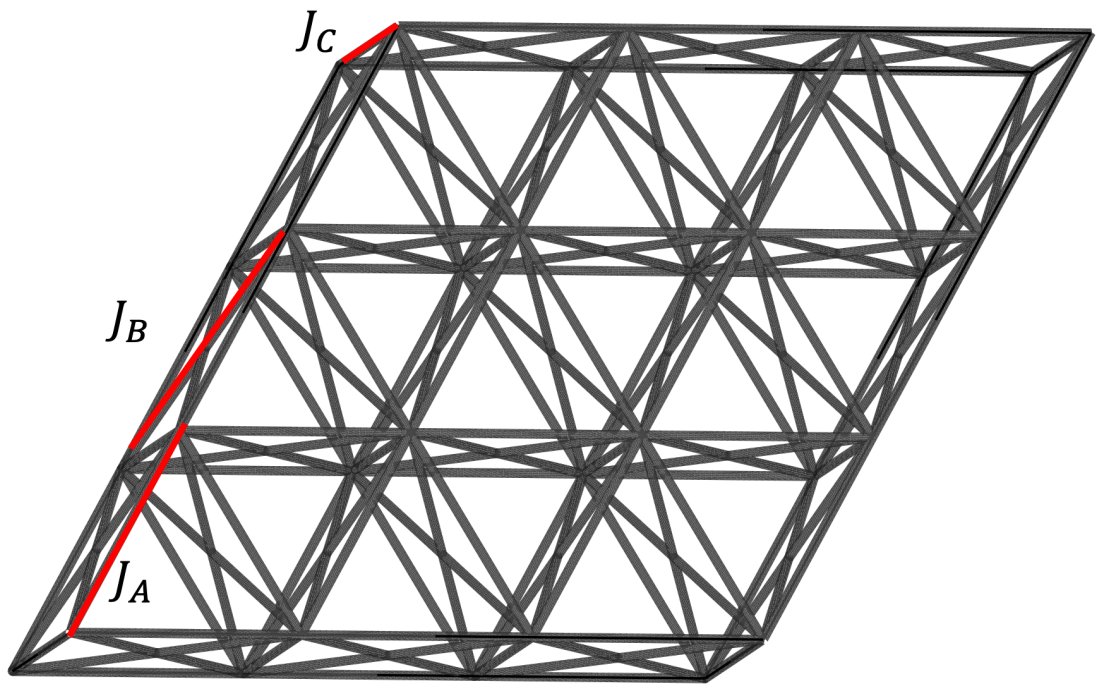

Figure 4.5: The bilayer triangular lattice model

Topological frustration is enriched when $J_A/J_B = 1$. At this point, we can define a new set of spin operators $\vec{T}_{i,j} = \vec{S}_{i,j,1} + \vec{S}_{i,j,2}$, and rewrite the Hamiltonian as

$$H_{bilayer(SETF)} = \frac{J_B}{2S(S+1)} \sum_{i,j} (\vec{T}_{i,j} + \vec{T}_{i+1,j} + \vec{T}_{i,j+1})^2. \tag{4.9}$$

Configurations with two spins on the same vertex pointing into opposite directions ($\vec{S}_{i,j,1} = -\vec{S}_{i,j,2}$) are the zero modes with two continuous degrees of freedom on each vertex. Therefore, the same form of SETF occurs in this bilayer triangular lattice model.

As we go from infinite S to a finite value of S, each spin operator $\vec{T}_{i,j}$ gives a local conserved quantity $T_{i,j}(T_{i,j}+1)$. A set of low energy eigenstates of the bilayer triangular lattice model is consisted of the ground states from different

sectors defining by infinite many conserved quantities $T_{i,j}(T_{i,j}+1)$. Some of those eigenstates come from well-known models that have been studied by previous works[39, 17, 12]. For example, when $T_{i,j}(T_{i,j}+1) = 2$ for all i, j, $H_{bilayer(SETF)}$ is reduced to spin-one Heisenberg triangular lattice model [See Fig.4.6(a)] which has the 120 degree magnetically ordered ground state[39]. We can also make some $T_{i,j}(T_{i,j}+1) = 0$ and some other $T_{i,j}(T_{i,j}+1) = 2$ to obtain spin-one Heisenberg honeycomb and kagome lattice models as shown in Fig.4.6(b) and (c). The ground state of spin-one Heisenberg honeycomb lattice model has been found to be a Neel state while a possible candidate for the ground state of spin-one Heisenberg kagome lattice model is the hexagon singlet solid[17, 12]. From the above analysis, we can study the spectra features with the benefit of being able to calculate some topological eigenstates from a simplified model based on a set of conserved quantities. Moreover, we can further infer the spectra features for some unsolved model such as kagome and pyrochlore antiferromagnets by understanding the fate of SETF.

4.5.3 Tensor network methods

For a generic model, understanding the fate of SETF and how it is preserved in the quantum limit relies on numerical simulations. In particular, tensor network methods have been shown powerful to handle low-dimensional frustrated spin systems. Especially in one-dimensional systems, tensor network methods have been well developed from the matrix product state[66]. Nevertheless, the challenge significantly grows in dealing with two-dimensional systems because of the need for large size tensors to obtain a wavefunction with acceptable accuracy. To overcome the challenge several algorithms such as the projected en-

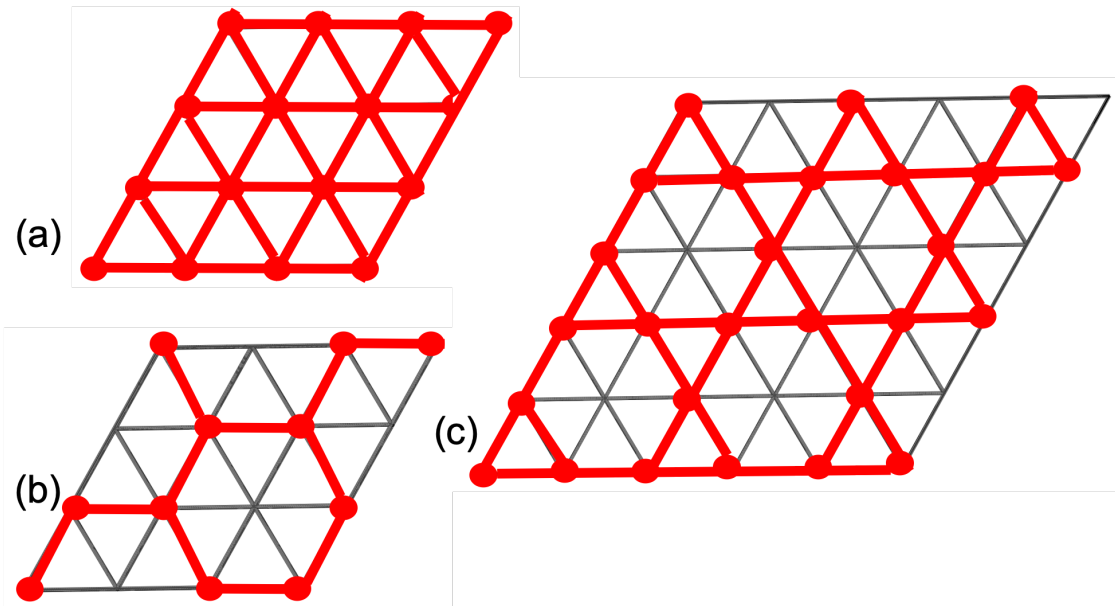

Figure 4.6: (a)A triangular lattice model (b)A honeycomb lattice model (c)A kagome lattice model

tangled pair states, the infinite projected entangled pair states, and infinite projected entangled simplex states have been developed to reduce fitting parameters of tensors based on symmetry[61, 25, 68]. The idea behind those algorithms implies that even with large size tensors one can still use only a small number of parameters by appropriately imposing structures on tensors. In other words, as we move to large spin cases, although the size of tensors may increase, it is possible to use fewer parameters to construct a tensor network representation of a wavefunction with the same accuracy as that in the spin-half or one case.

To see whether we can study the large spin cases in the spin ladder model with achievable computational resources, we first notice that mutual information I in the classical limit can be the analogy to entanglement entropy S_q. For the rung singlet phase, since knowing the directions of two spins at a certain rung does not give us any information on the directions of spins at other rungs,

the mutual information is zero, and so is the entanglement entropy. On the other hand, in the case of the Haldane phase, classically, once we know the direction of spins at a certain rung, the directions of the rest of the spins can be completely determined. Thus, both the mutual information and entanglement entropy are nonzero. The mutual information can be computed as follows. The (classically) entropy S_c for a chain with any size is always lnN where N is the number of states (assume a uniform grid N on a sphere) for an individual spin. Now if the system is divided into subsystem A and subsystem B, the mutual information between them would be

$$I = S_c(A) + S_c(B) - S_c(A + B) = lnN + lnN - lnN = lnN. \tag{4.10}$$

From the analog between mutual information and entanglement entropy, Eq.4.10 implies that the entanglement entropy has an asymptotic function $ln(2S+1)$ as S goes infinity where $2S+1$ is the degrees of freedom for a quantum spin-S. Thus a tensor network representation for a large spin-S Haldane state can be constructed by tensors with virtual bond dimension to the order of $2S+1$

To further confirm our claim, we perform the density-matrix renormalization group calculation for the Heisenberg spin chain as shown in Fig.4.7. Here we compare different spin cases with the same ratio of the virtual bond dimension χ to $2S+1$. The factor $2S+1$ is able to be factored out by using appropriate symmetric tensors because it comes from the global $SU(2)$ symmetry. With different values of $\chi/(2S+1)$, the entanglement entropy is always bounded by $ln(2S+1)$. Moreover, the entanglement entropy only increases slightly with the increasing S. As a result, we conclude that in the frustrated spin ladder model, the tensor network method can be used to study the large spin regime which would give us a better understanding of SETF.

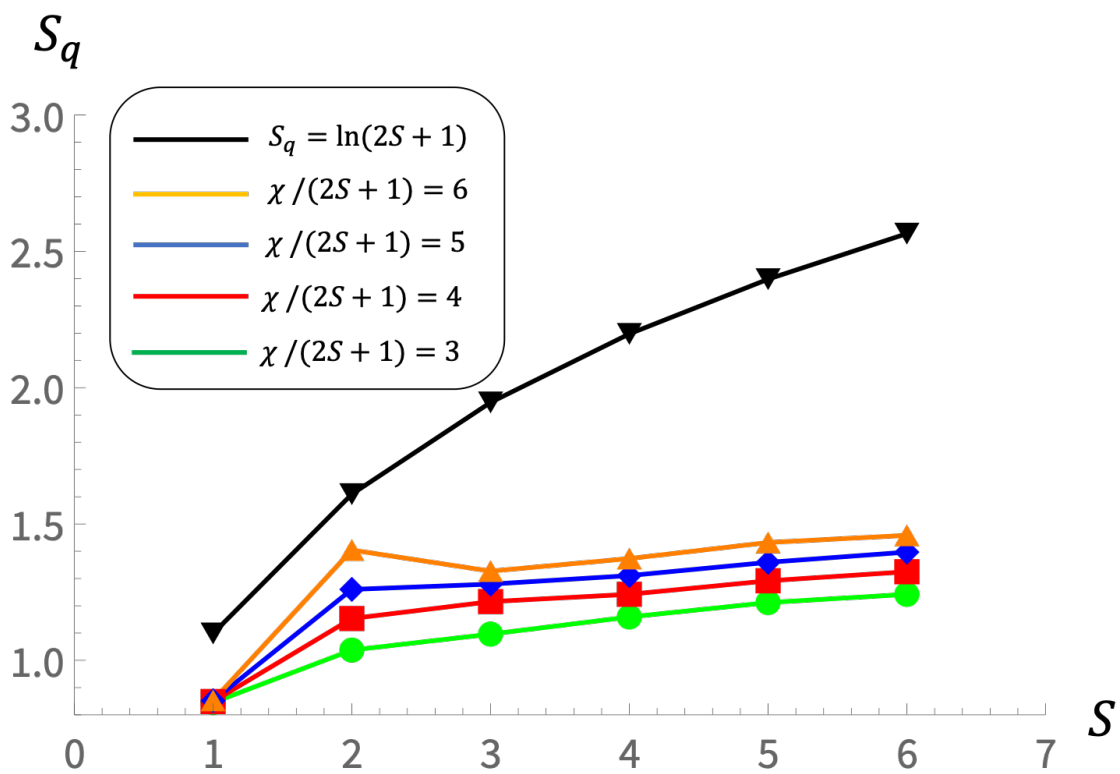

Figure 4.7: The density-matrix renormalization group calculation for the entanglement entropy as a function of S for different virtual bond dimension $\chi/(2S+1)$ of the Heisenberg spin chain (50 spins).

CHAPTER 5

CONCLUSION

In this thesis, we provide alternative ways to understand topology of quantum phenomenon with concrete classical pictures. Firstly, we conclude by emphasizing that new topological indices can be generated in similar manners following our prescription to classify nonlinear ZMs. For instance, a $n-1$-dimensional sphere around an isolated zero-energy configuration (solution) is chosen in this work as the base manifold to construct a bundle with $\mathbb{Z}$-type topological invariant. For higher-dimensional manifolds of such solutions, different choices of the base manifold can lead to different types of topological invariants [1]. Exploring the physical significance of those topological indices constitutes a new direction of searching for novel topologically protected nonlinear ZMs in the future.

Secondly, due to the similarity of mathematical frameworks, our prescription of defining topological indices suggests some connections between these topological indices and existing topological numbers in quantum theory. These connections lead to some analogy between classical mechanical systems and quantum systems that offers an alternatively way to understand the topology in quantum systems.

Last but not least, topological frustration is a classical phenomenon that is able to study in most frustrated spin systems, but does not draw much attention due to the ignorance of the connections between classical frustration and quantum magnets. In particular, combined with the role of symmetry, the fate of SETF and how SETF is preserved from infinite spin to a finite spin points out a new direction to study unsolved frustrated spin systems such as kagome and

pyrochlore antiferromagnets.

APPENDIX A

THE ORIGAMI CHAIN

The origami chain is a periodic origami fold pattern of degree-4 vertices constructed from quadrilaterals as shown in Fig. A.1. Each vertex, because it has a one-dimensional configuration space, can be parametrized by the fold angle of a single vertex so any finite number of vertices will have one degree of freedom. There are two degree-4 vertices in each unit cell with interior angles $\{\alpha_i, \beta_i, \phi_i, \psi_i\}$ for the ith vertex. When the interior angles around each internal vertex add up to 2π, the fold pattern can be realized as a flat structure; here, we will extend the calculation of Ref.[37] to the more general case of arbitrary interior angles.

The law of cosines applied to each vertex gives a constraint on the dihedral angles θ as,

$$\cos(\alpha_1)\cos(\psi_1) + \sin(\alpha_1)\sin(\psi_1)\cos\theta_1 = \cos(\beta_1)\cos(\phi_1) + \sin(\beta_1)\sin(\phi_1)\cos\theta_2$$

$$\cos(\alpha_2)\cos(\psi_2) + \sin(\alpha_2)\sin(\psi_2)\cos\theta_2 = \cos(\beta_2)\cos(\phi_2) + \sin(\beta_2)\sin(\phi_2)\cos\theta_3$$

After some manipulation, we obtain

$$A\sin^2\left(\frac{\delta\theta_1}{2}\right) - B\sin^2\left(\frac{\delta\theta_2}{2}\right) + \epsilon = 0, \tag{A.1}$$

where $\delta\theta_i = \pi - \theta_i$ and

$$\begin{aligned} A &= \sin\alpha_1 \sin\alpha_2 \sin\psi_1 \sin\psi_2, \\ B &= \sin\beta_1 \sin\beta_2 \sin\phi_1 \sin\phi_2, \\ 2\epsilon &= \sin(\alpha_2)\sin(\psi_2)\left[\cos(\alpha_1+\psi_1) - \cos(\beta_1)\cos(\phi_1)\right] \\ &\quad + \sin(\beta_1)\sin(\phi_1)\left[\cos(\alpha_2)\cos(\phi_2) - \cos(\beta_2+\phi_2)\right]. \end{aligned}$$

When the Gaussian curvature of both vertices is zero, $\epsilon = 0$.

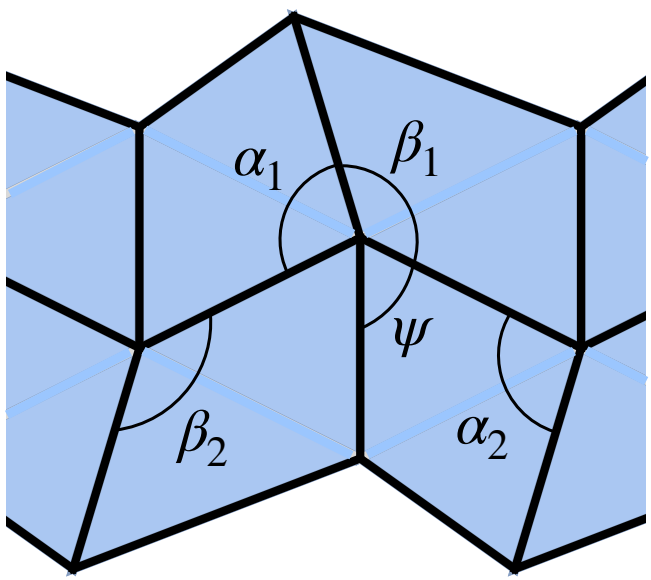

Figure A.1: The origami topological chain.

APPENDIX B

GAUGE THEORY

The connection between fermion and boson problems has been discussed in various perspectives. Many topological orders have been found in fermion systems. In classical mechanics, boson systems can also have some interesting topology. Topological quantum field theory (TQFT) is a theory which establishes a mathematical framework which relates one boson system to a fermion system. One of the branches of TQFT which can be understood as Nicolai map, BRST (where the BRST refers to Becchi, Rouet, Stora and Tyutin) theory, or Faddev-Popov (FP) gauge-fixing relates to classical constrained systems. The connection between them is established by a gauge theory in which constraints for a classical system are treated as gauge-fixing conditions.

One of the useful topological numbers in TQFT is the partition function. In general, a partition function sums over all paths by assigning each path a weight depending on the action. In TQFT all paths cancel and together contribute exactly zero except for the paths of ground states. Therefore, the partition function is simply the sum over all paths of ground states which have an action equal to $n\pi$. Due to this fact, the partition function can always be rewritten as an integration over a sum of several delta functions up to a sign. Thus, one can write a partition function of TQFT in an inverted way by starting with a gauge symmetry action and then fixing the gauge by imposing delta functions.

B.1 Toy model

To understand this gauge theory we first start with a toy model

$$Z_0 = \int dx \tag{B.1}$$

This partition function is infinity. We need to fix x to get a well-defined Z. Let's assume that the function $f(x) = x^2 - a^2$ is used to fix the degree of freedom. We define a gauge-fixed partition function as

$$Z_0 = \int dx \delta(f(x)) \frac{df(x)}{dx} \tag{B.2}$$

There are two solutions to $f(x) = x^2 - a^2 = 0$, namely, $x_s = \pm a$. The partition function becomes

$$Z_0 = \int dx[\delta(x-a) + \delta(x+a)]|\frac{df(x)}{dx}|^{-1}\frac{df(x)}{dx} = 1 + (-1) = 0 \tag{B.3}$$

which is a sum over the signs of the slops at $x_s = \pm a$.There are two reasons why we use $\delta(f(x))\frac{df(x)}{dx}$ instead of $\delta(f(x))|\frac{df(x)}{dx}|$. The first one is that $\frac{df(x)}{dx}$ can be mapped to a fermion action if we treat it as a Pfaffian. The second one is that with this definition, Z_0 is topological invariant in the sense that it is totally determined by the boundaries of $f(x)$. For $f(\infty) = f(-\infty) = \pm\infty$, $Z_0 = 0$; For $f(\infty) = -f(-\infty) = \pm\infty$, $Z_0 = \pm 1$. Therefore, Z_0 is robust to any local deformation of $f(x)$.

By treating $\frac{df(x)}{dx}$ as a Pfaffian, we rewrite Z_0 as

$$Z_0 = \int dx(id\Psi_A d\Psi_B)\delta(f(x))e^{(\frac{i}{2}\Psi_A\frac{df(x)}{dx}\Psi_B - \frac{i}{2}\Psi_B\frac{df(x)}{dx}\Psi_A)} \tag{B.4}$$

where Ψ_A and Ψ_B are real Grassmann numbers. Because Z_0 is robust to any local deformation of $f(x)$, we can write

$$Z_0 = \int dx(id\Psi_A d\Psi_B)\delta(f(x) - w)e^{(\frac{i}{2}\Psi_A \frac{df(x)}{dx}\Psi_B - \frac{i}{2}\Psi_B \frac{df(x)}{dx}\Psi_A)} \tag{B.5}$$

where w is a real number. Since Z_0 does not depend on the choice of w, we multiply Z_0 by $\int \frac{dw}{\sqrt{2\pi}} e^{-\frac{1}{2}w^2} = 1$ and get

$$Z_0 = \int dx(id\Psi_A d\Psi_B)\frac{dw}{\sqrt{2\pi}}\delta(f(x) - w)e^{-\frac{1}{2}w^2 + (\frac{i}{2}\Psi_A \frac{df(x)}{dx}\Psi_B - \frac{i}{2}\Psi_B \frac{df(x)}{dx}\Psi_A)} \tag{B.6}$$

Finally, integrating over w, we get a partition function

$$Z_0 = \int \frac{dx}{\sqrt{2\pi}}(id\Psi_A d\Psi_B)e^{-\frac{1}{2}(f(x))^2 + (\frac{i}{2}\Psi_A \frac{df(x)}{dx}\Psi_B - \frac{i}{2}\Psi_B \frac{df(x)}{dx}\Psi_A)} \tag{B.7}$$

This is a simplest example of TQFT. The partition function itself is a topological number. The other way to write this partition of function is simply replacing $\delta(f(x))$ by $\int \frac{dB}{\sqrt{2\pi}} e^{iBf(x)}$. We will have

$$Z_0' = \int \frac{dxdB}{\sqrt{2\pi}}(id\Psi_A d\Psi_B)e^{iBf(x) + (\frac{i}{2}\Psi_A \frac{df(x)}{dx}\Psi_B - \frac{i}{2}\Psi_B \frac{df(x)}{dx}\Psi_A)} \tag{B.8}$$

To get this, we don't need to assume the robustness of a local deformation of $f(x)$. This can be considered as a hard-constrained version of previous one.

The sign of slop for each solution also has a topological meaning. For a given solution, the partition function of fermion part is

$$Z_F(f(x_s)) = \int i d\Psi_A d\Psi_B e^{\frac{i}{2}\Psi_A \frac{df(x_s)}{dx}\Psi_B - \frac{i}{2}\Psi_B \frac{df(x_s)}{dx}\Psi_A} = |Z_F(f(x_s))|(-1)^{W(f(x_s))} \tag{B.9}$$

where $(-1)^{W(f(x_s))}$ is a topological number protected by the gap $\frac{df(x)}{dx}$. In other words, to go from $x_s = a$ to $x_s = -a$, one must continuously deform $f(x)$ such that at some step where $\tilde{f}(x)$ has a point at which both $\tilde{f}(x) = 0$ and $\frac{d\tilde{f}(x)}{dx} = 0$. In boson systems, this corresponds to a linear zero mode which might not be an actual zero mode in a non-linear constrained system. If one generalizes x to a field ϕ, then it is clear that $W(f(x_s))$ is the winding number.

B.2 Isostatic systems

This gauge theory can be applied to isostatic systems. For an elastic lattice, if the number of constraints is equal to the number of degrees of freedom, it is called isostatic. Our goal is to find the topology of zero modes for such systems. We first start with a one-dimensional lattice model with a rotor on each site rotating freely. Assume p_i and x_i are momentum and position of the ith ball attached to the end of the ith rotor, respectively. For the ground state, the constraints $p_i = 0$ is trivial, we directly drop the degrees of freedom of momentum. We take the stiff springs limit which will not change the ground states. In this limit, the extensions of springs would be the constraints for x_i. Thus, we start with a partition function.

$$Z_s = \int \prod_{i=0}^{n} dx_i \tag{B.10}$$

Then fix the gauge by imposing gauge-fixing conditions, $f_i(\overrightarrow{x}) = 0$ where $f_i(\overrightarrow{x})$ is the extension for ith spring. A gauge-fixed partition function is defined as

$$Z_s \int \prod_{i=0}^{n} dx_i \prod_{i=0}^{n} \delta(f_i(\overrightarrow{x})) det(\frac{\partial f_i(\overrightarrow{x})}{\partial x_j}) = \sum_{\overrightarrow{f}(\overrightarrow{x})=0}^{n} sign(det(\frac{\partial f_i(\overrightarrow{x})}{\partial x_j})) \tag{B.11}$$

If this topological number is robust to a local deformation of $f_i(\overrightarrow{x})$, we consider $det(\frac{\partial f_i(\overrightarrow{x})}{\partial x_j})$ as a Pfaffian, replace $\delta(f_i(\overrightarrow{x}))$ by $\delta(f_i(\overrightarrow{x}) - w_i)$, multiply the partition function by $\prod_{i=0}^{n} \int \frac{dw_i}{\sqrt{2\pi}} e^{-\frac{1}{2}w_i^2} = 1$, and integrate over all w_i. We will get

$$Z_s = \int \prod_{i=0}^{n} \frac{dx_i}{\sqrt{2\pi}} i d\Psi_{Ai} d\Psi_{Bi} e^{-\sum_{i=0}^{n} \frac{1}{2}(f_i(\overrightarrow{x}))^2 + \sum_{i=0}^{n} \sum_{j=0}^{n} (\frac{i}{2}\Psi_{Ai} \frac{\partial f_i(\overrightarrow{x})}{\partial x_j} \Psi_{Bj} + h.c.)} \tag{B.12}$$

The Hamiltonian has two terms. The first term is the potential energy. The second term is a Majorana chain. In a spring-ball system, $\frac{\partial f_i(\overrightarrow{x})}{\partial x_j}$ is the rigidity matrix. Therefore, the partition function is the sum of the signs of the determinants for the rigidity matrices of all ground states. Without the assumption of robustness, we can also write the partition function in an alternative form

$$Z_s = \int \prod_{i=0}^{n} \frac{dx_i dB_i}{\sqrt{2\pi}} i d\Psi_{Ai} d\Psi_{Bi} e^{i \sum_{i=0}^{n} B_i f_i(\overrightarrow{x}) + \sum_{i=0}^{n} \sum_{j=0}^{n} (\frac{i}{2}\Psi_{Ai} \frac{\partial f_i(\overrightarrow{x})}{\partial x_j} \Psi_{Bj} + h.c.)} \tag{B.13}$$

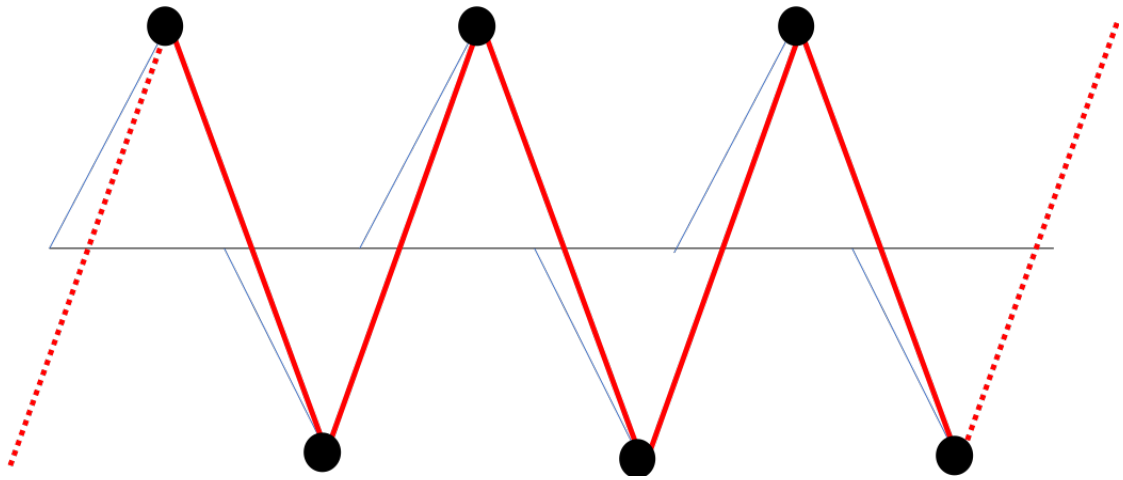

Take a Kane-Lubensky (KL) chain for an example. A closed KL chain is an example of isostatic systems. Each site of a KL chain has a rotor with radius r, and the distance between two sites is a. We define the angle θ_n of rotors on odd sites to be with respect to $+y$ clockwise, and with respect to $-y$ counterclockwise for even sites. The equilibrium angle θ_c for a given rest length $\bar{l}$ of springs satisfies the equation

$$l_{n,n+1}^2 = (rcos(\theta_{n+1}) + rcos(\theta_n))^2 + (a + rsin(\theta_{n+1}) - rsin(\theta_n))^2 = \bar{l}^2 \tag{B.14}$$

This equation can be simplified as

$$l_{n,n+1}^2 = a^2 + 2r^2 + 2r^2cos(\theta_{n+1} + \theta_n) + 2ar[sin(\theta_{n+1}) - sin(\theta_n)] = \bar{l}^2 \tag{B.15}$$

The extension of each spring is written as

$$e_n = \sqrt{l_{n,n+1}^2} - \bar{l} \tag{B.16}$$

There are four different solutions to $e_n = 0$ for all n, namely, $\theta_s = \theta_c, -\theta_c, \pi - \theta_c, \pi + \theta_c$.

$$\begin{pmatrix} -\Delta_+ & \Delta_- & 0 & ... & 0 \\ 0 & -\Delta_+ & \Delta_- & ... & 0 \\ 0 & 0 & -\Delta_+ & ... & 0 \\ ... & ... & ... & ... & ... \\ \Delta_- & 0 & 0 & ... & -\Delta_+ \end{pmatrix}$$

where $\Delta_+ = \frac{r}{l}[acos(\theta_s) + rsin(2\theta_s)]$ and $\Delta_- = \frac{\partial e_n}{\partial \theta_{n+1}} = \frac{r}{l}[acos(\theta_s) - rsin(2\theta_s)]$. The determinant is

$$(-1)^s[(\Delta_+)^s - (\Delta_-)^s] = [(\Delta_+)^s - (\Delta_-)^s] \tag{B.17}$$

where s is the number of sites and is always even. Thus

$$Z_{KL} = 1 + (-1) + 1 + (-1) = 0 \tag{B.18}$$

which means that we can deform a closed KL chain locally such that there is no configuration such that $e_n = 0$ for all n. In other words, those four solutions are topologically connected with a local deformation.

In this example, the sign of $\frac{\partial e_i(\vec{\theta})}{\partial \theta_j}$ determines the location (right or left edge) of the zero mode as we open the boundaries of KL chains. Each solution can also be mapped into a Kiteav chain, solutions with positive slope mapped into a trivial phase and solutions with negative slope mapped into a non-trivial phase. However, in a KL chain those solutions are not topologically protected with a local deformation. One can go from one solution to another by changing the length of springs locally. For example, one can consider an open KL chain as a local deformation of the length of the spring connecting the two rotors at boundaries.

B.3 Homotopy groups

Homotopy groups provide a standard way to define a topological number associated to any local critical point. Assume P is a critical point in n-dimensional space and S_p is an $(n-1)$-dimensional sphere which encloses the point P. We define an integral of $n-1$-form

$$\oint_{S_p} \frac{f_{i_1} df_{i_2} \wedge ... \wedge df_{i_n} \epsilon^{i_1,i_2,...,i_n}}{(f_1^2 + f_2^2 + ... + f_n^2)^{\frac{n}{2}}} \tag{B.19}$$

which is totally independent of the choice of surface S_p. In other words, this integral gives properties which only depend on the critical point P. In the theory of homotopy groups, the vector field $\overrightarrow{f}$ around the critical point P can be classified by $\pi_{n-1}(S^{n-1})$ which is a Z topological class. This number does not depend on the choice of surface S_p if there is no critical point other than P inside S_p.

Take limit of small S_p, the integral can be calculated as

$$\oint_{S_p} \frac{f_{i_1} df_{i_2} \wedge ... \wedge df_{i_n} \epsilon^{i_1,i_2,...,i_n}}{(f_1^2 + f_2^2 + ... + f_n^2)^{\frac{n}{2}}} = sign(det(\frac{\partial f_i}{\partial x_j})) \oint_{S_p} x_{i_1} dx_{i_2} \wedge ... \wedge dx_{i_n} \epsilon^{i_1,i_2,...,i_n} \tag{B.20}$$

The integral $\oint_{S_p} x_{i_1} dx_{i_2} \wedge ... \wedge dx_{i_n} \epsilon^{i_1,i_2,...,i_n}$ is the surface area of a unit $(n-1)$-dimensional sphere. The permutation of $\epsilon^{i_1,i_2,...,i_n}$ would give a factor $(n-1)!$. Therefore, the integral is

$$\oint_{S_p} \frac{f_{i_1} df_{i_2} \wedge ... \wedge df_{i_n} \epsilon^{i_1,i_2,...,i_n}}{(f_1^2 + f_2^2 + ... + f_n^2)^{\frac{n}{2}}} = sign(det(\frac{\partial f_i}{\partial x_j})) s_{n-1}(n-1)! \tag{B.21}$$

where s_{n-1} is the surface area of a unit $(n-1)$-dimensional sphere. Finally, we define the integral

$$\frac{1}{s_{n-1}(n-1)!}\oint_{S_p}\frac{f_{i_1}df_{i_2}\wedge ...\wedge df_{i_n}\epsilon^{i_1,i_2,...,i_n}}{(f_1^2+f_2^2+...+f_n^2)^{\frac{n}{2}}} = sign(det(\frac{\partial f_i}{\partial x_j})) \tag{B.22}$$

If $det(\frac{\partial f_i}{\partial x_j}) = 0$, one has to explicitly calculate the integral which can be any integer. For example, consider $f_1 = 2(x^2 - y^2)$ and $f_2 = 2xy$. The only critical point is $(x, y) = (0, 0)$ at which $det(\frac{\partial f_i}{\partial x_j}) = 0$. By parametrizing with $x = cos(t)$ and $y = sin(t)$, the integral of 1-form is

$$\frac{1}{2\pi}\oint_{S^1} cos(2t)dsin(2t) - sin(2t)dcos(2t) = \frac{1}{2\pi}\oint_{S^1} 2 = 2 \tag{B.23}$$

If the integral is over all space, this would be the same as what we found by gauge-fixing with gauge conditions f_i. This analog provides another perspective to look at constrained problems. A set of constraints is treated as a vector field which is generated by the topological charges at the critical points where the vector field is zero. The theory of homotopy groups also give richer topological number Z instead of Z_2. Topological numbers other than ± 1 come from the case when $det(\frac{\partial f_i}{\partial x_j}) = 0$ at critical points. Without imposing any symmetry, Z topological class is obtained from the non-linearity of constraints.

APPENDIX C

FIELD THEORY AND THE WITTEN INDEX

In the continuous limit, in a one-dimensional closed manifold, assume the constraint is $f(\theta, \frac{d\theta}{dx}) = g(\theta)\frac{d\theta}{dx} + V(\theta) = 0$. In this form, the topological number is robust to a local deformation (changing the rest lengths of springs, the lengths of rotors, or the distance between two sites locally). Therefore, we can write the partition function

$$Z_f = \int D\theta D\Psi_A D\Psi_B e^{\int dx[-\frac{1}{2}(f(\theta,\frac{d\theta}{dx}))^2+(\frac{i}{2}\Psi_A\frac{\delta f(\theta,\frac{d\theta}{dx})}{\delta\theta}\Psi_B+h.c.)]} = \sum_{V(\theta)=0} sign(g(\theta)\frac{\partial V(\theta)}{\partial\theta}) \quad \text{(C.1)}$$

We use a KL chain for an example. To derive a field theory for KL chain, we take the continuous limit. First, we replace θ_n by $\theta(x) - \frac{a}{2}\frac{d\theta(x)}{dx}$ and θ_{n+1} by $\theta(x) + \frac{a}{2}\frac{d\theta(x)}{dx}$ [**?**]. The dynamic length of a spring is

$$l^2(x) = a^2 + 4r^2cos^2(\theta(x)) + 2ar[sin(\theta(x) + \frac{a}{2}\frac{d\theta(x)}{dx}) - sin(\theta(x) - \frac{a}{2}\frac{d\theta(x)}{dx})] \quad \text{(C.2)}$$

we rewrite the constraint as

$$\frac{a}{r}cos(\theta(x))sin(\frac{a}{2}\frac{d\theta(x)}{dx}) + sin^2\theta_c - sin^2(\theta(x)) = 0 \quad \text{(C.3)}$$

where $sin^2\theta_c = \frac{a^2+4r^2-\bar{l}^2}{4r^2}$ and $0 < \theta_c < \frac{\pi}{2}$.

Take an approximation to the first order of $\frac{a}{2}\frac{d\theta(x)}{dx}$, we have

$$C_1cos(\theta(x))\frac{d\theta(x)}{dx} + sin^2\theta_c - sin^2(\theta(x)) = 0 \quad \text{(C.4)}$$

where $C_1 = \frac{a^2}{2r}$

There are four solutions to $sin^2\theta_c - sin^2(\theta(x)) = 0$, namely, $\theta_s = \theta_c, -\theta_c, \pi - \theta_c, \pi + \theta_c$. the sign for each solution is

$$sign(-C_1 cos(\theta_s) sin(\theta_s) cos(\theta_s)) = -sign(sin(\theta_s)) \tag{C.5}$$

So $Z_f = (-1) + 1 + (-1) + 1 = 0$ which means that we can deform a closed KL chain locally such that there is no solution to make the potential energy zero.

This topological number is related to Witten's index by construct a supersymmetric Hamiltonian

$$H_{wit} = [Q, Q^\dagger]_{anti} \tag{C.6}$$

where the supercharge Q is

$$Q = \begin{pmatrix} 0 & 0 \\ A & 0 \end{pmatrix} \tag{C.7}$$

The operator A is

$$A = \frac{d}{dx} + \frac{\partial V}{\partial x} \tag{C.8}$$

By defining two subspaces

$$\begin{pmatrix} boson \\ fermion \end{pmatrix} \tag{C.9}$$

and the operator F which is 1 for bosons and 0 for fermions. Then Witten's index can be calculated by

$$W_{wit} = Tr((-1)^F e^{-\beta H_{wit}}) \tag{C.10}$$

which is exactly the same as the partition function we defined.

Another way to understand Witten's supersymmetry is that there exist two Hamiltonians that have the same spectra except for zero energy states. The two corresponding Hamiltonians are

$$H_{\pm} = -\frac{d^2}{dx^2} + (\frac{\partial V}{\partial x})^2 \mp \frac{\partial^2 V}{\partial x^2} \tag{C.11}$$

Then we can combine those two Hamiltonians with an extra degree of freedom that is a Fermion number n_F. Then we can say that the states for H_+ have $n_F = 0$ (bosonic states) and the states for H_- have $n_F = 1$ (fermionic states). Therefore, the physical interpretation of Witten's index is the number of bosonic states minus the number of fermionic states. Since all non-zero energy states are paired, Witten's index is also equal to the number of bosonic zero modes minus the number of fermionic zero modes.

In a topological quantum field theory with BRST-exact form, the partition function can be calculated by simply summing over all classical solutions. The classical solutions are the points where $\frac{\partial V}{\partial x} = 0$. In $H_{\pm}$, the potential energy would be raised or lowered by the third therm depending on the sign of $\frac{\partial^2 V}{\partial x^2}$. Therefore, the classical solutions in a topological quantum field theory with positive slop would correspond to minimum of the potential energy for H_+, and the negative slop ones for H_-. In other word, we can map the solutions with positive slop to the states of H_+ and the solutions with negative slop to the states of H_-.

APPENDIX D

Z TOPOLOGICAL INVARIANT

A Kane-Lubensky chain can be mapped into a Su-Schrieffer-Heeger chain which is in BDI class. In one-dimensional space BDI class has Z topological invariant. However, the sign of determinant only gives two possible values $+1$ or -1 which seems more like a Z_2 topological invariant. To clarify this point, we track back to Z topological invariant by considering the determinant as the multiplication of all its eigenvalues. First we consider general cases of translational symmetric lattices with periodic boundary conditions. With periodic boundary conditions, we can transform the real space into k-space and find the eigenvalues in terms of k. The eigenvalue $h(k)$ is

$$h(k) = \sum_n w_n e^{ink} = r(k)e^{i\phi(k)} \tag{D.1}$$

where w_n is the coefficients of constraints at the nth nearest site. And the sign of determinant is

$$sign(det) = sign \prod_k h(k) = e^{i\sum_k \phi(k)} = e^{i\mu\pi} \tag{D.2}$$

where $\phi(k)$ is continuous in $-\pi < k \leq \pi$. Because $sign(det)$ can only be either $+1$ or -1, μ is an integer. Also, we can always add a $2n\pi$ phase to all $\phi(k)$, so μ is defined as a modular of $2N$ where N is the number of total sites. Therefore, μ have $2N$ possible values. Since all the elements in the matrix are real, $h(k) = h^*(-k)$, and thus all the phases (except for $\phi(0)$ and $\phi(\pi)$) would be canceled if $\phi(0) = 0$. On the other hand, if $h(0)$ is negative then we can choose $\phi(0) = \pi$. In this case, $N\pi$ would be added to the total sum over $\phi(k)$. Therefore, whether μ is in $[0, N)$ or $[N+1, 2N)$ totally depends on the sign of $h(0)$. Thus we can write μ as

$$\mu = \mu_1 N + \mu_2 \tag{D.3}$$

where $\mu_1 = \frac{1-sign(h(0))}{2}$. To determine μ_2, what we need to know is $\phi(\pi)$. Now imagine that we go from $k = -\pi$, when we encounter $h(k) < 0$, if the derivative of $\phi(k)$ is positive that would add a π phase to $\phi(\pi)$. On the other hand, if the derivative is negative that would add a $-\pi$ phase to $\phi(\pi)$. Therefore, we can calculate μ_2 by

$$\mu_2 = \sum_{h(k)<0} sign \frac{d[\phi(k)]}{dk} \tag{D.4}$$

which is exactly equal to the winding number. In conclusion, we can re-write the sign of determinant as

$$sign(det) = e^{i(\mu_1 N + \mu_2)\pi} \tag{D.5}$$

$$\mu_1 = \frac{1 - sign(h(0))}{2} \tag{D.6}$$

$$\mu_2 = \sum_{h(k)<0} sign \frac{d[\phi(k)]}{dk} \tag{D.7}$$

With this expression, we get a $Z_2 \otimes Z$ topological invariant. Here we have an extra Z_2 topological invariant because there is a mirror symmetry along the chain. In BDI class, the Z topological invariant is protected by both particle-hole symmetry and chiral symmetry. In this structure the translational symmetry of lattices directly gives a chiral symmetry. However, after opening the boundaries and rotating rotors, chiral symmetry would be broken. Therefore, the system would become in D class which has Z_2 invariant. In general, without translational invariant, we only have $Z_2 \otimes Z_2$ topological invariant in a KL chain.

Another perspective to see this question is that without any symmetry, the sign of determinant only gives two possible values. While if there are some symmetries, the matrix can be block-diagonalized. Therefore, the system would have richer topological phases. The topological number are the combination of the sign of the determinant of each block.

D.0.1 Example 1

In a Kane-Lubensky chain $w_0 = -\Delta_+$ and $w_1 = \Delta_-$. If $\Delta_+ > 0$, $\Delta_- > 0$, and $\Delta_+ > \Delta_-$, we have $h(0) < 0$ and $h(\pi) < 0$. The sign of $\frac{d[\phi(k)]}{dk}$ at $h(k) < 0$ can be written as

$$sign \frac{d[\phi(k)]}{dk}_{h(k)<0} = -sign \sum_n n w_n cos(nk) \tag{D.8}$$

So the topological number μ_2 is

$$\mu^{(1)}_{2,\Delta_+>\Delta_-} = (-1) + 1 = 0 \tag{D.9}$$

For $\Delta_+ > 0$, $\Delta_- > 0$, and $\Delta_+ < \Delta_-$, $h(k) < 0$ only at $k = \pi$. The topological number μ_2 is

$$\mu^{(1)}_{2,\Delta_+<\Delta_-} = 1 \tag{D.10}$$

D.0.2 Example 2

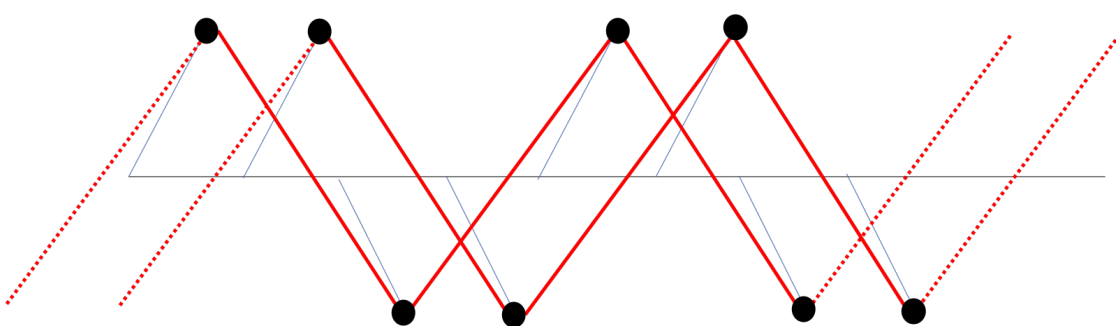

Now consider two separated KL chains, even sites for one KL chain and odd site for the other one. In this structure $w_0 = -\Delta_+$ and $w_2 = \Delta_-$. If $\Delta_+ > 0$, $\Delta_- > 0$, and $\Delta_+ > \Delta_-$, $h(k) < 0$ at four points, $k = 0$, $k = \pi/2$, $k = \pi$, and $k = 3\pi/2$. So the topological number μ_2 is

$$\mu^{(2)}_{2,\Delta_+>\Delta_-} = (-1) + 1 + (-1) + 1 = 0 \tag{D.11}$$

For $\Delta_+ > 0$, $\Delta_- > 0$, and $\Delta_+ < \Delta_-$, $h(k) < 0$ only at $k = \pi/2$ and $k = 3\pi/2$. The topological number μ is

$$\mu^{(2)}_{2,\Delta_+<\Delta_-} = 1 + 1 = 2 \tag{D.12}$$

D.0.3 Example 3

A spring-ball system with translational invariant can be mapped into a fermion system with a Hamiltonian

$$H = \sum_{i,j} w_{j-i} c^{\dagger}_{a,i} c_{b,j} + h.c. \tag{D.13}$$

This is a general form for a system with two sites, a and b, in one unit cell. In two coupled SSH chains, only w_{-1}, w_0, and w_1 are none-zero[33]. Assume that $w_{-1}, w_0, w_1 > 0$. If $w_0 > w_{-1} + w_1$, There is no point where $h(k) < 0$. Thus, $\mu_2 = 0$. If $w_0 < w_{-1} + w_1$, we have $h(k) < 0$ at $k = \pi$.

$$sign \frac{d[\phi(k)]}{dk}_{k=\pi} = -sign(w_{-1} - w_1) = sign(w_1 - w_{-1}) \tag{D.14}$$

Therefore, in this case, if $w_1 > w_{-1}$, $\mu_2 = 1$. On the other hand, if $w_1 < w_{-1}$, $\mu_2 = -1$.

APPENDIX E

LOCAL TOPOLOGICAL CHARGE APPROACH

The Kane-Lubensky (KL) chain shown in Fig.E.1 is a classical example to understand the topology of mechanical systems[26]. The winding number is defined via the dispersion of phonons at each zero energy point where all the extensions e_i of springs are zero. There are four different periodic solutions with zero energy which are the configurations with all angles being equal to θ_c, $-\theta_c$, $\pi - \theta_c$, or $\pi + \theta_c$ where $\theta_c = sin^{-1}(\frac{\sqrt{a^2+4r^2-L^2}}{2r})$ and a, r, and L are the distance between two nearest pivot points, the radius of rotors, and the length of springs, respectively. The dispersion of phonons is found to be the same form as the energy dispersion of the electronic states in the Su-Schrieffer-Heeger (SSH) chain. Therefore, the phonons in the KL chain and the electronic states in the SSH chain share the same topological properties.

A linear zero mode(ZM) located at one edge or the other after opening the boundaries can then be classified by the winding number[26]. The winding number is 0 for the solutions θ_c and $\pi - \theta_c$ which have a linear ZM at the right edge; the winding number is +1 for $-\theta_c$ and $\pi + \theta_c$ which have a linear ZM at the left edge. To continuously change the winding number from 0 to 1, one has to close the gap of phonons. Therefore, the winding number defined via phonons captures the topological invariant of linear ZMs protected by a gap.

However, those linear ZMs are indeed not localized and some of them are connected after opening the boundary. By building an exact model with rigid bars, a linkage initially located at one edge can propagate through the chain smoothly without any stretching or compressing deformations[14]. Therefore, the two linear ZMs with different winding numbers could actually be connected

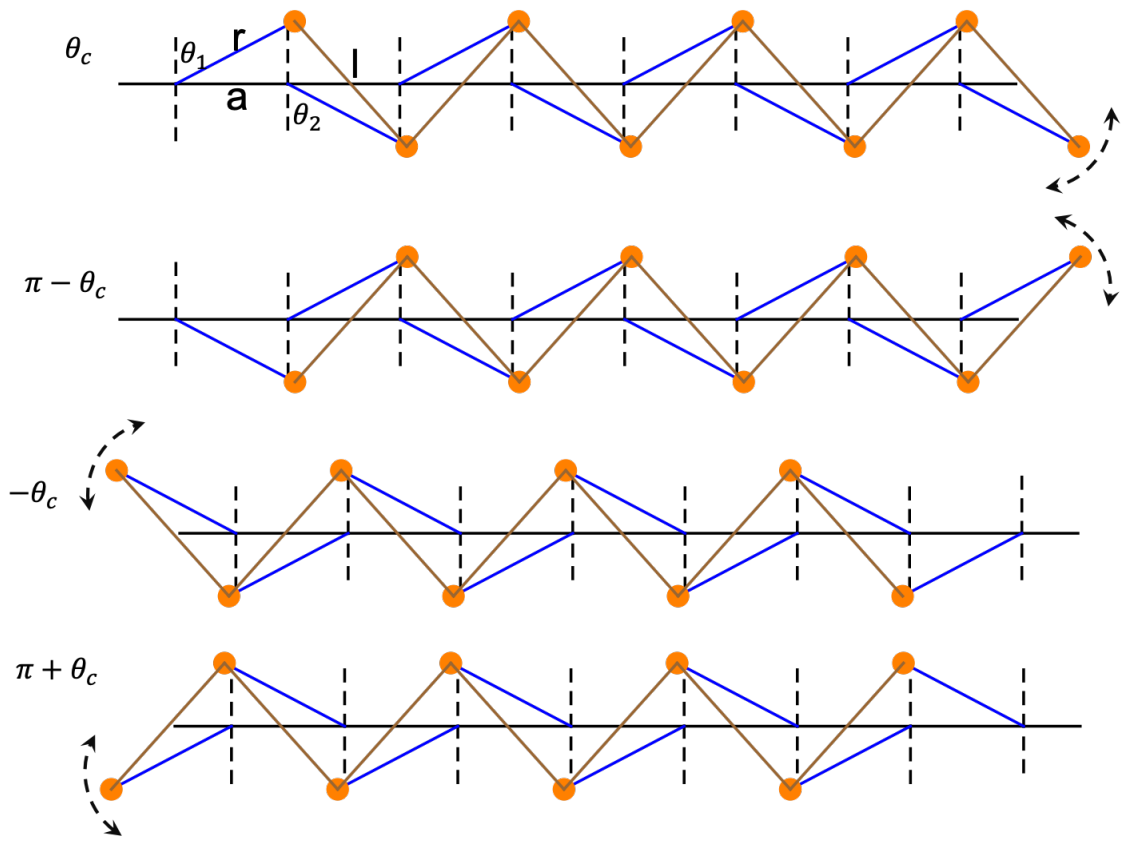

Figure E.1: Kane-Lubensky chain. Each site has a rotor (blue line) with radius r. The distance between two pivot points is a. Two adjacent rotors are connected by a spring (brown line) with rest length l. The rotating angle of ith rotor is θ_i. The opened KL chain has one linear zero mode located at one edge or the other. The configurations of θ_c and $\pi - \theta_c$ have a linear ZM at the right edge and their winding number is 0. The configurations of $-\theta_c$ and $\pi + \theta_c$ have a linear ZM at the left edge and their winding number is +1.

and belong to the same nonlinear ZM. This implies that the winding numbers defined via phonons are incompatible with the realistic nonlinear ZMs of the opened KL chain.

One can study whether a nonlinear ZM behaves like a soliton wave or is localized at one edge by using local topological charges. In the KL chain, a local topological charge for each unit cell is defined in the following way. Two nearest rotors are combined as a unit cell as shown in Fig.E.3(a). For each configuration of two rotors, by adding an extra spring that connects the second rotor back to the first rotor in a periodic way, it becomes a two-rotor model(Fig.E.2), and the the local topological charge for each configuration can be calculated by

$$\mu(p) = \frac{1}{s_{n-1}(n-1)!} \oint_{S_p} \frac{e_{i_1} de_{i_2} \wedge ... \wedge de_{i_n} \epsilon^{i_1, i_2, ..., i_n}}{(e_1^2 + e_2^2 + ... + e_n^2)^{\frac{n}{2}}} \tag{E.1}$$

The corresponding local topological charge $\mu(p)$ would tell us which one (θ_i or θ_{i+1}) is the dominant degree of freedom. The definition can be further promoted to a non-periodic point ($\theta_i \neq \theta_{i+1}$) by using the same definition.

$$\mu = \begin{cases} 1, & |\frac{\partial e_1}{\partial \theta_i}| > |\frac{\partial e_1}{\partial \theta_{i+1}}| \\ -1, & |\frac{\partial e_1}{\partial \theta_i}| < |\frac{\partial e_1}{\partial \theta_{i+1}}| \end{cases} \tag{E.2}$$

Imagine that we start with the configuration where all the local topological charges are +1 (the first configuration in Fig.E.1). The dominant rotor is initially identified in the last site. As we rotate rotors around this point, the changes of the angles would exponentially decay from the right to left. This property holds if the local topological charges stay the same. Therefore, the invariant of the local topological charges implies that the left edge is fixed if the chain is long enough. On the other hand, if the local topological charge changes, the dominant rotor would propagate from one site to the other.

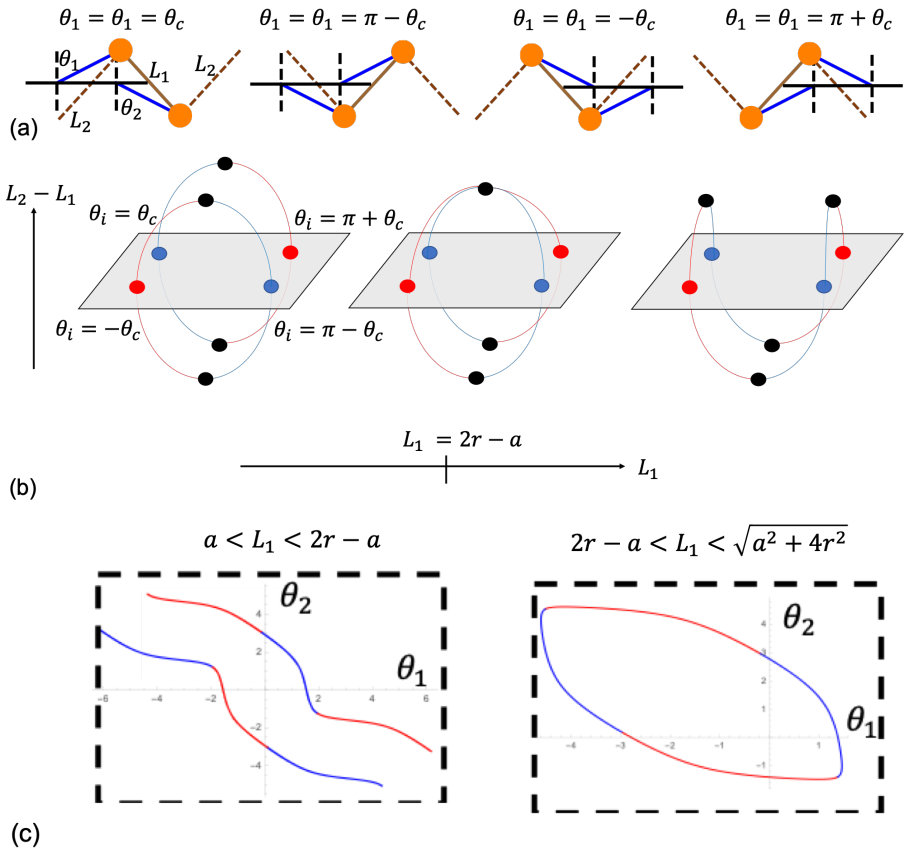

Figure E.2: Two-rotor model (a)Four solutions for the two-rotor model with the periodic boundary condition. An extra spring of length L_2 connects two rotors as the periodic boundary condition. (b)The dynamic of solutions with the continuous change of L_2. The blue (red) circles are the solution points for the periodic boundary condition with topological charge +1 (−1). The blue (red) lines are the solution points with topological charge +1 (−1) for different L_2. The black circles are the points where one positive and one negative topological charge combine. Two different nonlinear zero modes are separated by the phase transition point $L_1 = 2r - a$ where two black circles merge. (c)The plots of θ_1 versus θ_2. The blue lines are the points of configurations with +1 charge, and the red lines are the points of configurations with −1 charge. The curves of the left panel are periodic. The two red segments of the first curve are the same, and the two blue segments of the second curve are the same.

Imagine that we start with the configuration where all the local topological charges are +1 (The first configuration in Fig.E.1). The linear ZM is initially identified in the last unit cell. As we rotate rotors around this point, the changes of the θ_i would exponentially decay from the right to left. This property holds if the local topological charges stay the same. Therefore, the invariant of the local topological charge of a unit cell implies that the configuration of the unit cell stays topologically the same which makes the left edge almost fixed if the chain is long enough. On the other hand, if the local topological charge changes, the configuration of the unit cell would change significantly which implies that the linear ZM propagates from one unit cell to another.

Firstly, we consider a mildly disordered KL chain($a < L_i < \sqrt{a^2 + 4r^2}$). Start with a configuration in which all local topological charges are +1 as shown in Fig.E.3(a). Since the linear ZM is at the right edge initially, as we continuously rotate the rotors, only the last two unit cells would change significantly. As shown in Fig.E.3(b), the local topological charge in the last unit cell changes from +1 to −1, and then the local topological charge in the second to last unit cell also changes from +1 to −1. By looking at the relation of the nearest two unit cells for a mildly disordered KL chain, it shows that the local topological charges for all unit cells would change from +1 to −1 in the order from right to left. As a result, the nonlinear ZM behaves like a soliton wave which propagates through the chain.

For the second example, we introduce an extreme disorder for the last spring ($L_9 < a$) as shown in Fig.E.4(a). Similar to the previous example, the linear ZM is initially localized in the last unit cell. The configuration space of the last unit cell forms a loop and each point on the loop can be mapped into a point

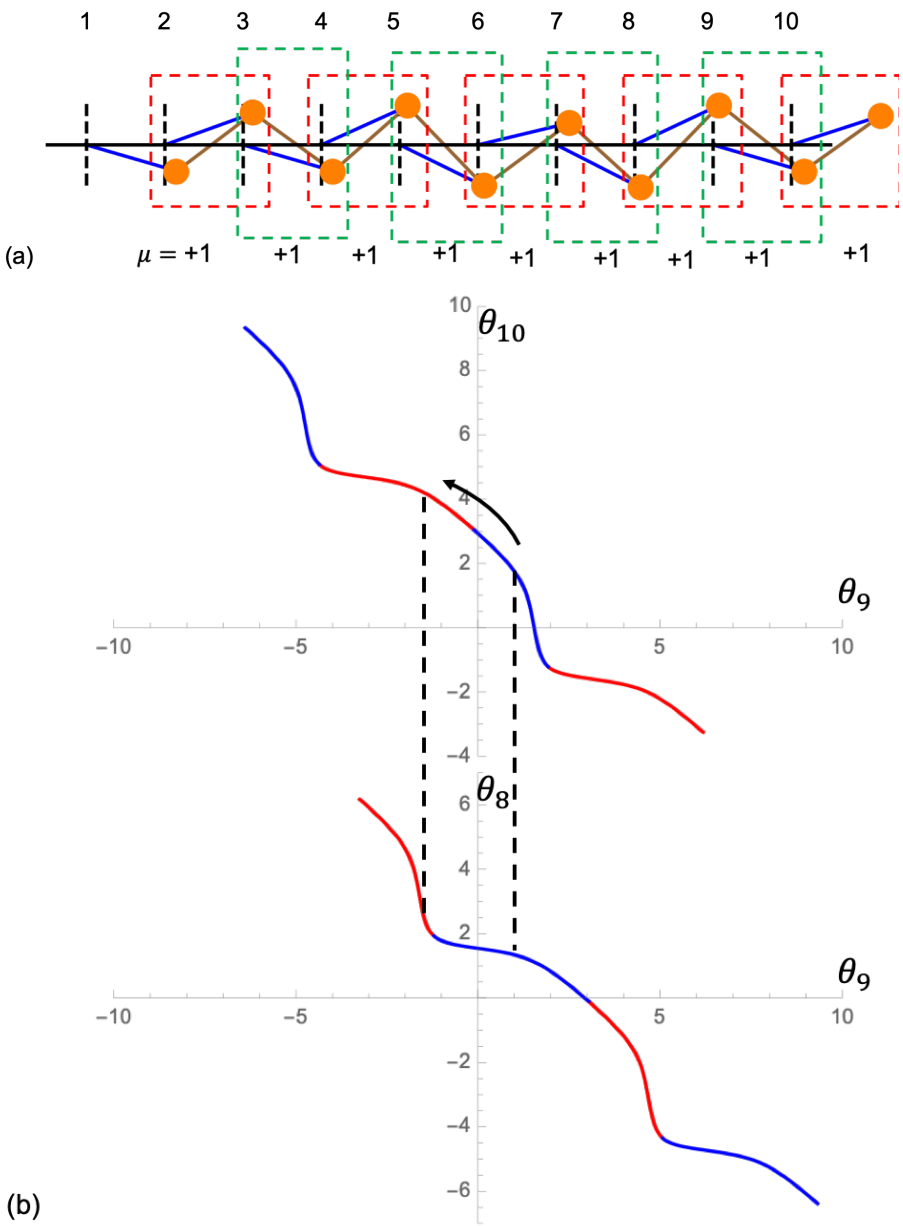

Figure E.3: Mildly disordered KL chain (a)Two nearest rotors are combined as a unit cell. Initially, all local topological charges are +1. (b)The relation between the last two unit cells. As continuously rotating rotors, the local topological charge in the last unit cell changes from +1 to −1, and then the local topological charge in the second to last unit cell also changes from +1 to −1.

with +1 charge in the second to last unit cell[See Fig.E.4(b)]. This condition is sufficient to guarantee that the linear ZM cannot propagate to the left-hand side. Therefore, the nonlinear ZM is localized at the right edge.

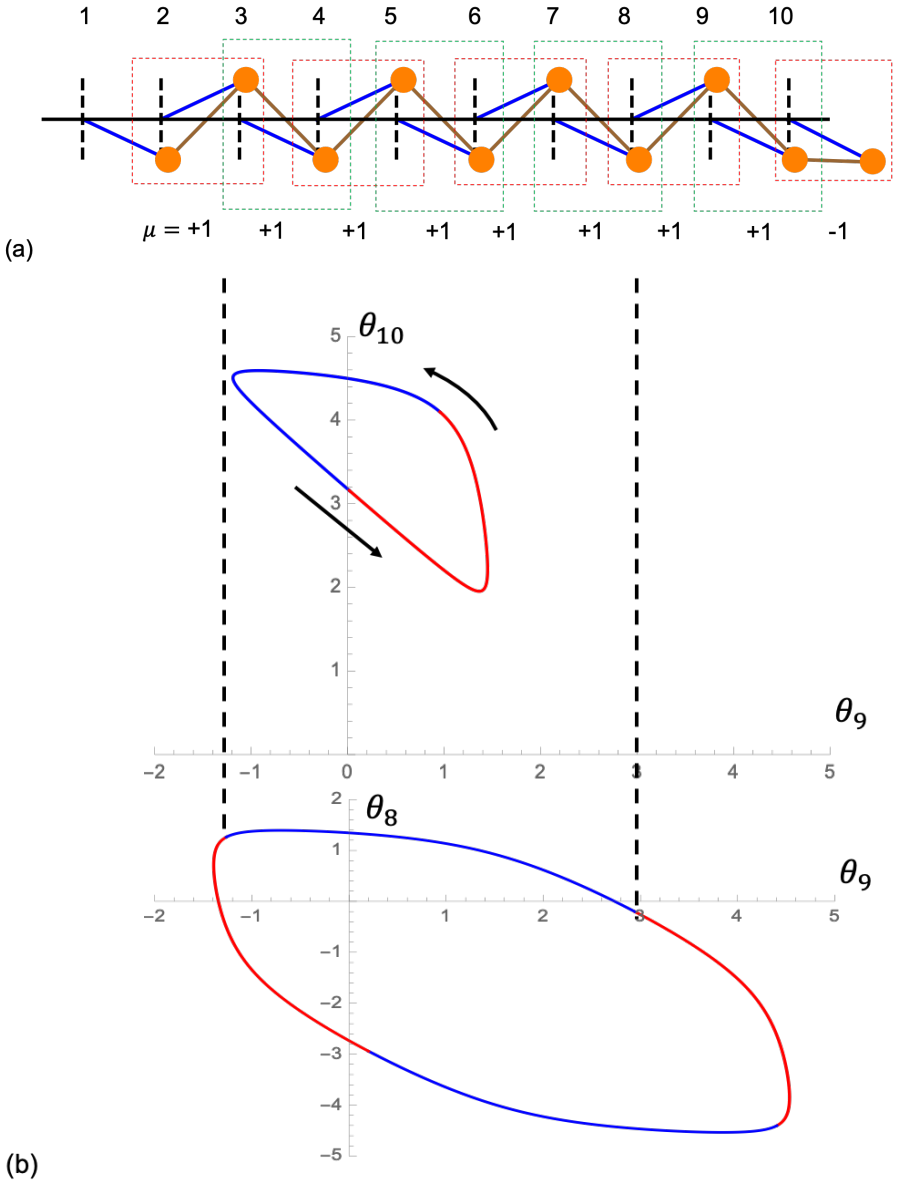

Figure E.4: Localized edge zero mode in a disordered KL chain (a)The initial configuration of a disordered KL chain in which the length of the last spring is smaller than a. (b)The configuration of the last unit cell forms a loop (the one at right-hand side). Each point on the loop can be mapped into a point with +1 charge in the second to last unit cell.

APPENDIX F

EXAMPLES OF SUPERSYMMETRY

linear constraints Let's consider $n = 2$ case. Assume that we have two linear constraints in a two-dimensional space. The solution to the two constraints is the intersecting point of two straight lines. Geometrically, we know that there always exists one single intersecting point for two non-parallel lines as shown in FigF.1(a).

Let's consider $x + y = 0$ and $x - y = 0$ as an example. In this case $Q_{net} = sign[1 \times (-1) - 1 \times 1] = -1$. We can map this constrained problem to a quantum system with the Hamiltonian

$$\begin{aligned} H_1 = -\frac{1}{2}(\frac{\partial^2}{\partial x^2} + \frac{\partial^2}{\partial y^2}) + (x^2 + y^2) \\ -\frac{1}{2}[(\frac{\partial}{\partial \Psi_1}\Psi_1 + \Psi_1\frac{\partial}{\partial \Psi_1}) + (\frac{\partial}{\partial \Psi_1}\Psi_2 + \Psi_2\frac{\partial}{\partial \Psi_1}) \\ +(\frac{\partial}{\partial \Psi_2}\Psi_1 + \Psi_1\frac{\partial}{\partial \Psi_2}) - (\frac{\partial}{\partial \Psi_2}\Psi_2 + \Psi_2\frac{\partial}{\partial \Psi_2})] \end{aligned} \tag{F.1}$$

In the $n_F = 0, 2$ sectors, we have

$$H_1(n_F = 0, 2) = -\frac{1}{2}(\frac{\partial^2}{\partial x^2} + \frac{\partial^2}{\partial y^2}) + (x^2 + y^2) \tag{F.2}$$

which is a two-simple-harmonic-oscillator system that has the lowest energy equal to $\sqrt{2}$. Thus, there is no zero mode in the even number fermion sections.

In the $n_F = 1$ sectors, we have

$$H_1(n_F = 1) = -\frac{1}{2}(\frac{\partial^2}{\partial x^2} + \frac{\partial^2}{\partial y^2})\mathbf{I} + (x^2 + y^2)\mathbf{I} - \mathbf{R} \tag{F.3}$$

where $\mathbf{R} = \begin{pmatrix} 1 & 1 \\ 1 & -1 \end{pmatrix}$ By rotating the two fermion basis, we get two non-interacting Hamiltonians

$$H_{1,\pm}(n_F = 1) = -\frac{1}{2}(\frac{\partial^2}{\partial x^2} + \frac{\partial^2}{\partial y^2}) + (x^2 + y^2) \pm \sqrt{2}. \tag{F.4}$$

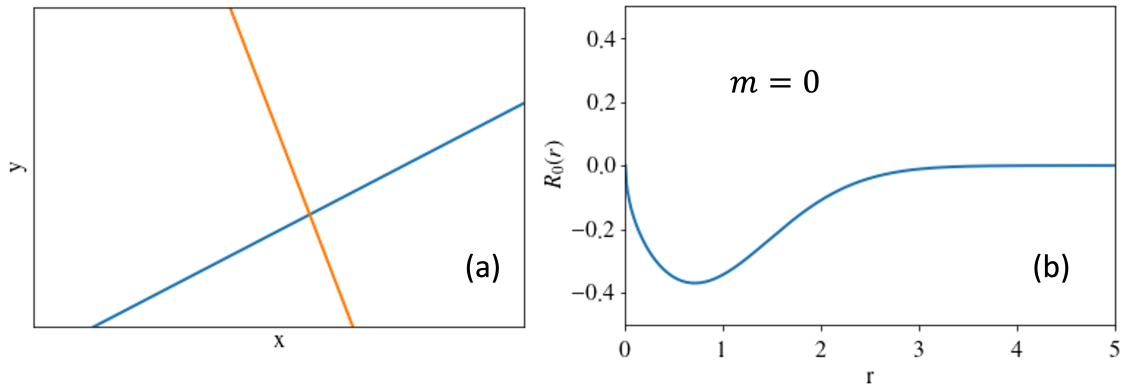

Figure F.1: (a)Geometrical topology: two non-parallel straight lines in a two-dimensional space always have one intersecting point. (b)The radial part of the wavefunction for the corresponding unbroken supersymmetric zero mode.

The ground state energy of $H_{1,+}(n_F = 1)$ is $2\sqrt{2}$ which is also nonzero. A zero mode comes from of $H_{1,-}(n_F = 1)$. The corresponding wavefunction is plot in Fig.F.1(a). Because we have a single zero mode in the odd number fermion section, the partition function Z_{susy} is equal to $(-1)^1 = -1$ that we can directly infer from Q_{net}. The unbroken supersymmetry in H_1 can therefore be understood as the geometric argument that two non-parallel lines must have a intersecting point.

F.1 nonlinear constraints

In general, nonlinear constraints can be any form. Here we consider the two hyperbola constraints as an example because of its special geometrically property. In a two dimensional space, two hyperbolas with non-parallel or non-perpendicular transverse axes always have two intersecting points as show in FigF.2(a). This topological property implies that there always exist two solution

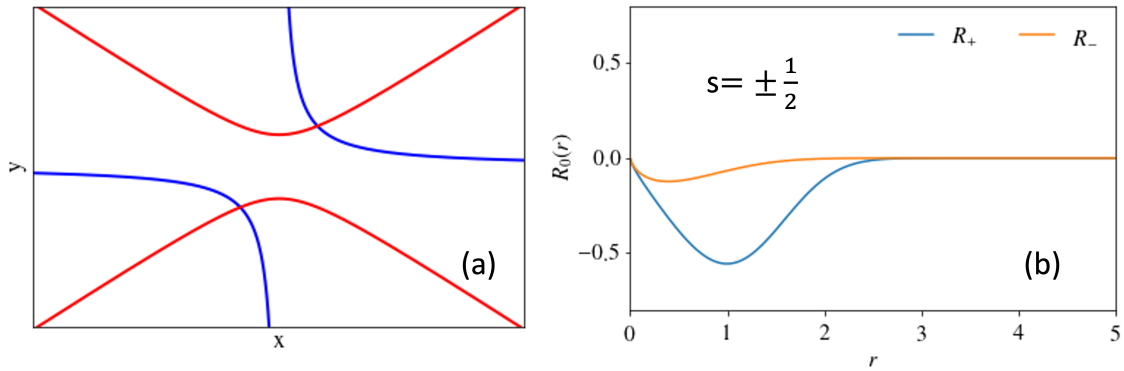

Figure F.2: (a)Geometrical topology: two hyperbolas with non-parallel or non-perpendicular transverse axes always in a two-dimensional space always have two intersecting points. (b)The radial part of the wavefunctions for the two corresponding unbroken supersymmetric zero modes.

points, and thus $Q_{net} = \pm 2$.

Let's consider $x^2 - y^2 = 0$ and $-2xy = 0$ as an example. In this case $Q_{net} = -2$. We can map this constrained problem to a quantum system with the Hamiltonian

$$\begin{aligned} H_2 = -\frac{1}{2}(\frac{\partial^2}{\partial x^2} + \frac{\partial^2}{\partial y^2}) + \frac{1}{2}(x^2+y^2)^2 \\ -\frac{1}{2}[2x(\frac{\partial}{\partial \Psi_1}\Psi_1 + \Psi_1\frac{\partial}{\partial \Psi_1}) - 2y(\frac{\partial}{\partial \Psi_1}\Psi_2 + \Psi_2\frac{\partial}{\partial \Psi_1}) \\ -2y(\frac{\partial}{\partial \Psi_2}\Psi_1 + \Psi_1\frac{\partial}{\partial \Psi_2}) - 2x(\frac{\partial}{\partial \Psi_2}\Psi_2 + \Psi_2\frac{\partial}{\partial \Psi_2})] \end{aligned} \tag{F.5}$$

which can be written in the polar coordinates as

$$\begin{aligned} H_2 = -\frac{1}{2}(\frac{\partial^2}{\partial r^2} + \frac{1}{r}\frac{\partial}{\partial r} + \frac{1}{r^2}(\frac{\partial^2}{\partial \theta^2}) + \frac{1}{2}r^4 \\ -r[cos\theta(\frac{\partial}{\partial \Psi_1}\Psi_1 + \Psi_1\frac{\partial}{\partial \Psi_1}) - sin\theta(\frac{\partial}{\partial \Psi_1}\Psi_2 + \Psi_2\frac{\partial}{\partial \Psi_1}) \\ -sin\theta(\frac{\partial}{\partial \Psi_2}\Psi_1 + \Psi_1\frac{\partial}{\partial \Psi_2}) - cos\theta(\frac{\partial}{\partial \Psi_2}\Psi_2 + \Psi_2\frac{\partial}{\partial \Psi_2})] \end{aligned} \tag{F.6}$$

In the $n_F = 0, 2$ sectors, we have

$$H_2(n_F = 0, 2) = -\frac{1}{2}(\frac{\partial^2}{\partial r^2} + \frac{1}{r}\frac{\partial}{\partial r} + \frac{1}{r^2}\frac{\partial^2}{\partial \theta^2}) + \frac{1}{2}r^4. \tag{F.7}$$

The θ dependent part of the wavefunction is e^{-im} with some integer m, and thus the term $\frac{1}{r^2}\frac{\partial^2}{\partial\theta^2}$ can be replaced by $-\frac{m^2}{r^2}$. Then we have

$$H_2(n_F = 0, 2) = -\frac{1}{2}(\frac{\partial^2}{\partial r^2} + \frac{1}{r}\frac{\partial}{\partial r}) + \frac{1}{2}r^4 + \frac{m^2}{2r^2}. \tag{F.8}$$

In the $n_F = 1$ sectors, we have

$$H_2(n_F = 1) = -\frac{1}{2}(\frac{\partial^2}{\partial r^2} + \frac{1}{r}\frac{\partial}{\partial r} + \frac{1}{r^2}\frac{\partial^2}{\partial\theta^2})\mathbf{I} + \frac{1}{2}r^4\mathbf{I} - 2r\mathbf{T} \tag{F.9}$$

where $\mathbf{T} = \begin{pmatrix} cos\theta & -sin\theta \\ -sin\theta & -cos\theta \end{pmatrix}$, The eigenvector of $\mathbf{T}$ with eigenvalue 1 is $e^{is\theta}\begin{pmatrix} -cos\frac{\theta}{2} \\ sin\frac{\theta}{2} \end{pmatrix}$ and eigenvector of $\mathbf{T}$ with eigenvalue -1 is $e^{is\theta}\begin{pmatrix} sin\frac{\theta}{2} \\ cos\frac{\theta}{2} \end{pmatrix}$ where s is a half integer. The term $\frac{1}{r^2}\frac{\partial^2}{\partial\theta^2}$ acting on the above two states gives the potential energy

$$\begin{pmatrix} \frac{\frac{1}{4}+s^2}{2r^2} & -\frac{is}{2r^2} \\ \frac{is}{2r^2} & \frac{\frac{1}{4}+s^2}{2r^2} \end{pmatrix} \tag{F.10}$$

Therefore, we $H_2(n_F = 1)$ can be written as

$$\begin{pmatrix} H_{hyper} - 2r & -\frac{is}{2r^2} \\ \frac{is}{2r^2} & H_{hyper} + 2r \end{pmatrix} \tag{F.11}$$

where $H_{hyper} = -\frac{1}{2}(\frac{\partial^2}{\partial r^2} + \frac{1}{r}\frac{\partial}{\partial r}) + \frac{1}{2}r^4 + \frac{\frac{1}{4}+s^2}{2r^2}$.

By explicitly solving $H_2(n_F = 0, 1, 2)$, we found that there are only two zero modes exist in $H_2(n_F = 1)$ with $s = \pm\frac{1}{2}$ as shown in Fig.F.2(b). Therefore, $Z_{susy} = -2$ which agrees with result from classical constrained problem. In this case, the two unbroken supersymmetric zero modes in H_2 is the topological result from the geometric reason that two hyperbolas with non-parallel or non-perpendicular transverse axes always have two intersecting points.

APPENDIX G

SPT EIGENSTATES

We study the spin-1/2 ladder model with 6 rungs to see what happens to the Haldane spin-one SPT eigenstates after breaking the staggered swap symmetry ($J_{\|,1} = J_{\|,2} = J_{X,1} = J_{X,2}$).

In the antiferromagnetic Heisenberg spin-one chain model, the lowest 4 eigenstates are separated by a gap from the other states as shown in FigG.1. Those four states are $S = 0$ singlet and $S = 1$ triplet. The excitation ($S = 1, S_z = -1, 1$) of the ground state ($S = 0$) is an edge state that has two spin-half particles separately at two edges where the expectation value of S_z is roughly 0.5 as show in Fig.G.2(a).

Now we start with the ladder model at the highly frustrated point $J_\perp = 2J_{\|,1} = 2J_{\|,2} = 2J_{X,1} = 2J_{X,2}$ and identify the corresponding $S = 0$ singlet and $S = 1$ triplet are the 54th, 61st, 62nd and 63rd excited states.

When we change $J_{\|,1}$ slightly without having any level crossing, S_z of those four states change as Fig.G.2(b) and (c). When $\Delta J_{\|,1} = 0.01 J_{\|,1}$, from the expectation values of S_z on different rungs we can see the states $S = 1, S_z = -1, 1$ evolve into the bulk. In these two states, $< S_z >$ at two edges decreases and $< S_z >$ of the middle rungs increases becoming comparable to $< S_z >$ at two edges[See Fig.G.2(b)]. When we increase $\Delta J_{\|,1}$ further to $0.01 J_{\|,1}$ as shown in Fig.G.2(c) the state $S = 1, S_z = -1$ significantly mixed with the state $S = 1, S_z = 0$. From the evolution of $< S_z >$ in Fig.4.7(a)-(c), we see that the edge states are not robust with the deformation (change of $J_\|$). In other words, these Haldane eigenstates are protected by the staggered swap symmetry ($J_{\|,1} = J_{\|,2} = J_{X,1} = J_{X,2}$) that is

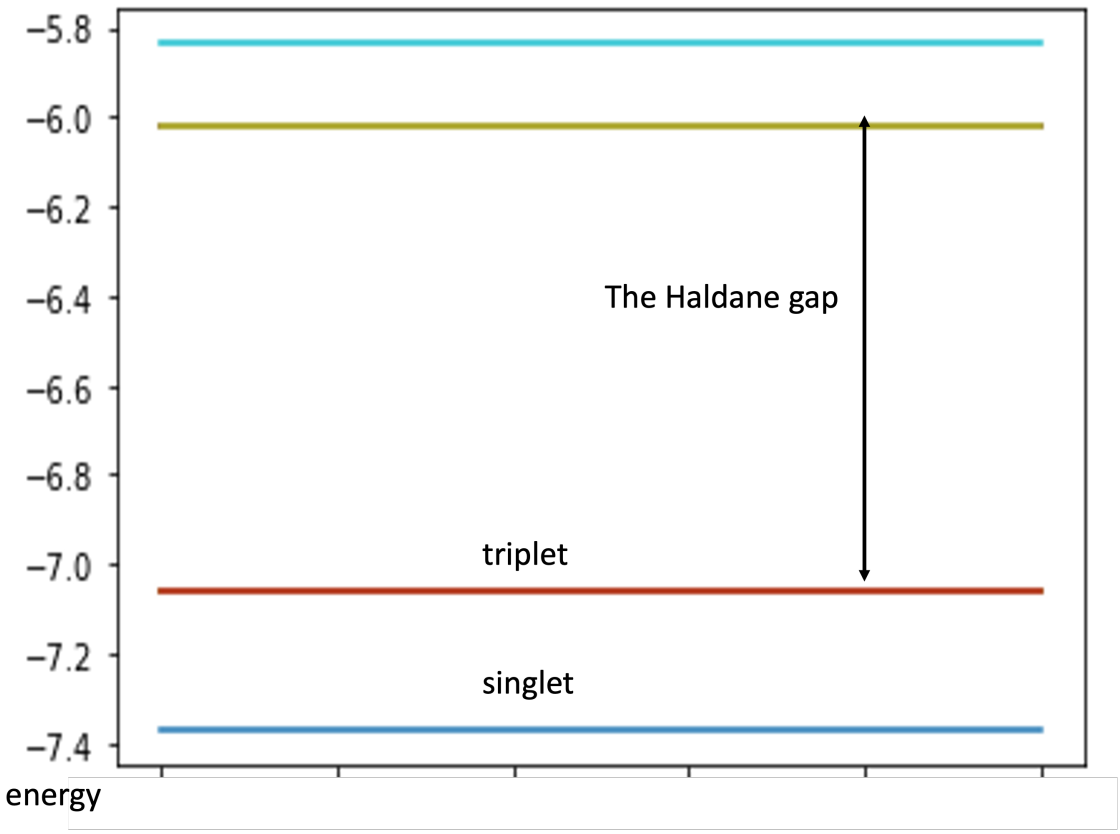

Figure G.1: The spectrum of the antiferromagnetic Heisenberg spin-one chain with 6 sites.

also the symmetry enriches the topological frustration in the classical limit.

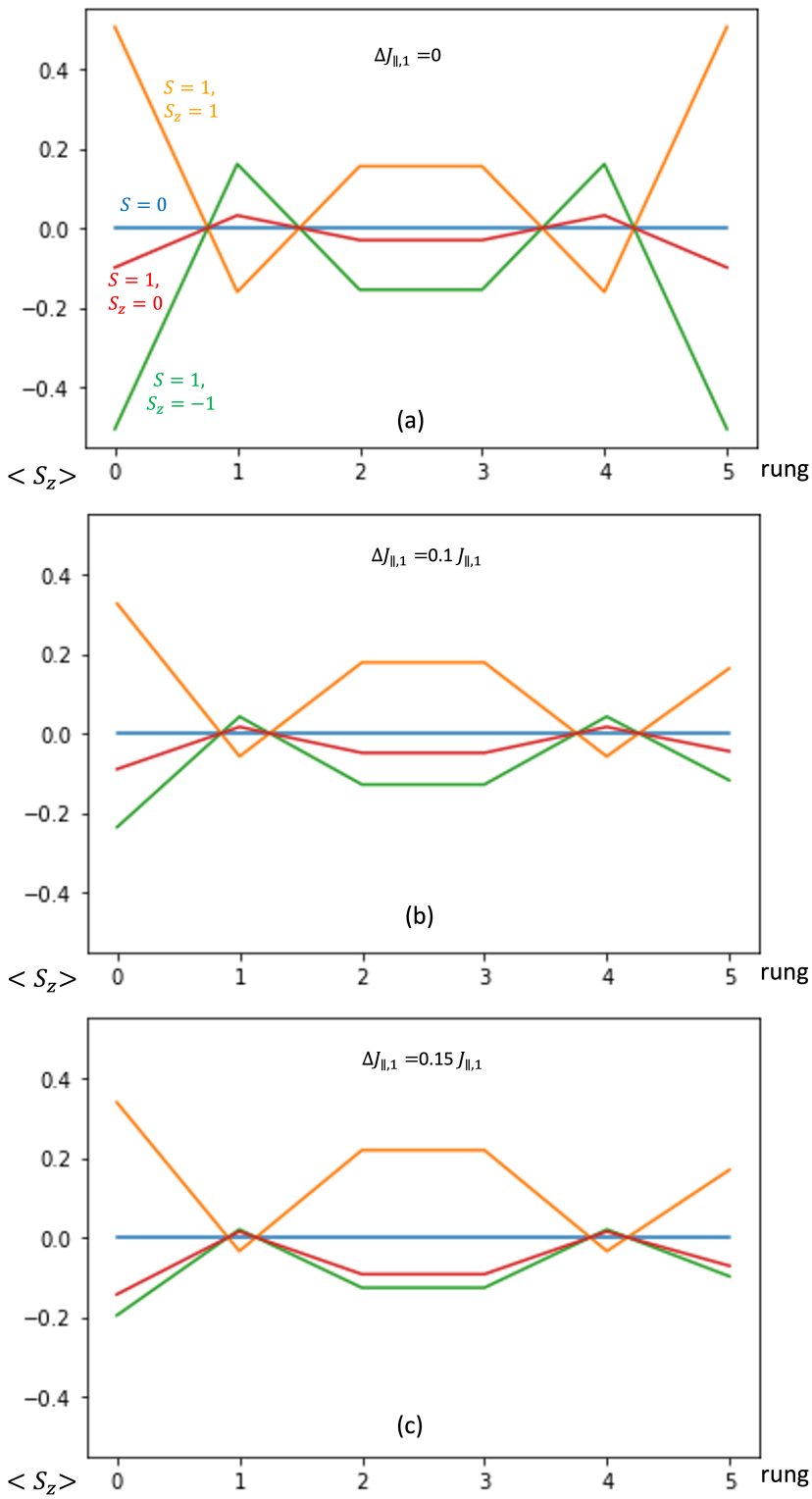

Figure G.2: (a)The expectation value of S_z on each rung for the $S = 0$ singlet and $S = 1$ triplet. (b) and (c) show the evolution of $< S_z >$ after breaking the staggered swap symmetry.

BIBLIOGRAPHY

[1] Michael Francis Atiyah. *K-theory (Advanced Book Classics)*. Addison-Wesley, 1989.

[2] C. Becchi, A. Rouet, and R. Stora. The abelian higgs kibble model, unitarity of the s-operator. *Physics Letters B*, 52(3):344 – 346, 1974.

[3] C Becchi, A Rouet, and R Stora. Renormalization of gauge theories. *Annals of Physics*, 98(2):287 – 321, 1976.

[4] B. Bernu, P. Lecheminant, C. Lhuillier, and L. Pierre. Exact spectra, spin susceptibilities, and order parameter of the quantum heisenberg antiferromagnet on the triangular lattice. *Phys. Rev. B*, 50:10048–10062, Oct 1994.

[5] D. Birmingham, M. Blau, M. Rakowski, and G. Thompson. Topological field theory. *Physics Reports*, 209:129–340, 1991.

[6] Indrani Bose and Saurabh Gayen. Hole motion in a coupled-chain model: Some exact results. *Phys. Rev. B*, 48:10653–10656, Oct 1993.

[7] Jean-Paul Brasselet, José Seade, and Tatsuo Suwa. *Vector fields on Singular Varieties*. Springer-Verlag Berlin Heidelberg, 2009.

[8] B. Canals and C. Lacroix. Pyrochlore antiferromagnet: A three-dimensional quantum spin liquid. *Phys. Rev. Lett.*, 80:2933–2936, Mar 1998.

[9] Luca Capriotti, Adolfo E. Trumper, and Sandro Sorella. Long-range néel order in the triangular heisenberg model. *Phys. Rev. Lett.*, 82:3899–3902, May 1999.

[10] J. T. Chalker and J. F. G. Eastmond. Ground-state disorder in the spin-1/2 kagomé heisenberg antiferromagnet. *Phys. Rev. B*, 46:14201–14204, Dec 1992.

[11] P. Chandra and B. Doucot. Possible spin-liquid state at large s for the frustrated square heisenberg lattice. *Phys. Rev. B*, 38:9335–9338, Nov 1988.

[12] Hitesh J. Changlani and Andreas M. Läuchli. Trimerized ground state of the spin-1 heisenberg antiferromagnet on the kagome lattice. *Phys. Rev. B*, 91:100407, Mar 2015.

[13] Bryan Gin-ge Chen, Bin Liu, Arthur A. Evans, Jayson Paulose, Itai Cohen, Vincenzo Vitelli, and C. D. Santangelo. Topological mechanics of origami and kirigami. *Phys. Rev. Lett.*, 116:135501, Mar 2016.

[14] Bryan Gin-ge Chen, Nitin Upadhyaya, and Vincenzo Vitelli. Nonlinear conduction via solitons in a topological mechanical insulator. *Proceedings of the National Academy of Sciences*, 111(36):13004–13009, 2014.

[15] Andrey V. Chubukov and Th. Jolicoeur. Order-from-disorder phenomena in heisenberg antiferromagnets on a triangular lattice. *Phys. Rev. B*, 46:11137–11140, Nov 1992.

[16] J. M. Deutsch. Quantum statistical mechanics in a closed system. *Phys. Rev. A*, 43:2046–2049, Feb 1991.

[17] Xiao-Yu Dong and D. N. Sheng. Spin-1 kitaev-heisenberg model on a honeycomb lattice. *Phys. Rev. B*, 102:121102, Sep 2020.

[18] L.D. Faddeev and V.N. Popov. Feynman diagrams for the yang-mills field. *Physics Letters B*, 25(1):29 – 30, 1967.

[19] Irene Fonseca, Nicola Fusco, and Paolo Marcellini. Topological degree, jacobian determinants and relaxation. *Bollettino dell'Unione Matematica Italiana*, 8-B(1):187–250, 2 2005.

[20] J. Clerk Maxwell F.R.S. L. on the calculation of the equilibrium and stiffness of frames. *The London, Edinburgh, and Dublin Philosophical Magazine and Journal of Science*, 27(182):294–299, 1864.

[21] Liang Fu and C. L. Kane. Topological insulators with inversion symmetry. *Phys. Rev. B*, 76:045302, Jul 2007.

[22] M. J. Harris, S. T. Bramwell, D. F. McMorrow, T. Zeiske, and K. W. Godfrey. Geometrical frustration in the ferromagnetic pyrochlore $\mathrm{ho_2ti_2}O_7$. *Phys. Rev. Lett.*, 79:2554–2557, Sep 1997.

[23] M. Z. Hasan and C. L. Kane. Colloquium: Topological insulators. *Rev. Mod. Phys.*, 82:3045–3067, Nov 2010.

[24] Uzi Hizi and Christopher L Henley. Effective hamiltonians for large-spyrochlore antiferromagnets. *Journal of Physics: Condensed Matter*, 19(14):145268, mar 2007.

[25] J. Jordan, R. Orús, G. Vidal, F. Verstraete, and J. I. Cirac. Classical simulation of infinite-size quantum lattice systems in two spatial dimensions. *Phys. Rev. Lett.*, 101:250602, Dec 2008.

[26] C. L. Kane and T. C. Lubensky. Topological boundary modes in isostatic lattices. *Nature Physics*, 10:39, Dec 2013.

[27] C. L. Kane and T. C. Lubensky. Topological boundary modes in isostatic lattices. *Nature Physics*, 10:39, Dec 2013.

[28] C. L. Kane and E. J. Mele. Z_2 topological order and the quantum spin hall effect. *Phys. Rev. Lett.*, 95:146802, Sep 2005.

[29] A Yu Kitaev. Unpaired majorana fermions in quantum wires. *Physics-Uspekhi*, 44(10S):131–136, oct 2001.

[30] Michael J Lawler. Emergent gauge dynamics of highly frustrated magnets. *New Journal of Physics*, 15(4):043043, 2013.

[31] Michael J. Lawler. Supersymmetry protected topological phases of isostatic lattices and kagome antiferromagnets. *Phys. Rev. B*, 94:165101, Oct 2016.

[32] P. Lecheminant, B. Bernu, C. Lhuillier, L. Pierre, and P. Sindzingre. Order versus disorder in the quantum heisenberg antiferromagnet on the kagomé lattice using exact spectra analysis. *Phys. Rev. B*, 56:2521–2529, Aug 1997.

[33] C. Li, S. Lin, G. Zhang, and Z. Song. Topological nodal points in two coupled su-schrieffer-heeger chains. *Phys. Rev. B*, 96:125418, Sep 2017.

[34] Po-Wei Lo, Chao-Ming Jian, and Michael J Lawler. Topology shared between classical metamaterials and interacting superconductors, 2022.

[35] Po-Wei Lo and Michael J. Lawler. The fate of topological frustration in quantum spin ladders and generalizations, 2022.

[36] Po-Wei Lo, Christian D. Santangelo, Bryan Gin-ge Chen, Chao-Ming Jian, Krishanu Roychowdhury, and Michael J. Lawler. Topology in nonlinear mechanical systems. *Phys. Rev. Lett.*, 127:076802, Aug 2021.

[37] T. C. Lubensky, C. L. Kane, Xiaoming Mao, A. Souslov, and Kai Sun. Phonons and elasticity in critically coordinated lattices. *Reports on Progress in Physics*, 78(7):1 – 30, July 2015.

[38] Dustin Nash, Lisa M.and Kleckner, Alismari Read, Vincenzo Vitelli, Ari M. Turner, and William T. M. Irvine. Topological mechanics of gyroscopic metamaterials. *Proceedings of the National Academy of Sciences*, 112(47):14495–14500, 2015.

[39] Ido Niesen and Philippe Corboz. Ground-state study of the spin-1 bilinear-biquadratic heisenberg model on the triangular lattice using tensor networks. *Phys. Rev. B*, 97:245146, Jun 2018.

[40] Paul Olum. Mappings of manifolds and the notion of degree. *Annals of Mathematics*, 58(3):458–480, 1953.

[41] Jayson Paulose, Anne S. Meeussen, and Vincenzo Vitelli. Selective buckling via states of self-stress in topological metamaterials. *Proceedings of the National Academy of Sciences*, 25:7639, Jun 2015.

[42] Hoi Chun Po, Yasaman Bahri, and Ashvin Vishwanath. Phonon analog of topological nodal semimetals. *Phys. Rev. B*, 93:205158, May 2016.

[43] I. Ritchey, P. Chandra, and P. Coleman. Spin folding in the two-dimensional heisenberg kagomé antiferromagnet. *Phys. Rev. B*, 47:15342–15345, Jun 1993.

[44] D. Zeb Rocklin, Bryan Gin-ge Chen, Martin Falk, Vincenzo Vitelli, and T. C. Lubensky. Mechanical weyl modes in topological maxwell lattices. *Phys. Rev. Lett.*, 116:135503, Apr 2016.

[45] D. Zeb Rocklin, Bryan Gin-ge Chen, Martin Falk, Vincenzo Vitelli, and T. C. Lubensky. Mechanical weyl modes in topological maxwell lattices. *Phys. Rev. Lett.*, 116:135503, Apr 2016.

[46] Rahul Roy. Z_2 classification of quantum spin hall systems: An approach using time-reversal invariance. *Phys. Rev. B*, 79:195321, May 2009.

[47] Krishanu Roychowdhury and Michael J Lawler. Classification of magnetic frustration and metamaterials from topology. *Physical Review B*, 98(9):094432, 2018.

[48] Krishanu Roychowdhury, D. Zeb Rocklin, and Michael J. Lawler. Topology and geometry of spin origami. *Phys. Rev. Lett.*, 121:177201, Oct 2018.

[49] Krishanu Roychowdhury, D. Zeb Rocklin, and Michael J. Lawler. Topology and geometry of spin origami. *Phys. Rev. Lett.*, 121:177201, Oct 2018.

[50] Adrien Saremi and Zeb Rocklin. Controlling the deformation of metamaterials: Corner modes via topology. *Phys. Rev. B*, 98:180102, Nov 2018.

[51] Adrien Saremi and Zeb Rocklin. Controlling the deformation of metamaterials: Corner modes via topology. *Phys. Rev. B*, 98:180102, Nov 2018.

[52] Koji Sato and Ryokichi Tanaka. Solitons in one-dimensional mechanical linkage. *Phys. Rev. E*, 98:013001, Jul 2018.

[53] E. F. Shender, V. B. Cherepanov, P. C. W. Holdsworth, and A. J. Berlinsky. Kagomé antiferromagnet with defects: Satisfaction, frustration, and spin folding in a random spin system. *Phys. Rev. Lett.*, 70:3812–3815, Jun 1993.

[54] Daniel Stanek, Oleg P. Sushkov, and Götz S. Uhrig. Self-consistent spin-wave theory for a frustrated heisenberg model with biquadratic exchange in the columnar phase and its application to iron pnictides. *Phys. Rev. B*, 84:064505, Aug 2011.

[55] Olaf Stenull, C. L. Kane, and T. C. Lubensky. Topological phonons and weyl lines in three dimensions. *Phys. Rev. Lett.*, 117:068001, Aug 2016.

[56] Roman Süsstrunk and Sebastian D. Huber. Observation of phononic helical edge states in a mechanical topological insulator. *Sciences*, 349:47–50, Jul 2015.

[57] D. J. Thouless, M. Kohmoto, M. P. Nightingale, and M. den Nijs. Quantized hall conductance in a two-dimensional periodic potential. *Phys. Rev. Lett.*, 49:405–408, Aug 1982.

[58] C. J. Turner, A. A. Michailidis, D. A. Abanin, M. Serbyn, and Z. Papić. Quantum scarred eigenstates in a rydberg atom chain: Entanglement, breakdown of thermalization, and stability to perturbations. *Phys. Rev. B*, 98:155134, Oct 2018.

[59] C. J. Turner, A. A. Michailidis, D. A. Abanin, M. Serbyn, and Z. Papić. Weak ergodicity breaking from quantum many-body scars. *Nature Physics*, 14(7):745–749, 2018.

[60] I. V. Tyutin. Gauge invariance in field theory and statistical physics in operator formalism, 1975.

[61] F. Verstraete and J. I. Cirac. Valence-bond states for quantum computation. *Phys. Rev. A*, 70:060302, Dec 2004.

[62] Pai Wang, Ling Lu, and Katia Bertoldi. Topological phononic crystals with one-way elastic edge waves. *Phys. Rev. Lett.*, 115:104302, Sep 2015.

[63] Pai Wang, Ling Lu, and Katia Bertoldi. Topological phononic crystals with one-way elastic edge waves. *Phys. Rev. Lett.*, 115:104302, Sep 2015.

[64] Yao-Ting Wang, Pi-Gang Luan, and Shuang Zhang. Coriolis force induced topological order for classical mechanical vibrations. *New Journal of Physics*, 17(7):073031, jul 2015.

[65] Zheng Weihong, V. Kotov, and J. Oitmaa. Two-chain spin ladder with frustrating second-neighbor interactions. *Phys. Rev. B*, 57:11439–11445, May 1998.

[66] Steven R. White. Density matrix formulation for quantum renormalization groups. *Phys. Rev. Lett.*, 69:2863–2866, Nov 1992.

[67] Y. Xian. Rigorous results on a first-order phase transition in antiferromagnetic spin-1/2 coupled chains. *Phys. Rev. B*, 52:12485–12488, Nov 1995.

[68] Z. Y. Xie, J. Chen, J. F. Yu, X. Kong, B. Normand, and T. Xiang. Tensor renormalization of quantum many-body systems using projected entangled simplex states. *Phys. Rev. X*, 4:011025, Feb 2014.

[69] Mengxing Ye and Andrey V. Chubukov. Quantum phase transitions in the heisenberg $J_1 - J_2$ triangular antiferromagnet in a magnetic field. *Phys. Rev. B*, 95:014425, Jan 2017.

[70] Yue Yu and Steven A. Kivelson. Phases of frustrated quantum antiferromagnets on the square and triangular lattices. *Phys. Rev. B*, 101:214404, Jun 2020.

[71] Leyou Zhang and Xiaoming Mao. Fracturing of topological maxwell lattices. *New Journal of Physics*, 20(6):063034, jun 2018.

[72] Leyou Zhang and Xiaoming Mao. Fracturing of topological maxwell lattices. *New Journal of Physics*, 20(6):063034, jun 2018.

[73] Di Zhou, Leyou Zhang, and Xiaoming Mao. Topological edge floppy modes in disordered fiber networks. *Phys. Rev. Lett.*, 120:068003, Feb 2018.

[74] Di Zhou, Leyou Zhang, and Xiaoming Mao. Topological boundary floppy modes in quasicrystals. *Phys. Rev. X*, 9:021054, Jun 2019.

[75] Yujie Zhou, Bryan Gin-ge Chen, Nitin Upadhyaya, and Vincenzo Vitelli. Kink-antikink asymmetry and impurity interactions in topological mechanical chains. *Phys. Rev. E*, 95:022202, Feb 2017.